

DISSERTATION

PHYSICOCHEMICAL CHARACTERIZATION OF SELF-ASSOCIATED CHROMATIN
OLIGOMERS

Submitted by

Ryan Rogge

Department of Biochemistry and Molecular Biology

In partial fulfillment of the requirements

For the Degree of Doctor of Philosophy

Colorado State University

Fort Collins, Colorado

Spring 2016

Doctoral Committee:

Advisor: Jeffrey Hansen

Karoline Luger

Jennifer DeLuca

Donald Mykles

Copyright by Ryan Rogge 2016

All Rights Reserved

ABSTRACT

PYSICOCHEMICAL CHARACTERIZATION OF SELF-ASSOCIATED CHROMATIN OLIGOMERS

The DNA of chromosomes is extensively compacted within the nuclei of eukaryotic nuclei. Chromosomes are composed of chromatin which is a repeating polymer of nucleosomes bound by additional chromatin proteins. Chromatin can be reconstituted *in vitro* using purified DNA and histone proteins to form nucleosomal arrays. Reconstituted chromatin fibers are structurally dynamic and the structures formed are highly dependent on the buffer conditions, particularly polyvalent cations. The addition of Mg²⁺ favors nucleosome-nucleosome interactions. At low concentrations nucleosomes on the same fiber interact resulting in folding, while at higher concentrations inter-fiber interactions result in chromatin self-association. Unlike folded chromatin, the oligomeric structure of chromatin is unknown, to address this deficiency, in this dissertation the oligomeric structures formed by 12-mer nucleosomal arrays were characterized by microscopy, sedimentation velocity, and SAXS experiments. The oligomeric chromatin complexes were globular throughout all stages of the cooperative assembly process, and ranged in size from ~50 nm to a diameter of ~1000 nm. The oligomer sedimentation coefficients under these conditions ranged from 5000-350,000S, corresponding to ~1-400 Mb DNA/oligomer. The nucleosomal arrays were packaged within the oligomers as interdigitated 10-nm fibers, rather than folded 30-nm structures. Linker DNA was freely accessible to micrococcal nuclease, although the oligomers remained partially intact after linker DNA digestion. The organization of chromosomal fibers in human nuclei *in situ* was stabilized by 1 mM MgCl₂, but became disrupted in 0 mM MgCl₂, conditions that also dissociated the oligomers *in vitro*. These results indicate that a 10-nm array of nucleosomes has the intrinsic ability to self-

assemble into large chromatin globules stabilized by nucleosome-nucleosome interactions, and suggest that the oligomers are good *in vitro* model for investigating the structure and organization of interphase chromosomes.

ACKNOWLEDGEMENTS

The people I would like to thank first are students who worked with me on my project. Ryan von Feldt, Erik Seidel, and Ken Lyon all helped me work on various experiments at some point. I would also like to thank the multitude of fellow graduate students I have worked with over the years. Many of the students in the always changing roster of graduate students have been incredibly helpful to me. Graduate students are frequently my first point of contact around the department when learning, planning, and gathering the supplies for new experiments. A large number of graduate students have also been my good friends and an invaluable social support system. I would also like to thank all the past researchers in the Hansen Lab. Dr. Anna Kalashnikova and Dr. Heather Szerlong were particularly helpful during my tenure in the lab, and there are a number of previous unmet members whose research and publications had laid the ground work for my results. I have also worked closely with our collaborators the in the lab of Dr. Kazuhiro Maeshima, who has provided assays useful for analyzing chromatin reconstituted in our lab particularly the SAXS experiments. Lastly, I would like to thank my advisor Dr. Jeffrey Hansen, whose support was always positive and who allowed me to work on a number of projects until finding interesting results.

The work of a few individuals was particularly invaluable on specific experiments. Suzanne Royer's help on the transmission electron microscopy results made those experiments possible. The advice of Dr. Borries Demeler and Virgil Schirf was useful in the execution and analysis of the interference sedimentation velocity experiments. The assistance of the DeLuca Lab in the fluorescence microscopy experiments was also important. Without the work of Dr. Jake Herman, and assistance from Dr. Eric Tauchman I would not have been able to complete those experiments. Lastly, I would like to thank my committee members, Dr. Karolin Luger, Dr.

Jake DeLuca, and Dr. Donald Mykles. They have contributed a number of hours in reviewing my writing and presentations, as well as guiding my research through constructive critiques.

TABLE OF CONTENTS

ABSTRACT	ii
ACKNOWLEDGEMENTS	iv
Literature Review and Introduction.....	1
1.1 Background Information: Chromatin Composition and Chromosome Structure	1
1.2 Nucleosomal Arrays as Model Chromatin	4
1.3 Chromatin Fiber Dynamics	5
1.4 Mechanisms for Chromatin Compaction and the Implications for Nuclear Architecture.....	8
1.5 Determinants of Chromatin Self-Association.....	10
1.6 Assays for Exploring Self-Association.....	14
Development of a Sedimentation Velocity Assay for Chromatin Oligomers	18
2.1 Introduction.....	18
2.2 Theory	18
2.3 Equipment	21
2.4 Setting up the Interferometer Laser: Laser Delay and Duration	21
2.5 Radial Calibration of Interference Detector	23
2.6 Final Considerations for Interference Sedimentation Velocity Run.....	23
2.7 Experimental	24
2.7.1 Reconstitution of chromatin fibers and assembly of chromatin oligomers	24
2.7.2 Choosing the Rotor Speed	25
2.8 Data Analysis	27
2.8.1 Systematic noise considerations.....	27
2.8.2 Time derivative method.	28
2.8.3 Other analysis methods	28
2.9 Discussion	29
2.9.1 Chromatin oligomers	29
2.9.2 Large complexes in general.....	32
Nucleosomal arrays self-assemble into supramolecular globular structures lacking 30-nm fibers	33
3.1 Introduction.....	33
3.2 Results	36
3.2.1 Nucleosomal arrays self-associate into large globular oligomers	36
3.2.2 Nucleosomal array monomers are packaged as extended 10-nm fibers not folded 30 nm fibers.....	50
3.2.3 Linker histones modulate oligomer structure, assembly, and subunit packaging	57

3.2.4 Low salt disassembles higher order chromatin structures in nuclei <i>in situ</i>	66
3.3 Discussion	71
3.4 Materials and Methods	75
3.4.1 Reconstitutions.....	75
3.4.2 Fluorescence light microscopy of nucleosomal arrays and isolated nuclei.	76
3.4.3 Transmission electron microscopy.....	78
3.4.4 Analytical ultracentrifugation.....	78
3.4.5 SAXS.....	79
3.4.6 Micrococcal nuclease digestion	80
3.4.7 Computer modeling.	81
Unpublished Experiments on Chromatin Oligomers and Future Directions	83
4.1 Introduction.....	83
4.2 Results	85
4.2.1 Sedimentation velocity of chromatin oligomers made with recombinant <i>Xenopus laevis</i> chromatin oligomers.	85
4.2.2 Accessibility of chromatin oligomers assayed using digestion by micrococcal nuclease.....	87
4.2.3 Unique internal structure of linker histone chromatin in solution containing high concentrations of Mg ²⁺ when examined by TEM.	89
4.3 Methods	91
4.3.1 Sedimentation velocity experiments on chromatin assembled with recombinant <i>Xenopus laevis</i> octamer.	91
4.3.2 Micrococcal nuclease digestion of chromatin oligomers.....	91
4.3.3 Transmission electron microscopy.....	92
4.4 Discussion, Future Directions, Speculations	92
4.4.1 Discussion of unpublished experimental results	92
4.4.2 Future avenues of investigation.....	96
4.4.3 Summary and conclusions.....	98

Chapter 1

Literature Review and Introduction

1.1 Background Information: Chromatin Composition and Chromosome Structure

The DNA molecules of living organisms are the longest biological polymers which make up cells. The genetic material of human cell, if added end to end is nearly two meters long. However the DNA is never arranged in this fashion and is instead separated into 46 chromosomes. The longest of these chromosomes is 8 cm long if fully extended. A single chromosome is never fully extended, and is instead folded through extensive interactions with proteins. The DNA of eukaryotic organisms is associated extensively with proteins, which neutralize some of the negative charge, and which allows the DNA to fold upon itself to form chromosomes. At the first level of DNA folding and organization, the core histone octamer proteins bind to 146bp of DNA, with the DNA forming two loops around the proteins. The core histone octamer is composed of two copies each of the histones H2A, H2B, H3, and H4. While in interphase the chromosome is then further folded into small local domains and eventually globular chromosome territories (Lieberman-Aiden *et al*, 2009; Bolzer *et al*, 2005). During cell division the mitotic chromosomes are further compacted into characteristic X-shaped structures to aid in the proper separation of the genetic material (Maeshima *et al*, 2014b; Ohta *et al*, 2010).

Native chromatin is always at least partially condensed in mammalian cell nuclei, with some regions of chromosomes more compacted than others. Tightly packed regions of chromatin are referred to as heterochromatin, and less densely packed regions as euchromatin. As cells begin to differentiate larger regions of compacted heterochromatin begin to appear (Ugarte *et al*, 2015). The organization of interphase chromosomes is significantly stochastic, with large variability in cell to cell chromatin contact maps, as determined in single cell

chromatin conformation experiments (Nagano *et al*, 2013). Condensation patterns of interphase chromosomes are different across cell types and also generally get progressively more condensed throughout cell differentiation. There are, however, still large scale patterns obvious in the nuclear architecture of eukaryotic nuclei. Regions of highly condensed heterochromatin tend to gather at the nuclear periphery with more open euchromatin regions located at the nuclear interior (Bazett-Jones *et al*, 2008). Interphase chromatin fibers interact extensively with many regions along the same chromosome, and have very few interactions with other chromosomes resulting in the formation of chromosome territories (Bolzer *et al*, 2005; Lieberman-Aiden *et al*, 2009) (Figure 1.1). These intra-chromosomal interactions could be the result of additional chromatin architectural proteins, or an intrinsic feature of nucleosome-nucleosome attractions along the chromatin fiber. The specific composition of the chromatin fiber has been shown to influence the structures formed by chromatin both *in vitro* and *in vivo*. Chromatin architectural proteins such as linker histones, CTCF, HP1, and many others have large scale effects on chromosomes (McBryant *et al*, 2006). Changes within the nucleosomes, such as histone variants, and post-translational modifications are also known to influence the structure of chromatin fibers *in vivo* (Bannister & Kouzarides, 2011; Maze *et al*, 2014) and *in vitro* (Muthurajan *et al*, 2011b; Allahverdi *et al*, 2011).

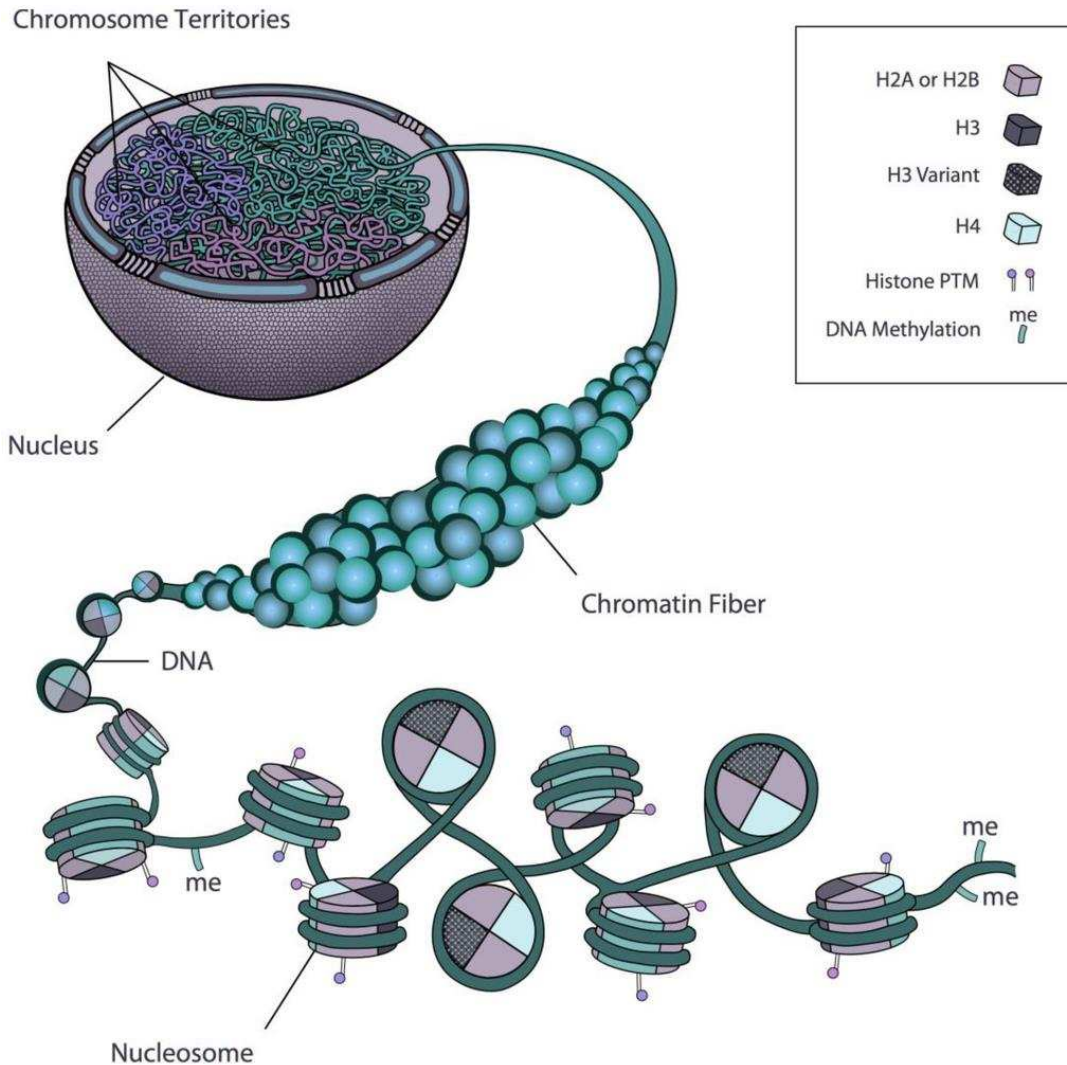


Figure 1.1 Schematic view of the organization of interphase chromatin fibers. The repeating unit of a chromatin fiber is the nucleosome. This includes the histone octamer which may contain variants of the canonical histone genes as well as a variety of post-translational modifications. Associations between the nucleosomes results in the compaction of the chromatin into intermediary structures and eventually forms chromosome territories. The actual compacted chromatin structures are still a point of contention.

Diagram from : Stefanie Rosa and Peter Shaw, Biology 2013, CC BY

1.2 Nucleosomal Arrays as Model Chromatin

In order to research the components of chromatin that affect the structural dynamics of chromatin fibers, researchers have performed extensive *in vitro* experiments. Early experiments utilized chromatin fibers isolated from native sources, frequently from chicken erythrocytes (Shaw *et al*, 1976). Recombinant DNA technologies have led to the use of defined model nucleosomal arrays, in which sequences of DNA with a propensity for forming well positioned nucleosomes are tandemly repeated and reconstituted with purified core histone octamers to form a string of well-defined nucleosomes (Hayes & Wolffe, 1993; Lowary & Widom, 1998). The model system we use to investigate the mechanisms by which chromosomes are organized utilizes nucleosome positioning sequences isolated from either the 5S rRNA gene or the Widom 601 nucleosome position sequence. The Widom 601 sequence is an artificial sequence produced by SELEX, which readily forms well positioned nucleosomes (Lowary & Widom, 1998). The 5S sequences strongly position nucleosomes (Dong *et al*, 1990), that differ from each other by multiples of 10 bp (Hansen *et al*, 1989) (and in this respect are more characteristic of *in vivo* chromatin fibers). The Hansen lab has extensive experience using both 5S and Widom repeats of 12 nucleosome positioning sequences for reconstitution of nucleosomal arrays *in vitro*. In order to make the nucleosomal arrays, first the isolated histone proteins are renatured into histone octamer and the octamer purified using size exclusion chromatography. Reconstitution of the nucleosomal arrays is accomplished by the addition of equimolar octamer proteins to the number of nucleosome positioning sequences, followed by repeated dialysis into solutions of decreasing sodium chloride concentration, and a final quality control step to check for saturation (Rogge *et al*, 2013). This method results in binding of all the added histones to the DNA, and as a result careful quality control measures must be taken in order to ensure that the final products contain no non-nucleosomal histone-DNA interactions due to over saturation with protein (Rogge *et al*, 2013). The 12-mer nucleosomal array has been well characterized in our lab and others (Hansen & Lohr, 1993; Muthurajan *et al*, 2011;

Carruthers *et al*, 2007). This allows for the use of sedimentation velocity experiments in the analytical ultracentrifuge (AUC) to control for the level of histone saturation on the DNA template. This combination of array reconstitution and sedimentation velocity experiments has been utilized extensively to study the folding of *in vitro* reconstituted chromatin into locally compacted 30nm fibers (Song *et al*, 2014; Dorigo *et al*, 2004; Schalch *et al*, 2005). Here I intend to utilize this model system to quantitatively study the self-association of nucleosomal arrays and H1 chromatin fibers, which have previously been characterized exclusively by a simple differential centrifugation assay.

One of the largest challenges of the *in vitro* model is the size compared to an entire chromosome. The largest human chromosome contains 250 Mbp of DNA and approximately 1.25 million nucleosomes, and so our model is only 1/100,000 the length of human chromosome 1. However, it has been suggested that self-association of short chromatin fibers *in vitro* is representative of long range interactions along a full-length chromosome (Lu *et al*, 2006). The interactions between distant regions along a single flexible polymer are unrestricted, and thus modelled relatively well by diffusing monomers (Lu *et al*, 2006). Self-association of arrays has not been studied using sedimentation velocity, and has been characterized only by a differential centrifugation assay (DCA) (Gordon *et al*, 2005). The DCA assay reports only the percentage of the sample which self-associated and provides no information about oligomer structure or assembly. In order to better characterize chromatin self-association we have developed new assays for interrogating chromatin oligomer structure.

1.3 Chromatin Fiber Dynamics

Short segments of chromatin fibers reconstituted *in vitro* have been shown to condense through nucleosome-nucleosome interactions. These interactions are salt dependent, and the nucleosomes interact in both an intra-fiber and inter-fiber fashion (Hansen, 2002). In low divalent salt concentrations (e.g., <0.5 mM Mg²⁺) nucleosomal arrays have an extended beads-

on-a-string conformation known as the 10 nm fiber. With increasing salt (e.g., 0.5-2 mM Mg²⁺), nucleosomal arrays fold into helical structures that are ~30-40 nm in diameter known as the ‘30 nm fiber’(Hansen, 2002). Two structures have been proposed for the 30 nm fiber, the solenoid model with neighboring nucleosomes interacting and the two start mode, in which n+2 nucleosomes are interacting (Robinson & Rhodes, 2006; Grigoryev *et al*, 2009). Folding occurs through intra-fiber nucleosome-nucleosome interactions mediated by the H4 N-terminal tail domain of one nucleosome interacting with the surface acidic patch of nearby nucleosomes (Kalashnikova *et al*, 2013a). Folded 30 nm fibers are stabilized by the H1 linker histones (Carruthers *et al*, 1998). A recent cryo-EM structure of folded chromatin with linker histone indicates a two-start helical structure as well as asymmetric binding of linker histone at the nucleosome dyad (Song *et al*, 2014). However, *in vivo* experiments indicate that 30nm fibers are not a prominent structure in mammalian nuclei (Eltsov *et al*, 2008; Nishino *et al*, 2012; Fussner *et al*, 2012).

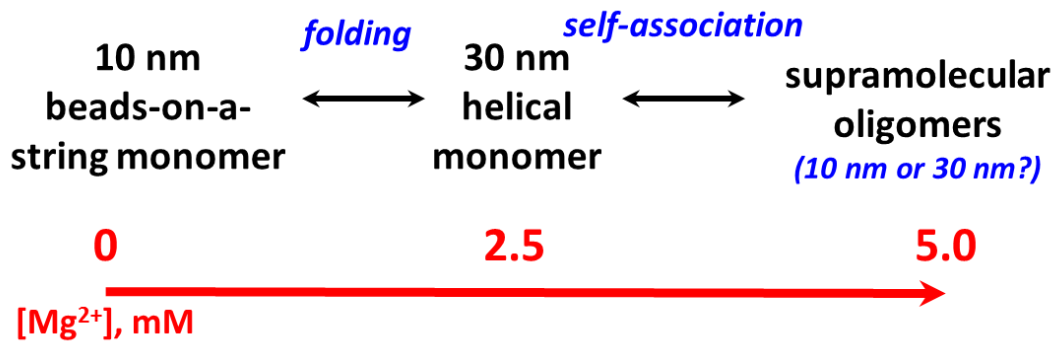


Figure 1.2. Chromatin structural dynamics with increasing Mg^{2+} . The formation of higher order structures observed in *in vitro* reconstituted chromatin fibers. With increasing divalent cations chromatin fibers first fold through intra-fiber interactions and eventually self-associate through inter-fiber interactions.

With increasing divalent cation concentrations into the physiological range (e.g., ≥ 3 mM Mg²⁺) (Strick *et al*, 2001), short nucleosomal arrays self-associate to form large oligomers that pellet immediately in a microfuge (Schwarz *et al*, 1996). Self-associated chromatin fibers have been studied much less extensively than the folded fibers. While self-association is mediated by inter-fiber nucleosome-nucleosome interactions distinct from those involved in folding (Hansen, 2002; Schwarz *et al*, 1996), nothing is known about the structure, subunit organization, and assembly of the chromatin oligomers due to their extreme size and the lack of available quantitative physicochemical assays. The underlying premise of my dissertation is that gaining a better understanding of the oligomers formed under physiological ionic conditions *in vitro* will shed light on how chromosomes condense and provide another *in vitro* model system for understanding how various chromatin components affect chromosome structure.

1.4 Mechanisms for Chromatin Compaction and the Implications for Nuclear Architecture

A large number of models for chromosome structure propose that extended chromatin is first folded into 30nm fiber structures, which is then folded and condensed further into chromosomes (Hansen, 2002; Maeshima *et al*, 2014b; Robinson & Rhodes, 2006; Alberts *et al*, 2007). If these models were accurate then the 30nm fiber should be a prevalent structure within nuclei. However, recent SAXS experiments, which can detect repeating structures within cells and nuclei, do not find that 30nm structures are prominent features within nuclei (Nishino *et al*, 2012). These results contradict a SAXS study which has long been cited as indication that nuclei contain 30nm structures (Langmore & Paulson, 1983), and suggests that the 30nm signal arises due to ribosomal components which exist within the nuclei. In addition electron microscopy techniques have not found evidence for 30nm fibers within nuclei. Specifically cryo-EM studies of interphase (Bouchet-Marquis *et al*, 2006) and mitotic chromosomes (Eltsov *et al*, 2008; Maeshima *et al*, 2010), and electron spectroscopic imaging studies of mouse cells

(Fussner *et al*, 2012), visualized packed 10 nm fibers but no folded 30 nm fibers, even in the highly condensed heterochromatin regions. These studies indicate that a different mechanism may be responsible for large scale chromatin compaction and the structure of chromosomes.

At the largest scale interphase chromosomes are arranged into chromosome territories, where each chromosome forms a globular discrete domain that is more likely to interact with itself than with other chromosomes (Cremer & Cremer, 2010). Chromosome conformation capture experiments coupled with high throughput sequencing (Hi-C) have begun to map interactions between entire chromosomes (Lieberman-Aiden *et al*, 2009). These experiments find evidence for discrete regions within a single chromosome which contain high probabilities of interaction. The highly interacting regions range in size from 0.1-10 Mb in size and were termed topologically associated domains (TADs) (Dekker *et al*, 2013; Smallwood & Ren, 2013). Fluorescence microscopy visualizations of nuclei have also found evidence for interacting globular domains of chromatin on the order of 1 Mb, with an average size of around 500 nm (Albiez *et al*, 2006). The chromatin globules also have been termed “topological domains” (Dixon *et al*, 2012), or “physical domains” (Sexton *et al*, 2012).

These new experimental results require that we rethink the textbook model of chromosome organization in which the 10 nm fiber goes through hierarchical folding into 30 nm structures and more compact fibers. Many other models of chromatin organization are independent of the requirement of 30nm fiber formation. Some require only long range nucleosome-nucleosome interactions between distal portions of the chromosome to form interdigitated clusters of chromatin, which are commonly referred to as polymer melts (Maeshima *et al*, 2014b, 2010). More detailed models have sought to define the path of chromatin within these globules, and recent experiments finding evidence in favor of a fractal globule rather than equilibrium globules (Lieberman-Aiden *et al*, 2009). More refined versions of this model from the same lab suggest that loops of chromatin, extruded by CTCF and cohesion proteins,

organize chromatin within smaller domains (Sanborn *et al*, 2015). Others require additional chromatin architectural proteins in order to condense chromatin into chromosomes (Barbieri *et al*, 2012). These newer models for chromosome structural organization suggest that we reconsider how the dynamics of our *in vitro* chromatin model systems relate to chromosome structure *in vivo*. As such, I plan to study the process of chromatin self-association in depth in order to determine how it may relate to chromosome structure and organization.

1.5 Determinants of Chromatin Self-Association

As mentioned previously the DCA assay has been used to characterize chromatin self-association in a number of studies. Many different variables in the chromatin fiber have been found to effect the self-association of chromatin. Solution conditions play a large role in whether self-association of chromatin will occur. This is not surprising given that a chromatin fiber is a large net-negative polyelectrolyte. Cations induce nucleosome-nucleosome interactions, as mentioned previously, with polyvalent cations having much more pronounced effects than monovalent cations. Divalent cations induce self-association with the following efficacy $Mn^{2+} = Zn^{2+} > Ba^{2+} > Mg^{2+} > Co^{2+} >> Cd^{2+}$ (Lu *et al*, 2006). The most prevalent divalent cations in the nucleus are Mg^{2+} and Ca^{2+} , which are present at 2-4 mM and 4-6 mM respectively (Strick *et al*, 2001). Biological polyamines such spermine and spermidine have also been found induce self-association of chromatin *in vitro* (Carruthers *et al*, 2007) and are present *in vivo* at concentrations of about 1 mM (Igarashi & Kashiwagi, 2000). The ionic conditions present in cells are in a range suggesting that significant portions of chromatin are self-associated over long distances. Furthermore, the dynamic self-association of chromatin *in vitro* in response to physiological salt concentration provides a simple mechanism by which researchers can study the intrinsic ability of chromatin fibers to form higher order structures in chromosomes.

The N-terminal disordered “tail” regions of the core histones, which also play a role in folding (Tse & Hansen, 1997), are necessary for self-association. Arrays treated with trypsin to

digest the tails, as well as arrays made with recombinant core histones lacking the tails, fail to self-associate under any solution conditions as judged by the DCA (Tse & Hansen, 1997). While all the tails have an effect of self-association the loss of the tails on the tetramer (H3/H4) is the most significant. The tails are also highly modified post-translation by acetylation, phosphorylation, methylation, ubiquitylation, and others (Bannister & Kouzarides, 2011). Given the intrinsic importance of the tails in chromatin condensation, it is not surprising that many of these modifications modify higher-order chromatin structures. An accumulating body of evidence suggests that histone modifications are an important type of epigenetic regulation of genomes. Histone acetylation is widespread histone modification *in vivo*, and the resulting charge neutralization of lysine residues is associated with more open chromatin structures and transcriptionally active portions of genomes *in vivo* (Eberharter & Becker, 2002). Arrays assembled with modified histones have demonstrated that acetylation of H4 tail lysines increases the concentration polyvalent cation required to induce self-association of arrays *in vitro*, as judged by the DCA (Shogren-Knaak *et al*, 2006). The dynamic and specific distributions of the other histone modifications, as well as their accompanying physical changes, suggest that they are likely to affect chromatin structure as well. Lysine methylation appears to have differential effects on chromatin which are highly dependent on extent (mono, di, or tri-methylated) and location of methylation (Black *et al*, 2012). Phosphorylation of serine and threonine residues alters the charge of nucleosomes and is associated with compacted chromatin *in vivo* (Rossetto *et al*, 2012). Histones can also be ubiquitinated and SUMOylated, and the addition of these peptides alters the steric profile of the nucleosome. Ubiquitination of H2A promotes self-association of *in vitro* chromatin (Jason *et al*, 2001). Many of these modifications significantly alter the physical characteristics of the nucleosome, and like acetylation are likely to alter structures formed by chromatin fibers. In addition to post-translational modifications, nucleosomes can be altered by the inclusion of histone variants.

Other than H4, each histone protein contains variants to its canonical form. The variants can cause significant changes to nucleosomes and chromatin structure. Some of these have been shown by the DCA to effect the self-association of chromatin fibers. Chromatin samples assembled with histone variant H2A.Z self-associated at significantly higher salt concentrations than those assembled with canonical H2A (Fan *et al*, 2002). Another H2A variant, macroH2A, had the opposite effect, promoting the formation of chromatin fiber oligomers in lower salt concentrations (Muthurajan *et al*, 2011). The variants of H2B are less prevalent and less well characterized, but appear to have a role in promoting compacted chromatin structures, particularly during the process of gametogenesis (Kamakaka & Biggins, 2005). Histone H3 has two very well studied variants, H3.3 and CENPA. The deposition of H3.3 *in vivo* indicates that this variant is associated with regions of active gene transcription (Ahmad & Henikoff, 2002). CENPA was originally discovered as a crucial component of centromeric regions of chromosomes, hence the different nomenclature. Despite its name CENPA, (known generically as CenH3 across species) is directly related to H3, and is also an epigenetic factor which is entirely responsible for determining where centromeres will form on chromosomes (Maze *et al*, 2014). The structural variations in nucleosomes which arise through the incorporation of histone variants, as well as those due to post-translational modifications are certain to result in regions of the chromosome fiber with intrinsically different structural characteristics.

In addition to structural variations which arise due to changes in the nucleosome a variety of chromatin architectural proteins exist. These proteins can have profound effects on chromatin structure and thus the entire biology of the cell. Linker histones share the name of the core proteins that make the nucleosome but are not structurally related to the core histones. Linker histones have tripartite domain organization, with a short disordered N-terminal domain, followed by a globular winged helix domain, and then a long disordered C-terminal domain (Allan *et al*, 1980; Gajiwala & Burley, 2000). The N-terminal domain is a short disordered region

The family of linker histones, of which 11 mammalian subtypes have been identified, are highly abundant in nuclei (Happel & Doenecke, 2009). While it is possible to knockout a single version of linker histone, the other subtypes are upregulated. Complete knockouts are lethal, but a triple knockout model has demonstrated that chromosomes and nuclei are expanded with reduced linker histone (Fan *et al*, 2003; Sirotkin *et al*, 1995). Footprinting experiments have demonstrated that linker histone binds at the nucleosome dyad and protects ~20bp of DNA (Hussain *et al*, 2010). Chromatin fibers reconstituted with linker histone form stabilized folded 30 nm fibers, and have an increased propensity for self-association between fibers (H1 chromatin self-associates at lower MgCl₂ concentrations than the parent nucleosomal arrays) (Carruthers *et al*, 1998). These results have demonstrated the important role linker histones play in the compaction of genomes. Newer experiments are beginning to expand our understanding of linker histones functions. Fluorescence recovery experiments have demonstrated that the majority of linker histone is diffusing rapidly through nuclei, and is not a static component of the chromatin fiber (Misteli *et al*, 2000). Affinity binding experiments using isolated nuclear and nucleolar extracts have suggested that linker histones are involved in many protein-protein interaction in the nucleus, and may be involved in a number of nuclear processes including RNA splicing as well as ribosome biogenesis (Kalashnikova *et al*, 2013c; Szerlong *et al*, 2015). Many experiments have demonstrated that linker histones have profound effects on chromatin structure, but its knowledge about its function is still expanding. Many other chromatin architectural proteins bind nucleosomes in lower abundances, and have unique effects on specific regions of the genome. For example, MeCP2, avian MENT, and Pcg proteins have all been shown to induce the formation of self-associated chromatin structures at lower salt concentration than nucleosomal arrays alone(McBryant *et al*, 2006). Recent experiments using next generation sequencing and chromatin conformation capture techniques (Hi-C), in conjunction with large data sets such as those in the ENCODE database, are identifying new chromatin architectural proteins. The protein CTCF binds to a specific DNA

sequence and appears to function as a boundary element between topologically associated domains (Ong & Corces, 2014). Through effecting domain organization and long range chromatin interactions CTCF can regulate enhancer-promoter interactions. Many currently recognized chromatin architectural proteins lack clear mechanisms by which they affect chromosome structure. Some of these proteins are likely to affect nucleosome-nucleosome interactions, so strong effects on chromatin fiber folding, and self-association are expected. In order to more completely understand genome organization we require better *in vitro* model systems, and assays for investigating the mechanisms by which proteins associated with chromosomes organize and regulate genomic information within nuclei.

1.6 Assays for Exploring Self-Association

Sedimentation velocity experiments using analytical ultracentrifugation (AUC) have been used extensively for studying the intramolecular folding of chromatin reconstituted *in vitro*. Measuring the rate of sedimentation allows one to monitor the mass and shape of the chromatin complexes. This has been used most frequently to report on the folding (intra-fiber interactions) of nucleosomal arrays (Carruthers *et al*, 1998; Fan *et al*, 2002; Lu & Simon, 2008). In contrast, attempts to perform sedimentation velocity experiments of chromatin oligomers have been stymied by the speed at which the concentration can be determined along the radius of the sample cell. The absorbance optics can capture only a single boundary for sedimenting chromatin oligomers, even at the minimum rotor speed of 3000 rpm (Schwarz *et al*, 1996). Accordingly, here I have utilized the interference detection system of the AUC in order to quantitate the sedimentation of oligomeric self-associated chromatin. The interference system captures the entire radial concentration profile at once allowing much quicker measurements of sedimentation to be made. Faster measurements in turn allow us to determine the sedimentation rate of much larger complexes. This is discussed in depth in the next chapter.

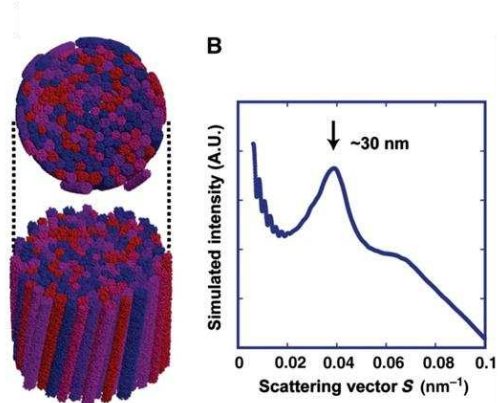
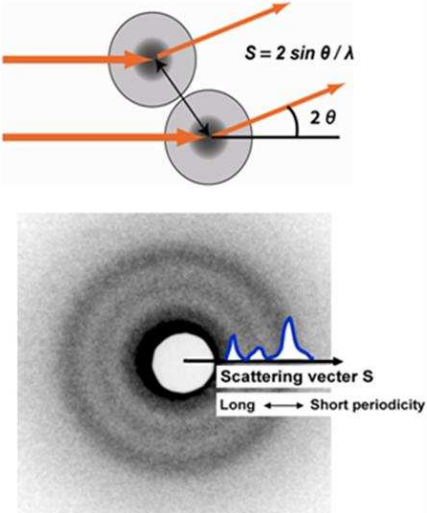
Microscopy experiments allow us to make qualitative determinations of size and morphology. In order to obtain images of self-associated chromatin complexes we have employed both transmission electron microscopy as well as fluorescence microscopy, each of which has unique benefits. Fluorescence microscopy experiments allow us to investigate the chromatin complexes in solution with minimal staining using the fluorescent DNA binding stain DAPI. However, light microscopy techniques are limited in resolution, and in order to discern the finer details of the self-associated chromatin complexes we have also utilized transmission electron microscopy. The transmission electron microscopy experiments have utilized negative staining with uranyl acetate and phosphotungstic acid, which has been used widely in the study of chromatin folding (Woodcock & Horowitz, 1991). While these experiments allow for a finer level of detail to be visualized, the heavy metal staining and dehydration of samples onto electron microscopy grids results in conditions much further from a biological context than those in the fluorescence microscopy conditions. Together these two visualization techniques allow us to cover a large range of resolution and control for any adverse artefactual results which may arise due to specific sample preparation conditions.

In order to investigate the subunit composition of the chromatin complexes, SAXS experiments were utilized. This technique, which was conducted by our collaborator Kazuhiro Maeshima and his lab, using chromatin reconstituted by me, can determine the size of repeating structures present in the self-associated samples. This allows insight into the conformation of the individual fibers within the oligomeric complex (i.e. are they 10 nm or 30 nm fibers?). The technique has been used in the past to investigate the internal structures of whole nuclei as well as isolated chromosomes (Nishino *et al*, 2012; Langmore & Schutt, 1980). Recently our collaborators have employed the technique to determine that mitotic chromosomes lack repeating 30nm structures after ribosomal components are removed from the isolated chromosomes. This technique will allow us to determine if our *in vitro* reconstituted structures and composed of oligomerized 30nm fibers or if the individual arrays are in a more extended

conformation (Fig 1.3). As such, these experiments will allow us to add important information in an ongoing discussion in the literature about the importance of 30nm fibers in chromatin structures, and how *in vitro* chromatin structure relates to *in vivo* chromosome composition.

We have also used micrococcal nuclease in order to assay the accessibility of oligomeric chromatin as well as the stability of complexes in the absence of linker DNA. Micrococcal nuclease has endo-exonuclease activity, but in chromatin the DNA bound to the histone proteins is protected from digestion. The rate at which the linker DNA of chromatin samples is digested is frequently used as an indirect reporter of the level of chromatin compaction due to the accessibility of the nuclease to the linker DNA (Fierz *et al*, 2011a; Ziv *et al*, 2006). These assays also result in conditions under which all of the linker DNA is digested, and it is under these conditions which we can assess the role of linker DNA in the stability of self-associated chromatin.

A $2d \sin \theta = n\lambda$,
Small angle X-ray scattering (SAXS)



Simulated scattering of packed 30nm fibers.

Nishino Y; et al – 2012 -
EMBO

Figure 1.3 Principle of biological SAXS for periodic structures and simulated scattering of self-associated 30nm fibers. A.) Braggs law and example of angular dependency of scatter x-rays for a demonstrated SAXS sample. Scattering vector is inversely proportional to the size regularly repeated structures in the sample. B.) Kratky plot for simulated oligomer of 30nm chromatin fibers. Adapted from Nishino Y, et al, 2012, EMBO, 10.1038/emboj.2012.35

Chapter 2

Development of a Sedimentation Velocity Assay for Chromatin Oligomers¹

2.1 Introduction

Analytical ultracentrifugation has been used extensively for the characterization of macromolecular assemblies like chromatin fibers(Lu & Hansen, 2004; Correll *et al*, 2012; Fan *et al*, 2002b; Muthurajan *et al*, 2011b). Sedimentation velocity experiments yield information regarding the mass and shape of molecules in solution allowing researchers to investigate molecular interactions and conformational changes. These experiments rely on determining the concentration in solution as a function of radial distance under centrifugal force. This is accomplished most frequently using the absorbance optics, which takes about one minute to scan a cell. The time to collect a scan is a limiting factor in monitoring massive macromolecular complexes that sediment very rapidly. The use of the interference optics, which collects data much faster, allows for monitoring molecules with sedimentation coefficients orders of magnitude larger than those that can be seen with the absorbance optics. The following protocol details the use of the interference system to characterize chromosome-sized oligomeric complexes of chromatin fibers using sedimentation velocity, but the principles will allow for expanded sedimentation velocity analyses of a variety of much larger biological assemblies.

2.2 Theory

The signal from the interference system is a pattern of light and dark horizontal bands called a fringe pattern (Figure 1). The vertical displacement (fringe shift, ΔY) of these fringes is due to differences in the optical path between the sample and reference channel. The

¹Rogge, R. A., & Hansen, J. C. (2015). *Sedimentation Velocity Analysis of Large Oligomeric Chromatin Complexes Using Interference Detection. Methods in enzymology* (1st ed.). Elsevier Inc.
doi:10.1016/bs.mie.2015.05.007

interference system measures concentration by tracking changes in refractive index in solution. The refractive index of a solution is altered by its component solutes. The fringe shift magnitude is given by $\Delta Y = Ic(dn/dc)/\lambda$, where I is the path length, c is the concentration, λ is the wavelength, and dn/dc is a property of the unique individual solutes. For DNA dn/dc is ~0.17 mL/g(Chincholi *et al*, 1974) and for proteins it averages ~0.189 mL/g; however, differences in protein composition can change this considerably(Zhao *et al*, 2011). Polysaccharides and phospholipids are difficult to use with the absorbance optics but have an average dn/dc of ~0.15 and ~0.16 respectively, which makes interference measurements ideal for these molecules(Tumolo *et al*, 2004). Importantly, the fringe pattern is projected onto a camera which makes data capture along the radius of the AUC cell simultaneous. A Fourier transform of the fringe pattern results in a concentration profile that is obtained in a matter of seconds compared to the minute necessary for the absorbance optics.



Figure 2.1) A typical fringe pattern for a sedimentation velocity experiment of self-associated chromatin fibers. The sample here are 601(207bp)-12 nucleosome arrays with endogenous chicken octamer self-associated in 8mM MgCl₂. The vertical arrow marks the meniscus of the sample sector and the double headed horizontal arrow marks the boundary region. Note the increased light scattering in the region to the right of the boundary area due to the presence of large particles.

The fast data acquisition of the interference system makes it ideal for monitoring the sedimentation of large molecules that sediment quickly. For example, self-associated chromatin oligomers have been examined using absorbance based sedimentation velocity experiments previously, but the experiments have failed to capture more than a single complete boundary. The interference system has some unique properties to consider when compared to the absorbance system. The first is that interference generally requires a significantly more concentrated sample than absorbance. However, this is dependent on the extinction coefficient of the molecule being studied. For instance, interference measurement of a nucleic acid sample will require around a 10 fold higher concentration than monitoring the samples absorbance at 260nm. A second consideration is the increased presence of systematic noise. Because all changes in the optical path will affect the fringe pattern, the concentration profiles contain a large amount of time invariant noise. Vibrations as well as instability of the Fourier transform will lead to radially invariant noise. Both radially invariant and time invariant noise can be minimized by good maintenance of the system, and can be further accounted for during data analysis.

2.3 Equipment

Beckman XL-I Analytical Ultracentrifuge (AUC)

An50-Ti or An60Ti rotor

AUC counterbalance and weights

Assembled Epon 2-channel centerpiece AUC cell with sapphire windows

2.4 Setting up the Interferometer Laser: Laser Delay and Duration

In ProteomeLab choose Interference > Laser Setup in the dropdown menu in order to access the laser delay and duration settings for each cell. These options allow you to fine tune the laser to generate an optimal fringe pattern. The laser delay controls where the laser turns on

in the course of a 360° rotation of the rotor. The laser duration controls how long the laser is on after the laser delay triggers. The laser delay defaults to values of 180°, 90°, and 0° for cell positions 1,2, and 3 respectively. The laser duration default is set to 0.6°, which should be close to appropriate. These values should be adjusted slightly to produce an optimal fringe pattern with good contrast. Under these conditions the laser turns on as the cell crosses the condenser lens, and turns off just as it has passed. For identical cells and rotors these values should not need to be changed.

The XL-I AUC must be spinning at a minimum of 3,000 rpm in order to generate interference data and to set the laser delay and duration. For very high molecular weight samples, the slowest possible speed is chosen to maximize the amount of data that can be collected during the experiment. Setting up the laser and the radial calibration should be performed on a double sector cell with both channels containing reference buffer. A cell with sapphire windows should be used to limit distortion of the windows. Set the laser conditions using this cell. Auto-detection can be used to allow the software to select a laser delay, and is a good option for those unfamiliar with the process. The software auto-select option will adjust the delay to optimize the fringe pattern at the radial position selected by clicking in the fringe display (red text in top left of display). The entire fringe pattern can then be optimized by making small changes manually, with high contrast, unbroken bands of light and dark at all radial positions being the goal. To set the laser delay manually, find the upper and lower limits at which the fringe pattern begins to deteriorate, and then select the midpoint. The laser duration should be adjusted to maximize fringe intensity without saturating the image. Values between 0.5° and 1° are typical for laser duration. The process of setting up the laser should also be done for the counter-balance reference holes. Clear fringe patterns should be visible through both reference holes.

2.5 Radial Calibration of Interference Detector

The counter balance contains two reference holes that are used to determine radial position. When examining the fringe display of the counter balance, this results in two regions of fringe pattern separated by a lack of signal. The inside edges of these holes and thus the edges of their fringe patterns mark the radial positions of 5.85 cm and 7.15 cm. Opening the Interference > Radial Calibration menu allows you to define these positions in the fringe display. To set the radial points first click within the fringe display at the inside edge of the fringe pattern (vertical position does not matter). Then click the inside/outside option and set radius to set the location to 5.85 (inside) or 7.15 cm (outside).

2.6 Final Considerations for Interference Sedimentation Velocity Run

There are a few parameters to adjust before starting an experimental run. The first is to set the number of pixels per fringe. This setting is in the Details menu of each cell. Selecting automatic will have the software calculate this value. This value can be estimated manually by dividing 96 (the number of pixels in a column) by the number of visible fringes. If the automatic value is significantly different from the manual estimation, the optical system is likely misaligned.

The next two options will affect the data files generated by ProteomeLab and are used to compensate for systematic noise. Note that the systematic noise can be removed using specific types of data analysis (see below), making these options unnecessary. However, if you wish to analyze interference data using a method that does not compensate for systematic noise it would be wise to consider the following options. Misalignment of the interference detector can lead to fringe patterns which are not horizontal. This can be corrected by manipulating the detector, or by rotating the fringe data in the Interference > Fringe Rotation menu by a set number of degrees. The other option for removing systematic noise is to subtract a blank scan from every scan generated. Blank scans should be taken from empty rotor positions so that subtracting

them will negate noise from defects inherent to the optical system. If subtracting a blank, scan the blank data should be collected using identical laser settings to those used for sample data collection. These options can reduce systematic noise in the data, but the subtraction of a blank scan will increase the amount of stochastic noise in the data.

2.7 Experimental

2.7.1 Reconstitution of chromatin fibers and assembly of chromatin oligomers

Oligomeric chromatin fibers provide a good example of very large biological complexes that can be studied using sedimentation velocity only in conjunction with interference optics. Model chromatin fibers are obtained by reconstituting purified histone octamers onto tandem repeats of nucleosome positioning DNA using a salt dialysis method as described (Rogge *et al*, 2013a). This protocol yields equally spaced arrays of nucleosomes with a defined length and composition (see below).

The structure of the chromatin fibers in solution and within the cell is highly dependent on ionic strength, particularly the concentration of divalent cations(Korolev *et al*, 2010; Strick *et al*, 2001). In low salt the model chromatin fibers are monomeric and adopt an extended, beads-on-a-string structure. As divalent salts (e.g., MgCl₂) are first titrated into solution, the chromatin fibers fold into helical 30 nm structures (Hansen *et al*, 1989). At physiological MgCl₂ concentrations (i.e., >3mM) the chromatin fibers self-associate to form large oligomeric complexes(Schwarz *et al*, 1996) (Figure 1.2). Sedimentation velocity analysis of the chromatin oligomers is not ideal using absorbance optics because the oligomers pellet before a set of scans with complete boundaries is collected, even at 3,000 rpm.

In our experiments, chromatin fibers consisting of 12 spaced nucleosomes were reconstituted from tandemly repeated “601” nucleosome positioning DNA and purified chicken

histone octamers and stored in a buffer of 10mM Tris pH 7.8 , 0.25mM EDTA , and 2.5 mM NaCl. The chromatin fibers were then diluted to a concentration of 0.215 mg/mL, and MgCl₂ added to a final concentration of 8 mM to assemble the oligomeric complexes. The rotor, optics, and AUC chamber were pre-cooled to one degree below the final desired temperature. The speed was 3,000 rpm (see below). Data were collected using the interference optics as described in sections 4-6 above. The oligomeric samples formed broad but discrete boundaries (Figure 4A), which were analyzed using the time derivative method as described in section 8b. Previous sedimentation velocity experiments of these oligomers have only captured either single or incomplete boundaries of chromatin oligomers(Schwarz *et al*, 1996; Blacketer *et al*, 2010).

2.7.2 Choosing the Rotor Speed

The rotor speed, number of cells per run and number of scans per run should be chosen based on how rapidly the samples sediment. The interference optical system captures data from the fringe display about every 8 seconds. In our analysis of the chromatin oligomers, the rotor speed was set at 3,000 rpm and only one cell was sedimented at a time. These conditions were necessary because the oligomers sediment in the range of 10,000-350,000 S. For samples that sediment in the range of hundreds to thousands of S, it may be preferable to use faster rotor speeds or analyze more than one cell per run. Scanning multiple cells increases the amount of time it takes to scan each individual cell, which decreases the maximum sedimentation coefficient that can be monitored.

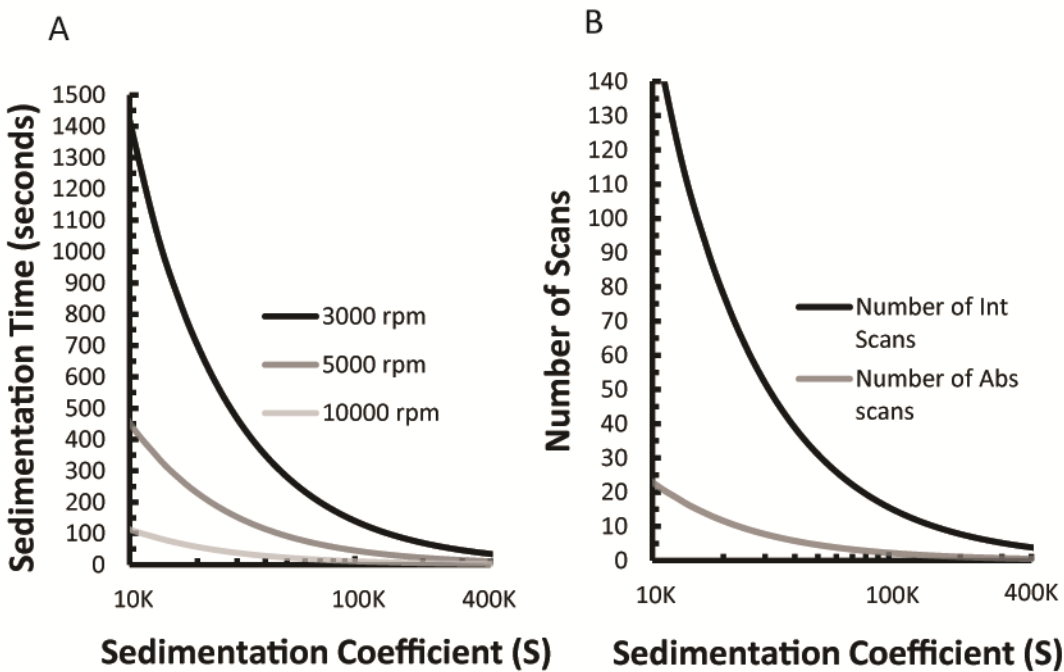


Figure 2.2) Calculations of amount of time spinning and scanning until an object has sedimented in the centrifuge. **A.** Time until sedimentation to bottom of cell. This calculation assumes the use of a two sector cell and a fluid column 1 cm. Rotor acceleration time is not considered so actual time will be shorter. **B.** Maximum number of possible scans collected for samples spun at the minimum rotor speed of 3000 rpm. Scan times are approximated at 9 seconds for the interference system and 60 seconds for the absorbance system.

The amount of time necessary to sediment the entire sample can be estimated if the sedimentation coefficient is known, according to $\times 10^{-13} s = \frac{.01 m}{\frac{t}{730 \times 9.8 \frac{m}{s^2}}}$, where S is the sedimentation coefficient in Svedbergs and t is the number of seconds for the object to sediment. The value of .01 is the length of the fluid column in meters, and 730 is the g force generated by the rotor at its minimum operational speed. Enter the desired number of scans in the Method menu. If the sample is being characterized for the first time, enter the maximum number of scans and stop the run after the boundary has reached the bottom of the cell. Under the Options menu select stop XL-I after last scan, so that the centrifuge will stop after the last scan is taken. Once the sample has been characterized in this manner, the rotor speed, number of cells sedimented and number of scans collected can be modified as appropriate.

If the sample is very heterogeneous, it is possible that smaller solution components will remain at the meniscus after the larger components have sedimented. For example, at intermediary Mg²⁺ concentrations chromatin samples will contain populations of both small monomeric and large oligomeric chromatin fibers. To characterize the smaller components a second run using higher speeds can be started after the first is completed. Smaller solutes are likely to take longer to sediment, so to avoid very large data sets use a scan delay time that can be found in the Method menu. The scan delay time adds time between captures of the fringe pattern, so that over the course of a longer run a smaller data set is generated.

2.8 Data Analysis

2.8.1 Systematic noise considerations

As mentioned above, interference data has relatively high amounts of systematic noise. The systematic noise can be further categorized as radially invariant and time invariant noise. Radially invariant noise arises due to vibrations in the detector as well and the nature of the fast

Fourier transform performed in the ProteomeLab software. Radially invariant noise appears visually as an offset in the baseline of the scan. The radially invariant component of the noise can be removed by aligning the scans in a consistent region, such as the air to air region, during data editing. Time invariant noise arises due to differences in the optical path between the reference and the sample sector. The differences due to the interference optical system and not the AUC cell can be removed by subtracting a blank scan, but this will lead to an increase in the stochastic noise. Alternatively the use of the time derivative method of data analysis, or the use of modelling software will allow for the removal of time invariant noise.

2.8.2 Time derivative method.

The time derivative method for determining distributions works by subtracting the subsequent scan in pairs of scans to determine how much the concentration has changed over time. A comprehensive explanation of the method can be found here(Stafford, 1992). Subtracting the subsequent scan from a pair removes time invariant noise, much in the same way subtracting a blank scan would, however the subsequent scan contains time invariant noise components which arise due to both the cell components and the interference optical system. Because this time invariant noise removal is more comprehensive than the subtraction of blank scan, it is an ideal method for the analysis of interference sedimentation velocity data. The primary limitation of this method for smaller solutes is that the sedimentation coefficient distribution will not be corrected for the effects of diffusion on the boundary. However, since diffusion is inversely proportional to solute size, the sedimentation coefficient distributions obtained using the time derivative method of very large macromolecular assemblies will be an accurate reflection of the actual composition of the sample.

2.8.3 Other analysis methods

Other data analysis can be used with the interference optics as well. Methods of modelling the data using software such as UltraScanIII and Sedfit contain methods for

decomposing and removing systematic noise contributions to the data(Schuck & Demeler, 1999; Demeler, 2005; Brown & Schuck, 2006). These programs generate a solution with a finite number of elements with sedimentation and diffusion coefficients, the model solutions concentration profile can then be compared against the experimental data. With prior knowledge or assumptions regarding the frictional coefficient or partial specific volume these models allow for the determination of molecular weight. The noise contributions determined during modelling are useful for other analysis methods such as the second moment and van Holde-Weischet(Holde & Weischet, 1978) methods, although with noise files subtracted these are no longer model independent analyses.

2.9 Discussion

2.9.1 Chromatin oligomers

The core of a eukaryotic chromosome is a single long chromatin fiber composed of 10^4 - 10^5 nucleosomes. An important outstanding question in the chromatin field is how the conformational dynamics of short array of nucleosomes in vitro relates to the structure and assembly of a chromosome in the cell. Most previous attention has focused on the local folding of the chromatin fiber into helical 30 nm structures(Fletcher *et al*, 1994; Dorigo *et al*, 2003; Allahverdi *et al*, 2011). Sedimentation velocity experiments using absorbance optics have proven very useful for analysis of this intramolecular conformational change(Ausio, 2000; Huynh *et al*, 2005; Fierz *et al*, 2011b). However, physicochemical studies of chromatin fiber oligomerization have lagged behind due to difficulties in characterizing the extremely large size of the oligomeric complexes. To overcome this hurdle we have developed sedimentation velocity together with the interference optical system as a quantitative assay for the structural features of chromatin oligomers. Our results demonstrate that the oligomers sediment in the range of 10,000-350,000 S (Figure 4B), spanning the size of range of eukaryotic chromosomes. This result indicates the self-association of a large number of the monomeric arrays, which

sediment in the range of 30 S (Figure 4B inset). By comparison, bacteriophage T7(Dubin *et al*, 1970) and the largest amyloid measured(MacRaild *et al*, 2003) sediment at 875 S and 3,000 S, respectively. This makes the chromatin oligomers the largest biological assemblies yet to be characterized by sedimentation velocity analytical ultracentrifugation.

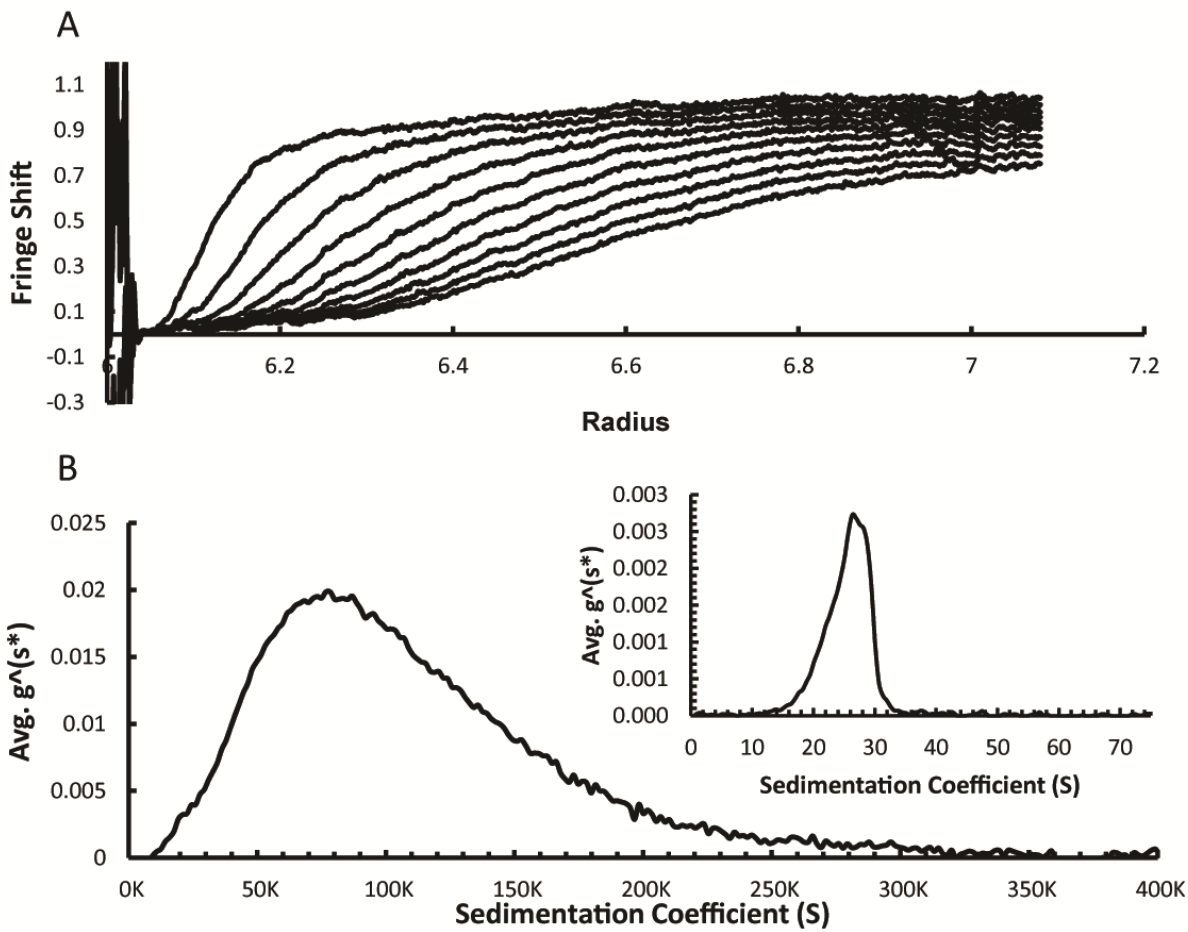


Figure 2.3) Sedimentation velocity experiments of self-associated chromatin fibers. This experiment used 601(207bp)-12mer DNA reconstituted with endogenous chicken octamers. **A.** A typical scan set used for the analysis of chromatin oligomer sedimentation. **B.** The $g^*(s^*)$ distribution of sedimentation coefficients for a sample of chromatin oligomers in 8mM Mg^{2+} . The inset shows the $g^*(s^*)$ distribution for monomeric arrays in the absence of Mg^{2+} .

It always is preferable to combine sedimentation velocity data with information obtained using complementary techniques. Toward this end, we have studied the chromatin oligomers using fluorescence microscopy, transmission electron microscopy and small angle x-ray scattering (manuscript in preparation)(Maeshima *et al*, 2015). Collectively, our studies have revealed that the oligomers are globular, assembled from smaller globular intermediates, and packaged as interdigitated 10 nm fibers. These physicochemical properties of the chromatin oligomers mimic the hierarchical organization of chromatin within an interphase chromosome(Bolzer *et al*, 2005; Lieberman-Aiden *et al*, 2009; Joti *et al*, 2012), indicating that future studies of chromatin fiber oligomerization using sedimentation velocity and the interference optics will yield much new molecular-based insight into how eukaryotic chromosomes are structured, assembled, and maintained.

2.9.2 Large complexes in general

One of the major challenges facing biochemists and biophysicists is to develop ways to deal with sample complexity. One common type of complexity is compositional heterogeneity. Sedimentation velocity analytical ultracentrifugation allows analysis of complex mixtures due to the availability of data analysis methods that determine sedimentation coefficient distributions(Demeler & van Holde, 2004b). Another type of complexity is sample size. The line between biochemistry and cell biology is increasingly becoming blurred as it becomes possible to isolate or reconstitute supramolecular biological assemblies. Successful characterization of these large macromolecular complexes requires a technical means to quantitatively characterize the structure and assembly of complex samples that sediment in excess of 5,000 S. Our studies of chromatin oligomers pave the way for general application of sedimentation velocity together with interference optics to the analysis of very large biological samples in heterogeneous mixtures.

Chapter 3

Nucleosomal arrays self-assemble into supramolecular globular structures lacking 30-nm fibers²

3.1 Introduction

In a typical human nucleus about two meters of DNA is packaged into nucleoprotein structures termed chromatin, and then into chromosomes. At its core a chromosome consists of a single ~50-250 Mb DNA molecule assembled into a chain of ~10⁵-10⁶ nucleosomes. The nucleosome is composed of ~147 bp of DNA bound to an octamer of core histone proteins (H2A, H2B, H3, H4) (Luger *et al*, 1997). Nucleosomes repetitively spaced along DNA at ~160-210 bp intervals and connected by stretches of free linker DNA are called nucleosomal arrays (Hansen, 2002). Chromatin refers to nucleosomal arrays bound to linker histone H1 and (or) other chromosome-associated proteins. The long linear chromatin molecule is condensed extensively within an interphase chromosome, such that chromosomal DNA can fit inside the nucleus, and during mitosis the long chromatin chain is further packaged into a mitotic chromosome (Hirano, 2015; Maeshima *et al*, 2014b; Ohta *et al*, 2010).

Physicochemical studies of short nucleosomal arrays, typically 12-60 nucleosomes in length, have shown that chromatin condensation *in vitro* is salt-dependent and driven by

²Maeshima K*, Rogge R*, Joti Y, Hikima T, Tamura S, Szerlong H, Krause C, Herman J, Ishikawa T, Seidel E, DeLuca J & Hansen JC (*co-first authors) (2016) Nucleosomal arrays self-assemble into supramolecular globular structures lacking 30nm fibers. *EMBO In Press*.

All of the *in vitro* chromatin samples were assembled in the Hansen Lab by Rogge R. and Seidel E. The sedimentation velocity experiments and DCA assays were also performed by the Hansen Lab. The fluorescence microscopy experiments were first carried out by the Hansen Lab in collaboration with the DeLuca lab and the results were repeated and improved upon by the Maeshima Lab. The fluorescence microscopy results shown here, were collected by the Maeshima Lab. The TEM results were collected by Rogge R. and the Hansen Lab with the assistance of Suzanne Royer.

both intra-fiber and inter-fiber nucleosome-nucleosome interactions (Hansen, 2002; Pepenella *et al*, 2014). At very low salt concentrations (e.g., <0.5 mM Mg²⁺) nucleosomal arrays have an extended beads-on-a-string conformation termed the 10-nm fiber (Hansen, 2002). As salt initially is titrated into solution (e.g., 0.5-2 mM Mg²⁺), nucleosomal arrays fold into helical structures that are ~30-40 nm in diameter, generically referred to as the '30-nm fiber'. Folding is mediated by intra-fiber interactions involving the H4 N-terminal tail domains of one nucleosome with the surface acidic patch domains of neighboring nucleosomes (Kalashnikova *et al*, 2013a; Luger *et al*, 1997). Folded 30-nm fibers are stabilized by the H1 linker histones (Hansen, 2002). The structure of the 30-nm fiber has been proposed to be a one-start solenoid, a two-start zig-zag, or a heteromorphic combination of the two (Grigoryev *et al*, 2009; Robinson & Rhodes, 2006). At higher divalent cation concentrations (e.g., ≥3 mM Mg²⁺), short nucleosomal arrays self-associate to form large oligomers that pellet immediately in a microfuge (Hansen, 2002). While self-association is mediated by inter-fiber nucleosome-nucleosome interactions distinct from those involved in folding (Hansen, 2002), nothing is known about the structure, subunit organization, and assembly of the chromatin oligomers due to their extreme size and the lack of available quantitative physicochemical assays.

The widely held paradigm for chromosome structure and assembly holds that the chromosomal fiber first forms a helical 30-nm chromatin structure (Finch & Klug, 1976; Langmore & Paulson, 1983; Woodcock *et al*, 1984; Widom & Klug, 1985; Dorigo *et al*, 2004; Gilbert *et al*, 2004; Schalch *et al*, 2005b; Robinson *et al*, 2006; Song *et al*, 2014), mimicking the folding of a nucleosomal array as salt is added into solution. A central premise of this paradigm is that the 30-nm fiber is a requisite folding intermediate in the assembly and maintenance of condensed interphase and mitotic chromosomes. However, small angle x-ray scattering (SAXS) experiments indicated that no repetitive structures

beyond the 10-nm fiber were present in the chromatin of isolated nuclei (Joti *et al*, 2012) or mitotic chromosomes (Nishino *et al*, 2012). Similarly, cryo-EM studies of interphase (Bouchet-Marquis *et al*, 2006; Gan *et al*, 2013) and mitotic chromosomes (Elsov *et al*, 2008), and electron spectroscopic imaging studies of mouse cells (Fussner *et al*, 2012), visualized packed 10-nm fibers but no folded 30-nm fibers, even in the highly condensed heterochromatin regions. More recent super-resolution imaging also showed heterogeneous groups of nucleosomes called ‘clutches’ (Ricci *et al*, 2015). Based on these results an alternative model has been proposed in which chromosomes are assembled through long-range interactions of extended 10-nm fibers to form an interdigitated polymer melt-like structure (Maeshima *et al*, 2010, 2014b). In the established paradigm, formation of condensed domains beyond the 30-nm fiber occurs through continuous twisting and coiling of the chromosomal chain of nucleosomes (Alberts *et al*, 2007). Conversely, chromosome conformation capture experiments (e.g., 3C, HiC) suggest that interphase chromosomes are organized into 0.1-10 Mb-sized globular structures such as “topologically associating domains” (TADs) (Dekker *et al*, 2013), which further self-associate into discrete chromosomal territories (Cremer & Cremer, 2010). Similarly, globular chromatin domains of ~1 Mb in size have been observed using fluorescence microscopy imaging, as foci of DNA replication via pulse labeling (Albiez *et al*, 2006). Altogether, the new data support a view of chromosome structure and assembly that fundamentally differs from the textbook model. This in turn requires a reexamination of the relationships between chromatin folding and oligomerization *in vitro* and chromosome assembly *in vivo*.

The present studies aim to improve our understanding of chromatin oligomerization and its relevance to chromosome structure and organization. We hypothesize that the fiber-fiber interactions that mediate oligomerization of short nucleosomal arrays *in vitro* are equivalent to the long-range fiber-fiber interactions that help assemble and organize higher

order chromatin domains within the nucleus. A direct prediction of this hypothesis is that the chromatin oligomers will possess many of the same structural features as an intact interphase chromosome. To test our hypothesis and its predictions we have used fluorescence light (FM) and transmission electron (TEM) microscopy, sedimentation velocity analytical ultracentrifugation (SV-AUC), and SAXS to quantitatively characterize the structure of the oligomers formed by salt-dependent self-association of 12-mer nucleosomal arrays, and micrococcal nuclease to determine the role of linker DNA in oligomer stability. We also examined the salt-dependence of chromatin organization and compaction *in situ*. The *in vitro* studies have yielded novel information regarding the size, morphology, subunit packaging, and mechanism of assembly of the nucleosome oligomers, and have revealed the effects of linker histones on the oligomerization transition. The *in vitro* data indicate that the ability to self-assemble through interdigitated packaging of 10-nm fibers into globular structures with diameters of ~50-1000 nm is an intrinsic property of an array of nucleosomes. In the case of the *in situ* experiments, low salt conditions that disassemble oligomers *in vitro* disrupt heterochromatin and euchromatin compartments and cause extensive chromatin decondensation in isolated nuclei. Collectively, our data support a new paradigm in which long-range interactions of the 10-nm chromatin fiber are important determinants of the structure and organization of interphase chromosomes. Our results further suggest that the chromatin oligomers provide a good *in vitro* model system for investigating eukaryotic chromosome structure and function.

3.2 Results

3.2.1 Nucleosomal arrays self-associate into large globular oligomers

The standard assay for nucleosomal array oligomerization is differential centrifugation (Schwarz & Hansen, 1994; Tse & Hansen, 1997b). This assay determines

the fraction of the chromatin sample that pellets after a short microfuge spin. Figure 3.1A shows a control differential centrifugation experiment performed with linear 12-mer 601 (Lowary & Widom, 1998) and 5S (Simpson *et al*, 1985) nucleosomal arrays reconstituted to an average of 11-12 nucleosomes per DNA template. In both cases, all of the nucleosomal arrays in 0-2 mM MgCl₂ remained in the supernatant, indicating no oligomerization had occurred under these conditions. About 10% of the samples pelleted in 3 mM MgCl₂, 30% in 4 mM MgCl₂, 60% in 4.5 mM, and 90% by 6 mM MgCl₂. Altogether, the pelleting curves for the 601 and 5S nucleosomal arrays were superimposable. While these data indicate that both the 601 and 5S nucleosomal arrays formed rapidly sedimenting oligomers in ≥3 mM MgCl₂, this assay yields no structure-based information.

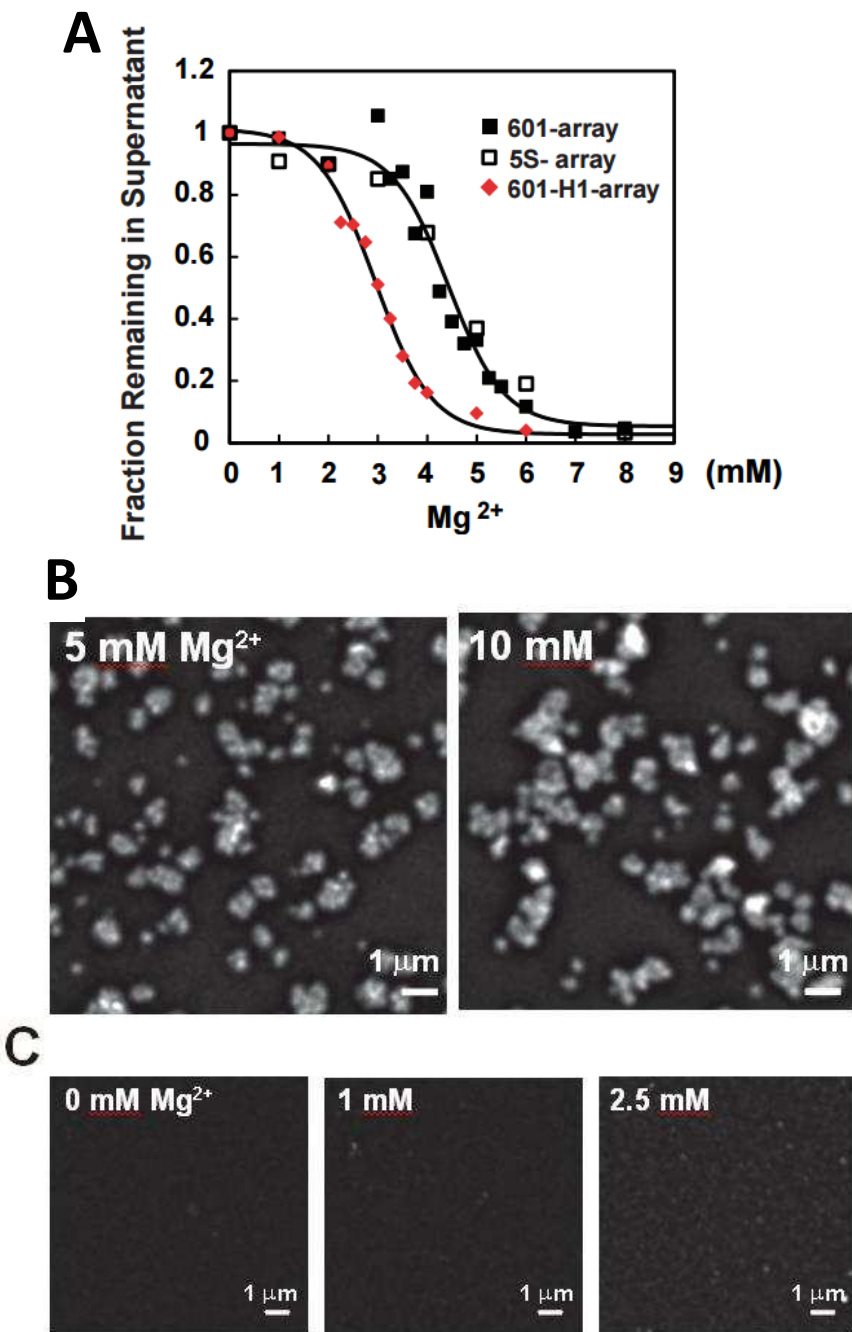


Figure 3.1) Differential centrifugation assay for the oligomer formation of 601-nucleosomal array, 5S-array, and H1-array, and fluorescence microscopy (FM) imaging of 5S-array oligomers. **A)** The differential centrifugation assay was performed as described in (Gordon et al., 2005). **B)** 5S-array oligomers were stained with DAPI and examined using FM as described in the Materials and Methods section. Shown are representative images obtained in 5 mM and 10 mM MgCl₂. **C)** Control FM images obtained in 0, 1 and 2.5 mM MgCl₂.

To determine oligomer size and morphology, samples were analyzed by FM and TEM. Representative FM images of the 601 oligomers obtained in 4.5 and 10 mM MgCl₂ are shown in Figure 3.2A. In both salt conditions the oligomers were globular and had diameters ranging from several hundred to ~1000 nm. Moreover, the ~1000 nm particles were the largest oligomers present in 4.5 and 10 mM MgCl₂, suggesting that there is an upper size limit to the self-association process. No particles were observed in control images taken at 0-2.5 mM MgCl₂ (Fig. 3.2B), consistent with the lack of oligomerization seen by the differential centrifugation assay (Fig. 3.1A). Of note, the size and morphology of the 5S oligomers assembled in 5 and 10 mM MgCl₂ (Fig. 3.1B) were quite similar to those of the 601 oligomers in Figure 3.2A. Thus, formation of large globular oligomers was not critically dependent on the nearly perfect nucleosome positioning of the 601 nucleosomal arrays. The 601 oligomers next were characterized by TEM as described by Woodcock (Woodcock & Horowitz, 1991). This protocol involves glutaraldehyde fixation to preserve macromolecular interactions and gross structure, adsorption to a carbon grid, negative staining, and dehydration. Figure 3.2C shows representative images of the oligomers visualized in 4.5 and 10 mM MgCl₂. In both salt conditions the predominant oligomers observed were globular and ~400 nm in diameter (Fig. 3.2C, left panels), in agreement with the FM results. Darker regions in the TEM images result from pooling of the negative stain, indicating that the surfaces of the oligomers were uneven and textured (Fig. 3.2C, left panels). The edges of the oligomers were irregular, and in some cases smaller globules could be seen at the periphery of the larger particles (Fig. 3.2C, left panels). At higher magnification, individual nucleosomes could be seen in the interior of the oligomers as bright 10 nm diameter particles that were closely packed and in physical contact (Fig. 3.2C, right panels). No regular repetitive folded structures such as the 30-nm fiber could be identified at the higher magnifications.

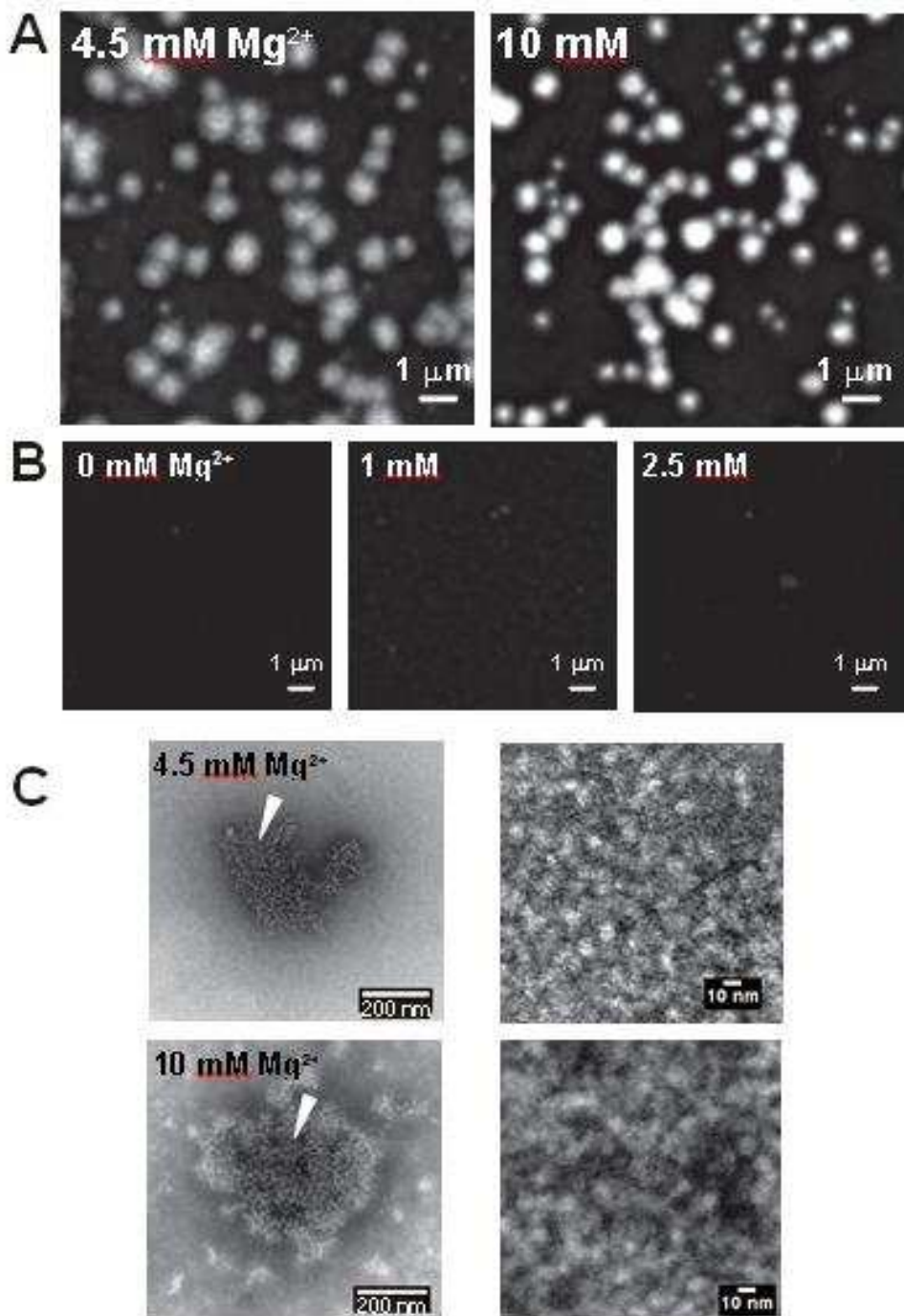


Figure 3.2) Nucleosomal array oligomers are globular **A)** Nucleosomal array oligomers were stained with DAPI and examined using FM (fluorescence microscopy) as described in the Materials and Methods section. Shown are representative images obtained in 4.5 mM and 10 mM MgCl₂. **B.)** Control FM images obtained in 0, 1 and 2.5 mM MgCl₂. **C.)** Nucleosomal array oligomers were negatively stained and visualized by TEM as described under Materials and Methods. Shown in the left panels are representative images obtained in 4.5 mM, and 10 mM MgCl₂. Shown in the right panels are images of the interior of the oligomers (white arrows, left panels) after cropping and re-scaling.

The FM studies (Fig. 3.1) suggest that a population of oligomers exists in solution at any given salt concentration, and that the oligomers reach a maximum size of about 1000 nm in ≥ 4.5 mM MgCl₂. An ideal complimentary technique to address these questions under native solution conditions and quantitatively characterize macromolecular self-association is SV-AUC (Schuck, 2013). However, in the past it has not been possible to study oligomerization using SV-AUC and the standard absorption optical system because the oligomers pellet before data can be collected. To overcome this hurdle we employed the interference optical system, which measures concentration based on refractive properties of the sample, and collects a complete concentration versus radial distance dataset in ~2-3 sec (compared to about ~90 sec for the absorbance optics) (Rogge & Hansen, 2015). The scans obtained from a typical interference SV-AUC experiment in 10 mM MgCl₂ are shown in Appendix Fig. 3.3. Under these conditions the samples formed broad but discrete boundaries during sedimentation, qualitatively indicating that there was a heterogeneous population of oligomers with upper and lower size limits.

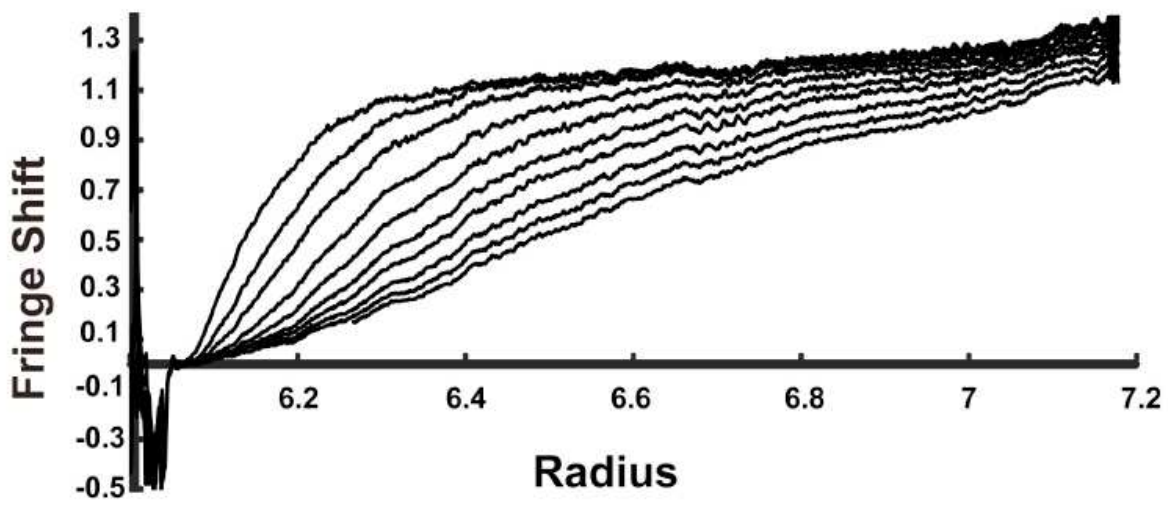


Figure 3.3) Interference scans collected in 10mM MgCl₂. Scan baselines were normalized at and just after the position of the meniscus. No blank scans have been subtracted.

To quantitatively analyze the boundaries we first calculated the weight averaged second moment sedimentation coefficients (ssm) of the 601 oligomers as a function of MgCl₂ (Fig. 3.4A). In 4.0 mM MgCl₂ (~30% oligomerized) the ssm was ~30,000S (S, a unit of time equal to 10^{-13} sec). The ssm increased to ~100,000S in 4.5 mM MgCl₂ (~60% oligomeric) before plateauing at ~200,000S in 5-10 mM MgCl₂ (75-100% oligomeric). By comparison, bacteriophage T7 (875S) (Dubin *et al*, 1970) and amyloid fibrils (3000S) (MacRaild *et al*, 2003) are the largest biological assemblages previously characterized by SV-AUC. Thus, our studies have substantially increased the size threshold for SV-AUC experiments. The plateau in the ssm at ≥ 5 mM MgCl₂ was reproducible (Fig. 3.4A, inset). In 4 mM MgCl₂ the ~70% of the sample that did not pellet during centrifugation sedimented as monomeric folded 35-45S nucleosomal arrays (Fig. 3.6). The existence of only nucleosomal array monomers and large oligomers at intermediate extents of self-association demonstrates that oligomerization is highly cooperative. The boundaries of the experiment shown in Figure 2A next were analyzed by time derivative method to obtain the distribution of sedimentation coefficients $g(s^*)$ (Stafford, 1992). In this analysis, the subsequent scan in a pair of scans is subtracted from the previous scan to determine the change in sample concentration over time. Because the oligomers were extremely large and the sedimentation times very short, the sedimentation coefficient distributions were not expected to be affected by diffusion. In 4.0 mM MgCl₂ the sedimentation coefficient distribution of the 601 oligomers ranged from ~5000-60,000S, with a peak in the plot at ~25,000S (Fig. 3.4B). In 4.5 mM MgCl₂ the distribution of sedimentation coefficients was shifted to ~25,000-130,000S, and the peak in the $g(s^*)$ plot increased to ~70,000S. In 5 mM MgCl₂ the 601 oligomers sedimented from ~40,000-250,000S, with a peak in the $g(s^*)$ plot at ~110,000S. In 8 and 10 mM MgCl₂ the $g(s^*)$ plots were very similar and yielded sedimentation coefficient distributions from

~40,000-350,000S and a peak at ~130,000-140,000S. The overlapping g(s*) plots in 8 and 10 mM MgCl₂ (Fig. 3.4B) are consistent with the plateau observed in the ssm vs. MgCl₂ plot (Fig. 3.4A) and indicate that the 601 oligomers reach a maximum average size of ~140,000S and a maximum absolute size of ~350,000S under ionic conditions that promote self-association of 100% of the sample. When the 601 nucleosomal arrays were exposed to 8 mM MgCl₂ and the sample returned to TE buffer, the oligomers dissociated into a homogeneous population of unfolded ~27-29S monomers (Fig. 3.5), demonstrating that all steps in Mg²⁺-induced assembly of the oligomers are reversible (also see (Schwarz *et al*, 1996)).

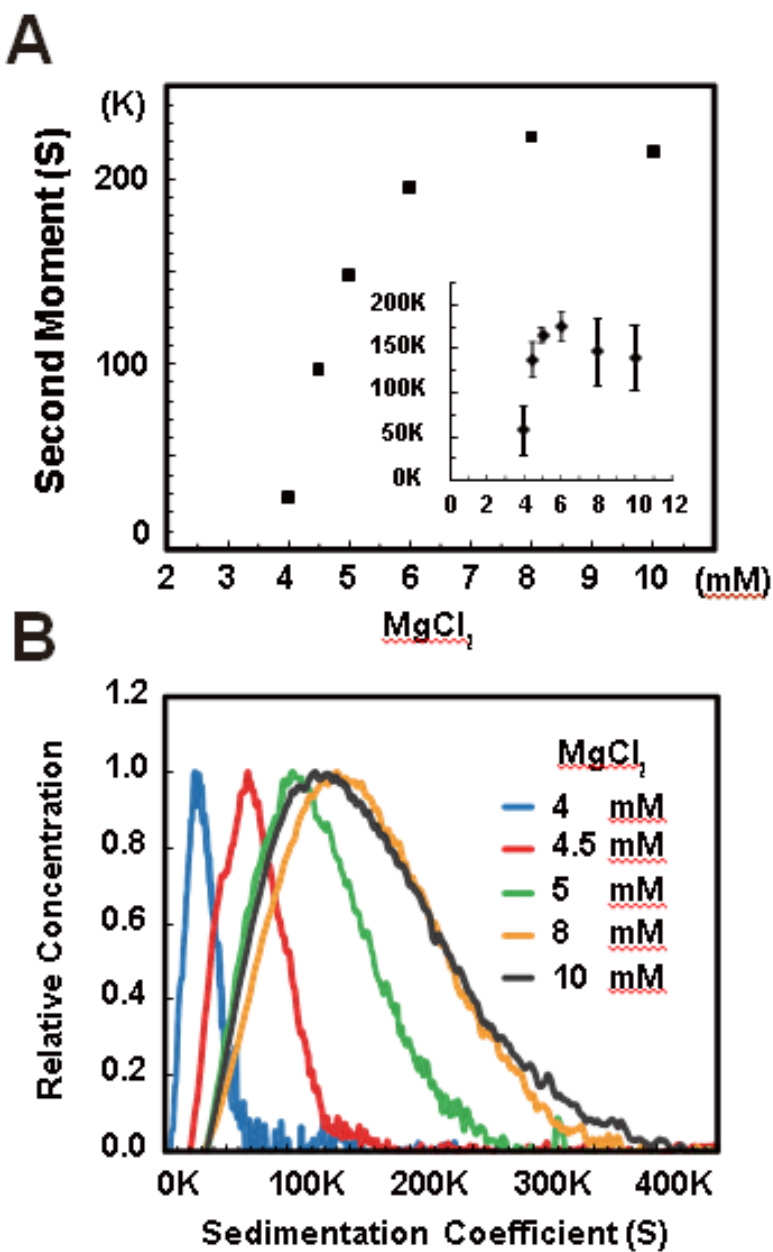


Figure 3.4) Sedimentation velocity analysis of the salt-dependent assembly of nucleosomal array oligomers. **A.)** Representative experiment showing the second moment sedimentation coefficients of the oligomeric nucleosomal arrays as a function of MgCl_2 . The second moment sedimentation coefficient is equivalent to the mass average sedimentation coefficient for the entire sample (see Materials and Methods). The inset shows the mean second moment sedimentation coefficient \pm the standard error for three replicated experiments. **B.)** Analysis of the same raw data as in panel (A) by the time derivative method to yield the sedimentation coefficient distribution, $g(s^*)$.

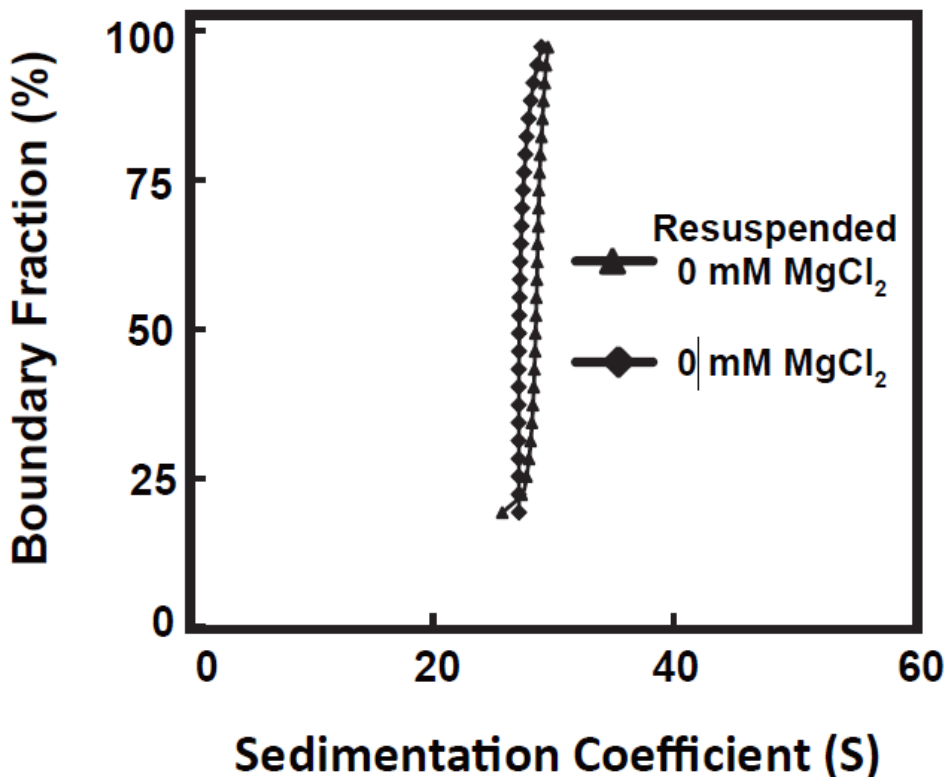


Figure 3.5) Nucleosomal array oligomerization is reversible upon the removal of salt. Sedimentation velocity analysis of reconstituted nucleosomal arrays in 10mM Tris pH 7.8, 0.25mM EDTA, 2.5mM NaCl (0mM MgCl₂ buffer). Shown is the integral distribution of sedimentation coefficients (diamonds). A portion of the same sample was then incubated in 8mM MgCl₂ to induce oligomerization. The oligomers were pelleted, the supernatant removed from the cell, and the pelleted oligomers resuspended in 0mM MgCl₂ buffer. The cell was shaken and left at room temperature for one hour. Triangles show the integral distribution of sedimentation coefficients of the resuspended oligomers.

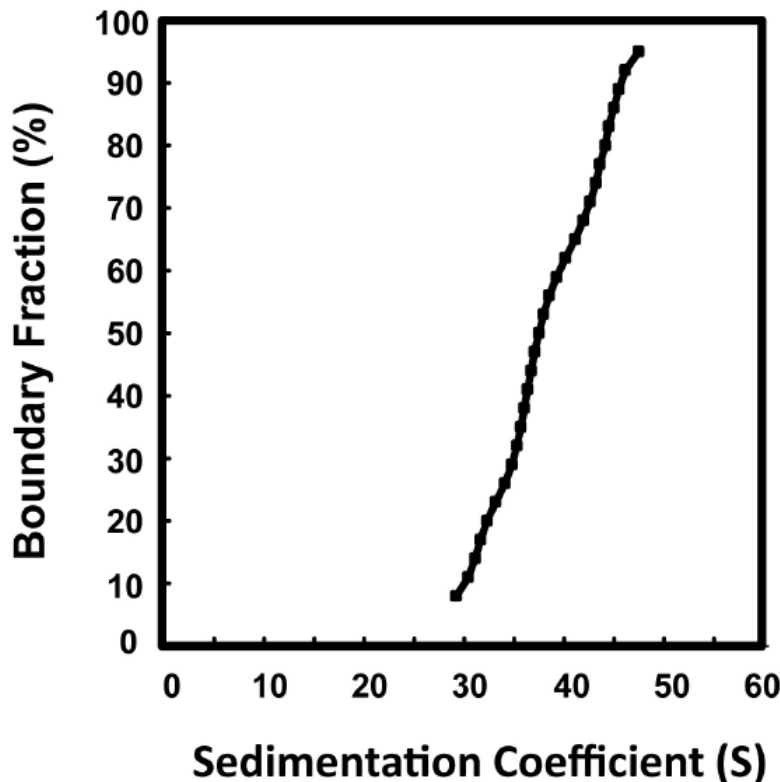


Figure 3.6) Nucleosomal array oligomerization is cooperative. Nucleosomal arrays were incubated in 4mM MgCl₂ and initially centrifuged at 3000 rpm to pellet the oligomers. The speed of the centrifuge was then increased to 25,000 rpm to monitor the fraction of the sample that did not pellet at 3000 rpm. Shown is the integral distribution of sedimentation coefficient obtained after analysis of the data by the method of Demeler and van Holde. The 30-50S sedimentation coefficient distribution indicates that the non-pelletable fraction in 4 mM MgCl₂ was monomeric and folded. The existence of only supramolecular oligomers and monomers at intermediate extend of oligomerization indicate that oligomerization is highly cooperative.

The microscopy studies indicate that the oligomers are globular throughout the assembly process. Consequently, a number of physical properties of the oligomers can be calculated from the measured sedimentation coefficients assuming a spherical structure (Table 3.1). The smallest oligomers detected during the early stages of self-association in 4 mM MgCl₂ sedimented at ~5000S while the largest oligomers observed in 8 and 10 mM MgCl₂ sedimented at ~350,000S. The 5000S oligomers were estimated to consist of 4.5×10^3 nucleosomes and have a mass of 1×10^9 Da. The Stokes radius, equivalent to the radius of a sphere calculated from the frictional coefficient, was 65 nm and the 5000S oligomers contained ~1 Mb DNA/oligomer. At the other extreme, the 350,000S oligomers were estimated to have 2×10^6 nucleosomes and a mass of 5×10^{11} Da. The Stokes radius was ~500 nm and the 350,000S particles contained ~450 Mb DNA/oligomer. The estimated Stokes radii are in the range determined by FM and TEM under the same ionic conditions (Fig. 3.2). The calculated mass and Mb DNA/oligomer indicate that the globular oligomers assembled *in vitro* as a function of increasing salt spanned the size range of the chromatin domains found in interphase nuclei (Dekker *et al*, 2013; Dixon *et al*, 2012; Eagen *et al*, 2015; Nora *et al*, 2012; Rao *et al*, 2014; Sexton *et al*, 2012).

Table 3.1

S	Oligomer Mass (Da) ^a	# Arrays ^b	# Nucleosomes ^c	Stokes R (nm) ^d	f ^e	Mb/Oligomer ^f	% Chromosome 1 ^g
5000	1.05E+09	3.75E+02	4.50E+03	64.71	1.22E-06	0.94	0.37
25000	1.18E+10	4.19E+03	5.03E+04	144.70	2.74E-06	10.48	4.19
75000	6.11E+10	2.18E+04	2.61E+05	250.62	4.74E-06	54.45	21.78
150000	1.73E+11	6.16E+04	7.39E+05	354.44	6.71E-06	154.00	61.60
300000	4.89E+11	1.74E+05	2.09E+06	501.25	9.49E-06	435.56	174.23

a.) A minimum mass of the complexes was calculated by using a spherical shape to determine a minimum frictional coefficient for a given sedimentation coefficient. A mass can then be calculated by a rearrangement of the Svedberg equation

$$s_s = \frac{M(1-\bar{v}\rho)}{N_A 6\pi\eta \left(\frac{3\bar{v}M}{4\pi}\right)^{1/3}}$$

b.) The number of arrays was calculated by dividing the minimum mass by the theoretical mass of a saturated array (2805206 Da)

c.) The estimate for the number of nucleosomes in each complex is 12 times the number of arrays.

d.) The stokes radius is the radius of the sphere which these calculations are based on and is $r_s = \left(\frac{3\bar{v}M}{4\pi}\right)^{1/3}$

e.) The frictional coefficient of the theoretical sphere is $f = 6\pi\eta \left(\frac{3\bar{v}M}{4\pi}\right)^{1/3}$

f.) As each array contains 2.5 kb of DNA, the number of arrays in a complex was used to determine the number of bp.

g.) The percentage of chromosome one was based on the Mb of DNA per oligomer divided by 250 Mb.

3.2.2 Nucleosomal array monomers are packaged as extended 10-nm fibers not folded 30 nm fibers

An important question is whether the nucleosomal array subunits are packaged within the oligomers as 10-nm or 30-nm fibers. The subunit structure of the oligomers was determined by SAXS, which is able to detect periodic structures in non-crystalline biological materials in solution (Maeshima *et al*, 2014a; Roe, 2000), and in particular has proven useful for determining the repetitive structures within the bulk chromatin of both mitotic chromosomes (Nishino *et al*, 2012) and intact nuclei (Joti *et al*, 2012). As in the pioneering work of Langmore and co-workers (Langmore & Paulson, 1983), scattering data are presented as plots of $\log(I \times S^2)$ vs. $1/S$ (I , intensity; S , scattering vector (1/nm)). A peak in the curve is indicative of a periodic structure in the sample with a diameter of inverse of S ($1/S$ nm) (Maeshima *et al*, 2014a; Roe, 2000). We first analyzed the structure of 601 nucleosomal arrays in 0-2.5 mM MgCl₂. In TE buffer without MgCl₂ the nucleosomal arrays sedimented at ~27S (Fig. 3.7), indicating they were monomeric and in the extended 10-nm beads-on-a-string conformation (Hansen, 2002). The scattering curve of the nucleosomal arrays in 0 mM MgCl₂ (Fig. 3.8A) had a broad peak between $1/S = 10-20$ nm resulting from the distances between the nucleosomes in the extended conformation, and a minor peak at ~6 nm corresponding to the width of the nucleosome disc (face-to-face positioning) (see also Fig. 3.8C). No peak at ~30-40 nm due to folded nucleosomal arrays (i.e., 30-nm fibers) was present under these low salt conditions, consistent with the SV-AUC data. Of note, the experimental scattering curve is very similar to the modeled scattering profile for an extended dinucleosome (Fig. 3.8D). Addition of salt to the solution causes the nucleosomal arrays to rapidly equilibrate between 10-nm and 30-nm conformations (Hansen, 2002), resulting in a progressively increased integral distribution of sedimentation coefficients in 1 and 2.5 mM MgCl₂ (Fig. 3.7). Importantly, a small peak at ~40 nm corresponding to folded

nucleosomal arrays appeared in the scattering curves in 1 and 2.5 mM MgCl₂ (arrow in Fig. 3.8A), in addition to the 10-20 nm and 6 nm peaks that were seen for the extended 10-nm fiber. A prominent ~40 nm peak was also present in the calculated scattering profile when either solenoid or zigzag 30-nm structures made from the 12-mer nucleosomal arrays were modeled (Figs. 3.8E and 3.8F). The experimental (Fig. 3.8A) and modeling (Figs. 3.8E and F) data provide important controls showing that SAXS is a valid assay for nucleosomal array folding, including being able to detect even small amounts of folded 30-nm structures when they are present.

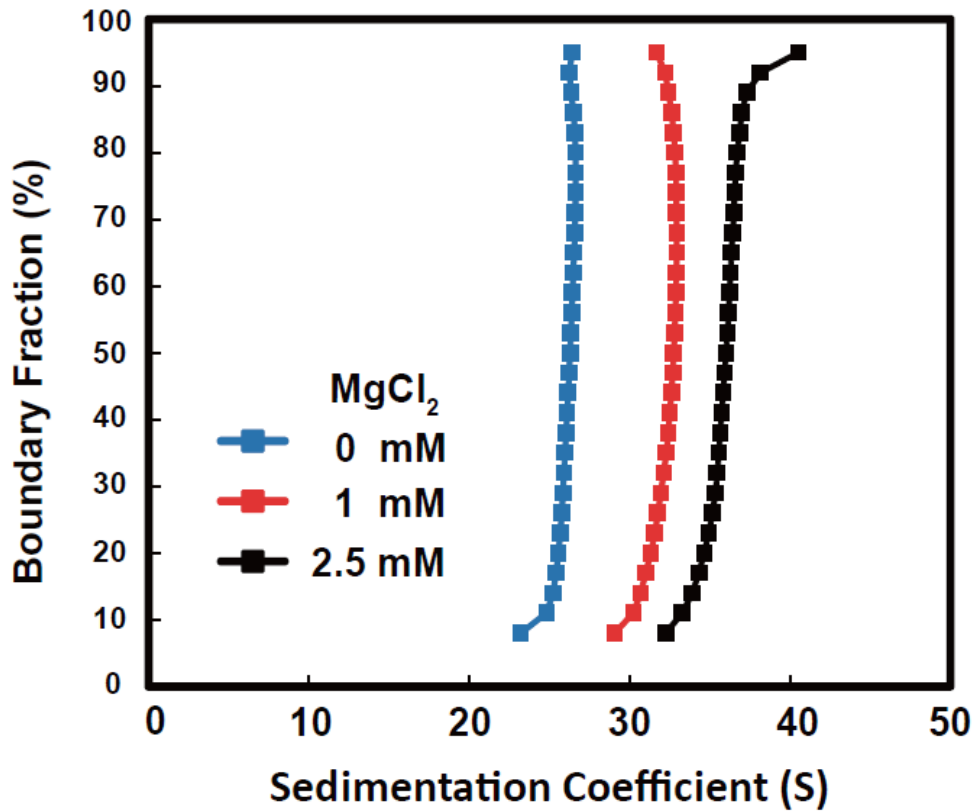


Figure 3.7) Nucleosomal arrays fold with increasing concentrations of salt. Sedimentation velocity experiments of reconstituted nucleosomal arrays in 0 mM (blue), 1 mM Mg (red), and 2.5 mM MgCl₂ (black) analyzed to obtain the integral distribution of sedimentation coefficients.

The scattering curves obtained for the 601 oligomers assembled in 5 and 10 mM MgCl₂ are shown in Figure 3.8B. In the range of $1/S > 20$ nm the slope of the curve was sharply downturned. This feature was observed in previous SAXS analyses of mitotic chromosomes (Nishino *et al*, 2012) and isolated nuclei (Joti *et al*, 2012), and results from the very large size of the oligomers. No ~40 nm peak was observed in the oligomer samples, indicating that the nucleosomal arrays subunits were not in a folded 30-nm conformation. The broad peaks at $1/S = 10\text{-}20$ nm and 6 nm seen for the extended arrays (Fig. 3.8A) were still present in the oligomeric samples, although between $1/S = 4\text{-}30$ nm the slope of the curve was sharply positive (Fig. 3.8B). For proteins the upward slope is characteristic of a denatured polypeptide chain (Doniach, 2001), implying that the nucleosomal arrays remain somewhat mobile within the oligomers. Collectively, the SAXS analyses of monomeric and oligomeric nucleosomal arrays indicate that the oligomers consist of packaged 10-nm fibers.

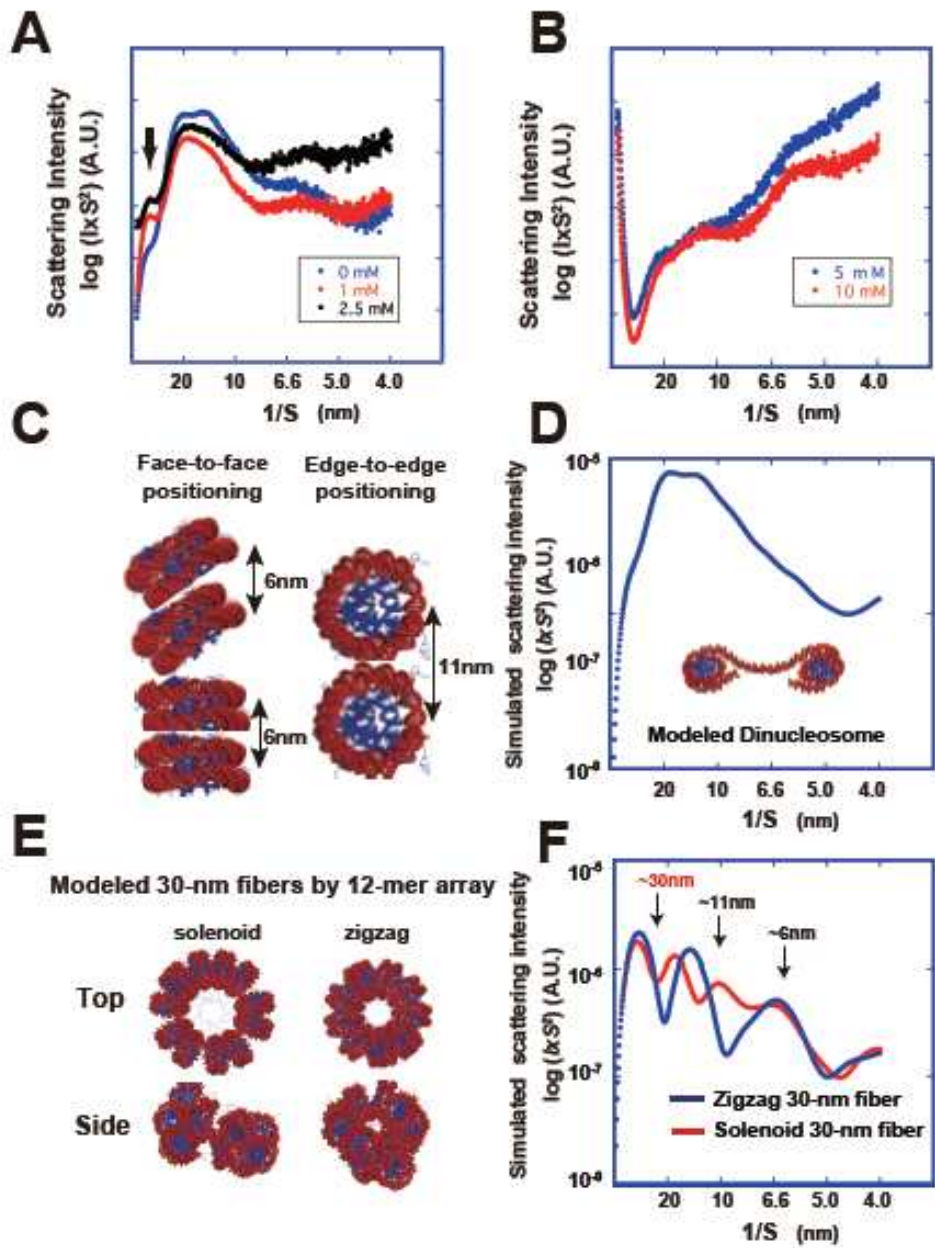


Figure 3.8) SAXS profiles of nucleosomal array oligomers and reconstructed *in silico* models. **A, B**) SAXS profiles of the nucleosomal arrays in 0 (TE), 1, 2.5 mM MgCl₂ (**A**) and 5, 10 mM MgCl₂ (**B**) are shown as plots of log($I \times S^2$) vs. $1/S$ (I , intensity; S , scattering vector (1/nm)). **C**) Two types of nucleosome positioning: face-to-face, at ~6-nm spacing, and edge-to-edge, at ~11-nm spacing. The image was made based on the structural information published in (Luger et al., 1997). **D**) The modeled scattering profile of an extended dinucleosome structure based on its atomic coordinate (for details, see Materials and Methods). Note that the modeled profile is similar to that of the nucleosomal arrays in 0 mM MgCl₂ (**A**). **E**) Two structural models of 12-mer 30-nm fibers: solenoid (left) and zigzag (right) as a top and side view. The models were constructed using MolScript (Kraulis, 1991). **F**) The scattering profiles of the solenoid (red line) and zigzag (blue line) 30-nm fibers were made from their atomic coordinates computationally. Note that the 30-40 nm peak is prominent in both fiber models.

We next asked whether the packaged linker DNA within the oligomers could be completely digested by MNase, and if so, whether the oligomers remained intact after digestion. Nucleosomal arrays were incubated in digestion buffer containing either 0.5 or 5 mM MgCl₂. The arrays were ~100% monomeric in 0.5 mM MgCl₂ and ~85% oligomeric in 5 mM MgCl₂ as judged by the differential centrifugation assay (Fig. 3.9A). For the oligomers in 5 mM MgCl₂, the presence of only mononucleosomal DNA in the deproteinized MNase digest indicated that the linker DNA was completely accessible and digested to completion under the conditions used (Fig. 3.9B). When the oligomers in 5 mM MgCl₂ were digested to completion with MNase and examined by FM we still observed oligomeric particles, but both the size (Fig. 3.9C) and number (Fig. 3.9A) of the oligomers were reduced compared to the undigested control. Thus, both attractive nucleosome-nucleosome interactions (Liu *et al*, 2011) and linker DNA contribute to oligomer stability.

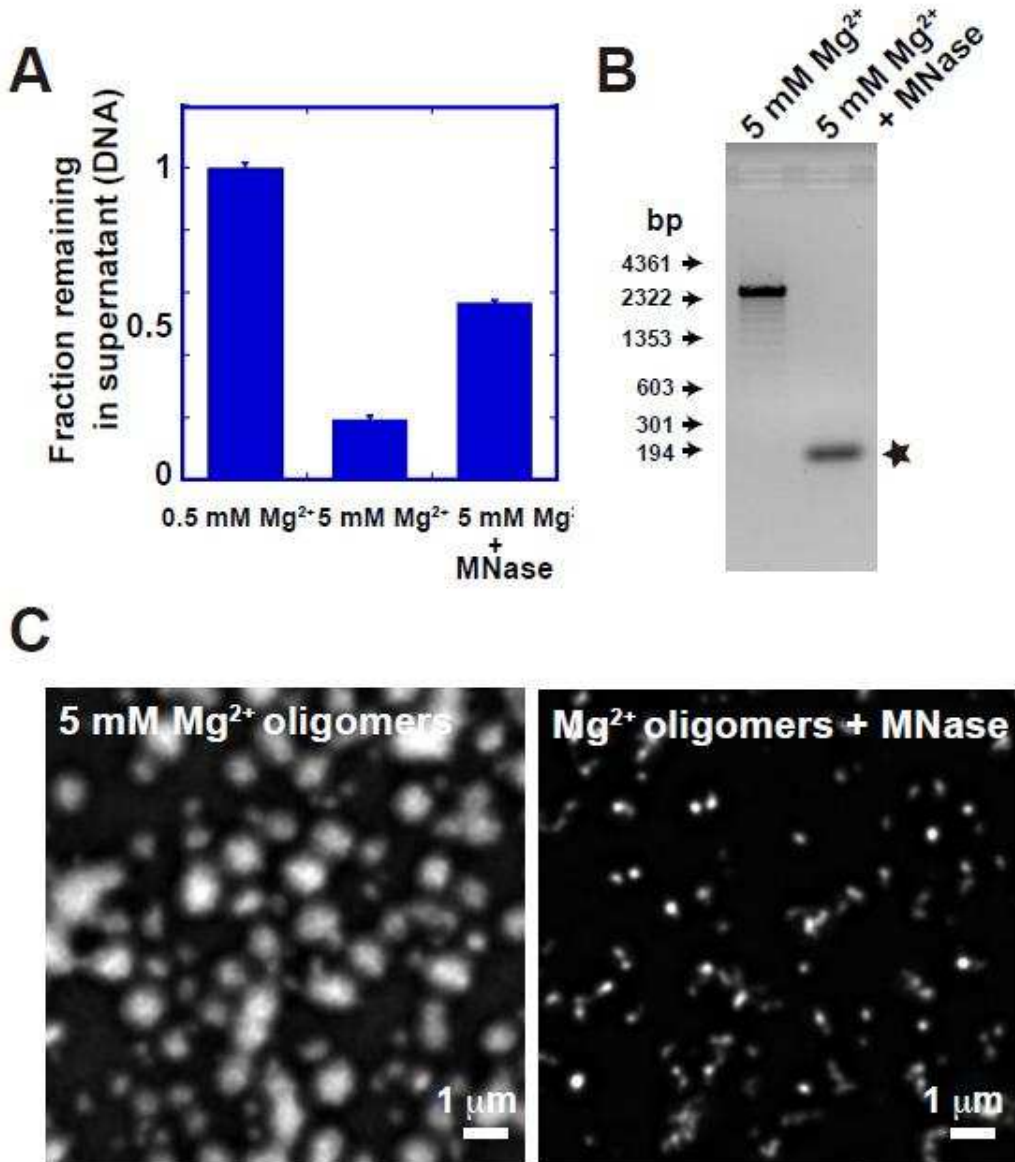


Figure 3.9 Effect of MNase digestion on oligomer structure. **A)** 601-nucleosomal arrays were incubated in 0.5, 5 mM MgCl₂, 5 mM MgCl₂ + MNase, and analyzed by the differential centrifugation assay to determine the fraction oligomeric. The amounts of DNA in the supernatant fraction were measured. Note that for the MNase- digested oligomers the supernatant fraction also includes the digested free linker DNA. Each value is the mean of three measurements and the error bars represent the standard deviation. **B)** Verification of complete MNase digestion. DNA was purified from the nucleosomal arrays incubated in 5 mM MgCl₂ or 5 mM MgCl₂ + MNase, and then electrophoresed on agarose gel. The position of mono nucleosome is marked with a star symbol. **C)** Nucleosomal array oligomers (left) or with MNase treatment (right) were stained with DAPI and examined using FM. Shown are representative images obtained. Note that the sizes of MNase-treated oligomers are much smaller than those of the control oligomers (left and Fig. 1A).

3.2.3 Linker histones modulate oligomer structure, assembly, and subunit packaging

Linker histones are the most abundant chromatin-associated proteins in most eukaryotic cells (Woodcock *et al*, 2006), and promote chromatin condensation *in vitro* (Hansen, 2002) and *in vivo* (Fan *et al*, 2005; Hashimoto *et al*, 2010). We therefore determined how linker histones affected nucleosomal array oligomerization. When characterized by the differential centrifugation assay, the plot for the H1-bound nucleosomal arrays was shifted to the left relative to that obtained for the nucleosomal arrays alone, although the shapes of the curves otherwise were very similar (Fig. 3.1A). While this indicates that linker histones in some way influence oligomerization, to more quantitatively address this question the H1-bound nucleosomal arrays were characterized by microscopy, SV-AUC, and SAXS as a function of salt.

Typical FM images obtained in 4 and 5 mM MgCl₂ for the 601 H1-oligomers are shown in Figure 3.11A. The H1-oligomers visualized in 4 and 5 mM MgCl₂ (~75% and 90% oligomerized, respectively) were globular and ~100-300 nm in size. Control FM images in 0, 1, and 3 mM MgCl₂ are shown in Figure 3.11B. Very small particles were faintly visible in 1 and 3 mM MgCl₂ but not at the lower salt concentration. In 4 mM MgCl₂ the predominant oligomers observed by TEM were globular, and had diameters of ~200-300 nm (Fig. 3.11C, left), consistent with the diameters seen in the FM images under the same conditions (Fig. 3.11A). As with the nucleosomal array oligomers (Fig. 3.11C, right panels), at higher magnification one could see individual close packed nucleosomes, but no regular repetitive folded structures such as the 30-nm fiber (Fig 3.11C, right panel). The *ssm* of the H1-oligomers as a function of MgCl₂ are shown in Figure 3.11A. The *ssm* in 3 mM MgCl₂ was ~650S, which increased to ~13,000S in 4 mM MgCl₂. While these sedimentation coefficients are very large, the *ssm* of the H1-oligomers were smaller than

the *ssm* of the nucleosomal array oligomers under equivalent extents of self-association (Fig. 3.10A), consistent with the FM analysis (compare Figs. 3.2A and 3.11A). Above 5 mM MgCl₂ the oligomers pelleted immediately and the *ssm* were too large to measure, even with the interference optical system (Fig. 3.12A). Analysis by the time derivative method yielded the distribution of H1-oligomer sedimentation coefficients present at each salt concentration. In 3 mM MgCl₂ the sedimentation coefficient distribution ranged from ~200-1400S, with a peak in the plot at ~600S (Figs. 3.12B,C). In 3.5 mM MgCl₂ the distribution of observed sedimentation coefficients was shifted to ~600-3000S, and the peak in the g(s) plot increased to ~1100S (Fig. 3.12C). In 4 mM MgCl₂ the range of H1-oligomer sedimentation coefficient increased significantly, extending from ~2000-50,000S with a peak in the g(s) plot at ~12,000S (Fig. 3.12B). To directly determine the effect of H1 on oligomer size, the oligomer sedimentation coefficient distributions determined in 4 mM MgCl₂ in the absence and presence of H1 were converted to Mb DNA/oligomer (as in Table 3.1). In both cases the DNA content of the H1- oligomers ranged from <1 to ~30 Mb/oligomer. However, the average for the H1-oligomers was 4 Mb DNA/oligomer compared to 12 Mb DNA/oligomer for the nucleosomal array oligomers under these conditions (Fig. 3.10B).

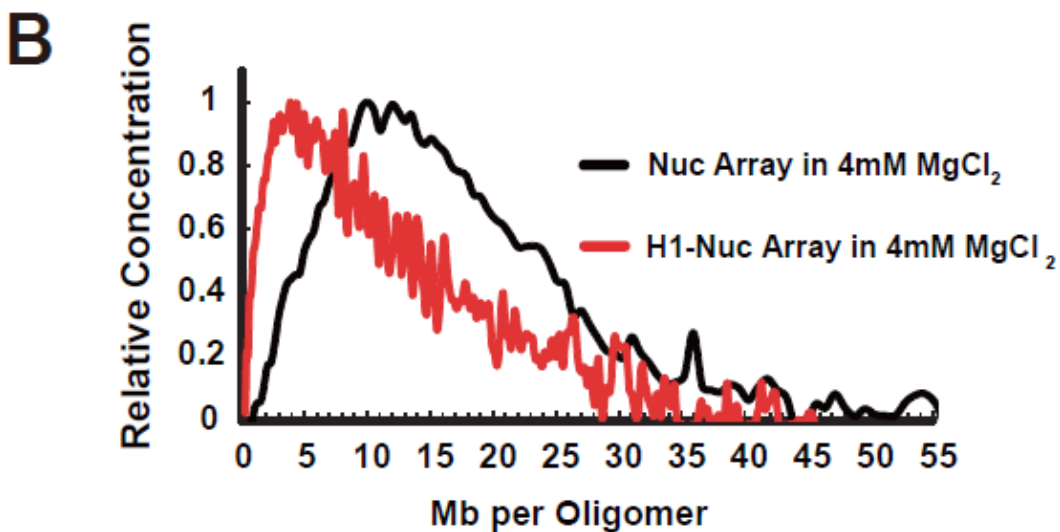
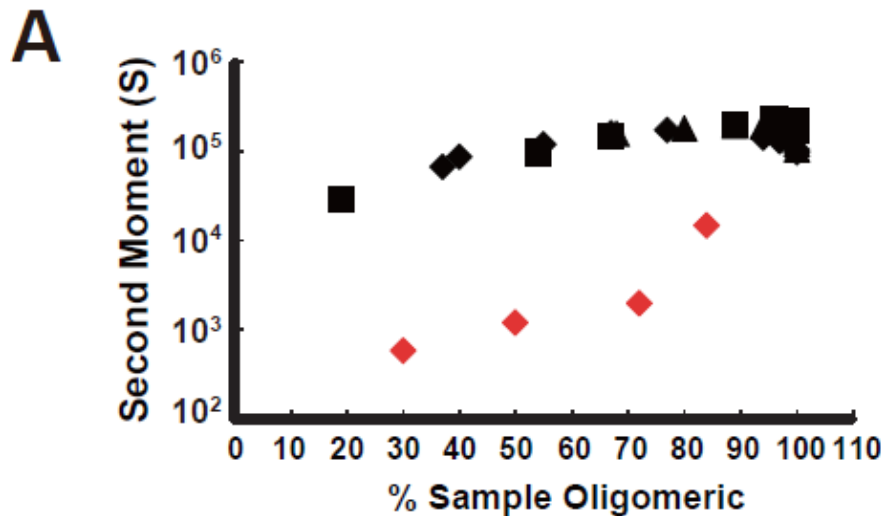


Figure 3.10) H1-oligomers are smaller than nucleosomal array oligomers at equivalent extents of self-association. **A)** The second moment sedimentation coefficients for oligomeric nucleosomal arrays (black) and H1-arrays (red) are plotted against the fraction of the sample that is oligomeric. **B)** The sedimentation data for nucleosomal arrays and H1-nucleosomal arrays in 4 mM MgCl₂ were analyzed by the time derivative method to obtain the g(s*), which was then converted to the distribution of Mb DNA per oligomer as in Table 3.1.

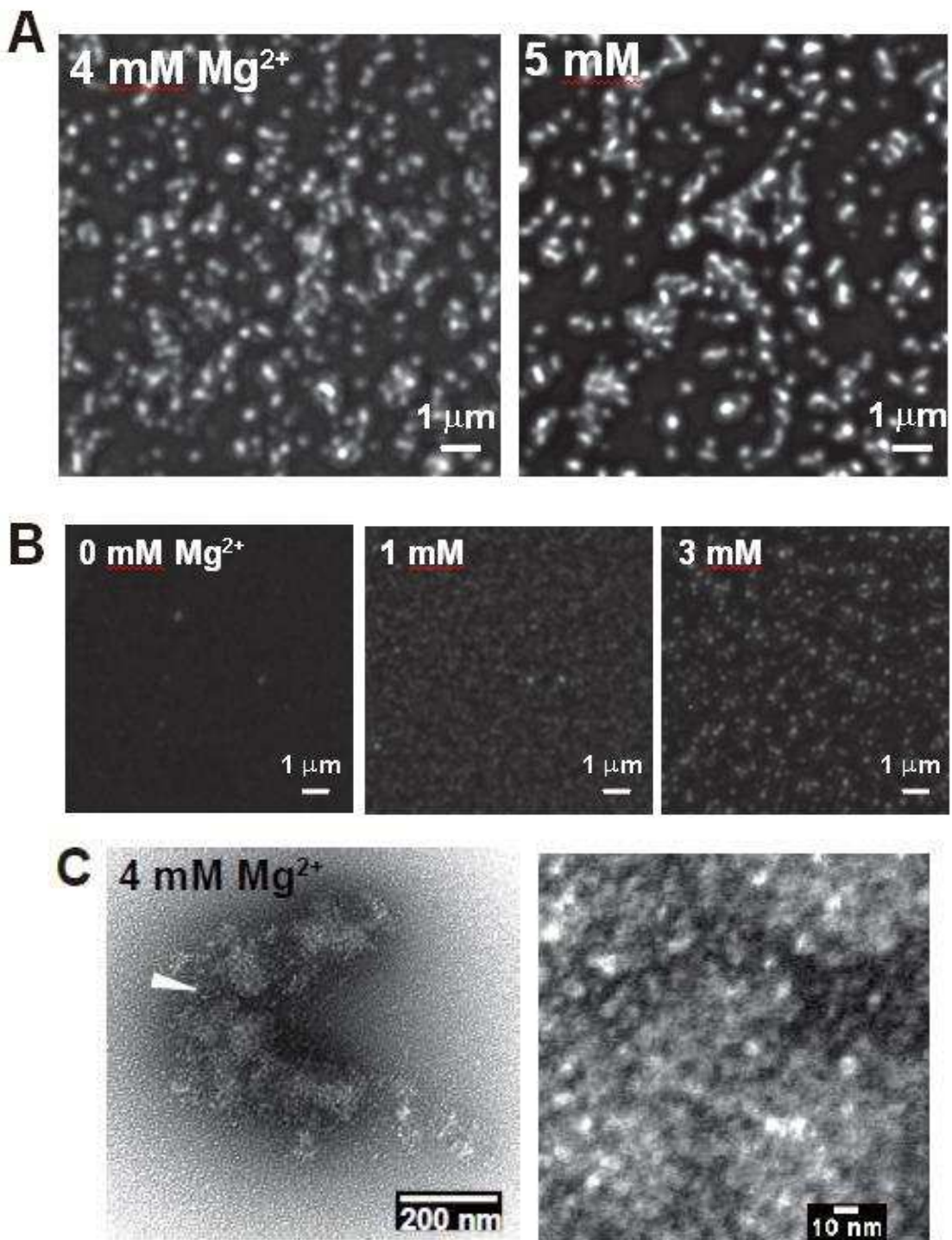


Figure 3.11) H1-oligomers are globular. **A)** Oligomers assembled from H1-nucleosomal arrays were stained with DAPI and examined using FM. Shown are representative images obtained in 4 mM and 5 mM $MgCl_2$. **B)** Control FM images obtained in 0, 1 and 3 mM $MgCl_2$. **C)** H1-nucleosomal array oligomers were negatively stained and visualized by TEM. Shown in the left panel is a representative image obtained in 4 mM $MgCl_2$. Shown in the right panel is an image of the interior of the oligomer (white arrow, left panel) after cropping and re-scaling.

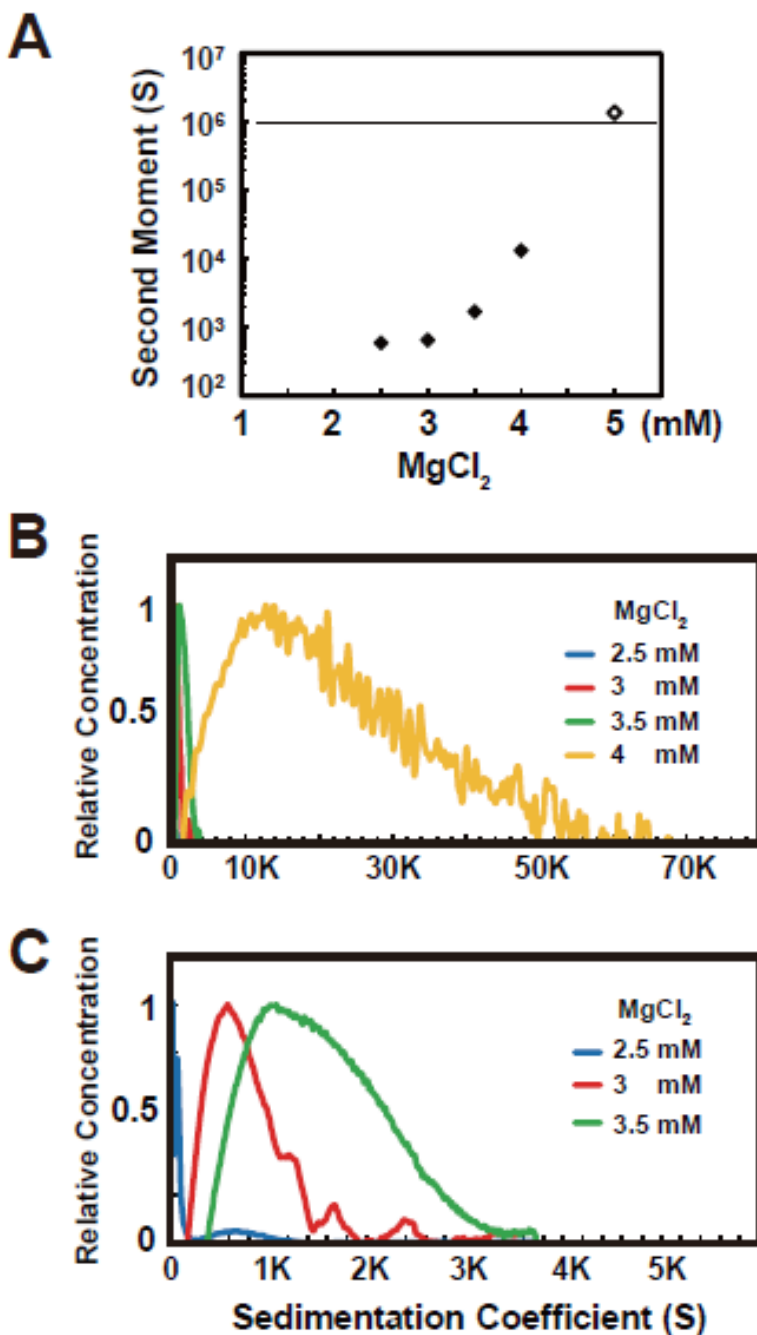


Figure 3.12) Sedimentation analysis of salt-dependent H1-oligomer assembly. **A)** Representative experiment showing the second moment sedimentation coefficients of the H1-oligomers as a function of MgCl_2 . The dashed line indicates the upper limit of measurable sedimentation coefficients ($\sim 10^6 \text{ S}$). The white symbol is intended to show that the sedimentation coefficient of the H1-oligomers in 5 mM MgCl_2 is beyond the detectable limit. **B)** Analysis of the same raw data as in panel (A) by the time derivative method to yield the sedimentation coefficient distribution, $g(s^*)$. **C)** The $g(s^*)$ profiles in 2.5 mM, 3 mM, and 3.5 mM from panel (B) are re-plotted on a smaller scale.

Given that H1 stabilizes folded 30-nm structures *in vitro* (Hansen, 2002; Li & Zhu, 2015; Robinson *et al*, 2006), we wanted to determine whether the subunit structure of the H1-oligomers was the 30 nm fiber. As a control we first compared the results obtained by SV-AUC and SAXS for H1-bound nucleosomal arrays in 0-2.5 mM MgCl₂. In 0 mM MgCl₂ the H1-arrays sedimented at ~32S (Fig. 3.13), indicating they were monomeric and extended (Carruthers *et al*, 1998). The scattering curve of the H1-arrays in 0 mM MgCl₂ resembled that of parent nucleosomal arrays under the same conditions, with a broad peak at 10-20 nm, a minor peak at ~6 nm, but no peak at ~30-40 nm corresponding to folded fibers (Fig. 3.14A). This indicates that the H1-bound arrays in the absence of salt had an extended structure with 10 to 20 nm internucleosomal distances in solution. In 1 mM MgCl₂ the H1 arrays began to form folded structures, as indicated by the increase in the maximum sedimentation coefficient to 45S (Fig. 3.13). Under these conditions a significant peak at 30- 40 nm appeared in the SAXS profile (arrow in Fig. 3.14A), consistent with the similar peak seen for the modeled 30-nm fibers (Figs. 3.8E-F). SV-AUC analysis of the H1-array samples in 2.5mM MgCl₂ indicated two major populations of fibers; one sedimented at ~32-55S, while the other sedimented from ~90-130S. The former corresponds to a distribution of folded monomers, while the latter is indicative of small oligomers that do not pellet at 3000 rpm. Importantly, the SAXS profile in 2.5 mM MgCl₂ was dominated by a major peak at 30-40 nm. A comparison of the SAXS data for monomeric nucleosomal arrays (Fig. 3.8A) and H1-bound arrays (Fig. 3.14A) demonstrates that H1 stabilizes folded 30-nm fibers, as has been observed by SV-AUC (Fig. 3.13) and other techniques (Li & Zhu, 2015; Robinson *et al*, 2006).

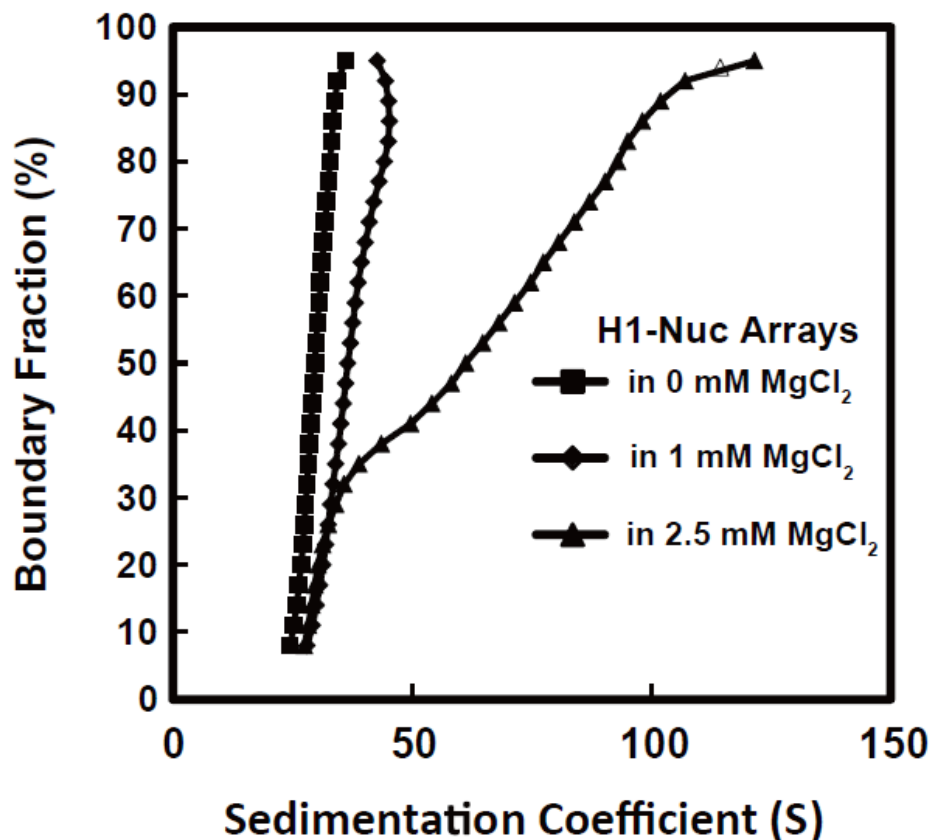


Figure 3.13) H1-array folds extensively in the presence of salt. Shown are the integral distributions of sedimentation coefficients obtained for H1-arrays in 0 mM, 1 mM and 2.5 mM MgCl₂

SAXS analyses of the H1-oligomers assembled in 5 and 10 mM MgCl₂ are shown in Figure 3.14B. In the range of $1/S > 20$ nm the slopes of the curves were sharply downturned due to the large size of the oligomers. The ~30-40 nm peak seen in the 1 and 2.5 mM MgCl₂ control samples was absent in the H1-oligomers. Between $1/S = 4-10$ nm the slopes of the scattering curves was flat and prominent peaks at 6 and 11 nm were apparent (Fig. 3.14B). The 6- and 11-nm peaks have been proposed to come from edge-to-edge and face-to-face positioning of nucleosomes, respectively (Langmore & Paulson, 1983) (see Fig. 3.8C). Several important conclusions can be drawn from these data. First, the 12-mer nucleosomes within the H1-oligomers were not folded into regular 30-nm fibers. Second, H1 abolished the upward slope between $1/S = 4-10$ nm seen in the plots of the nucleosomal array oligomers (Fig. 3.8B), suggesting tighter subunit packing. Lastly, H1 sharpened the diffuse 6 and 11 nm peaks present in the control H1 samples (Fig. 3.14A) and the nucleosomal array oligomers (Fig. 3.8B). The scattering curves for isolated native chicken chromatin fragments (which contain heterogeneous linker DNA lengths and near stoichiometric levels of H1) were essentially identical to those obtained for the 601 H1-arrays, but with lower concentration of MgCl₂ (Figure 3.14C), indicating that SAXS results were not dependent on the regular positioning of the 601 arrays. We next modeled the SAXS curve for *in silico* oligomers composed of 100 randomly and tightly packed 12-mer nucleosomal arrays in the 30-nm conformation (Figs. 3.14E-F). The nucleosome concentration of the *in silico* oligomers was about ~0.5 mM, comparable to that of mitotic chromosomes (Hihara *et al.*, 2012). The scattering profile of the *in silico* oligomers closely resembled the experimental scattering profile for the H1- oligomers, except for the presence of peaks at ~30-40 nm in the modeled curve (arrow in Fig. 3.14F). The modeling results further support the conclusion that the subunit structure of the H1-oligomers is not the folded 30-nm fiber.

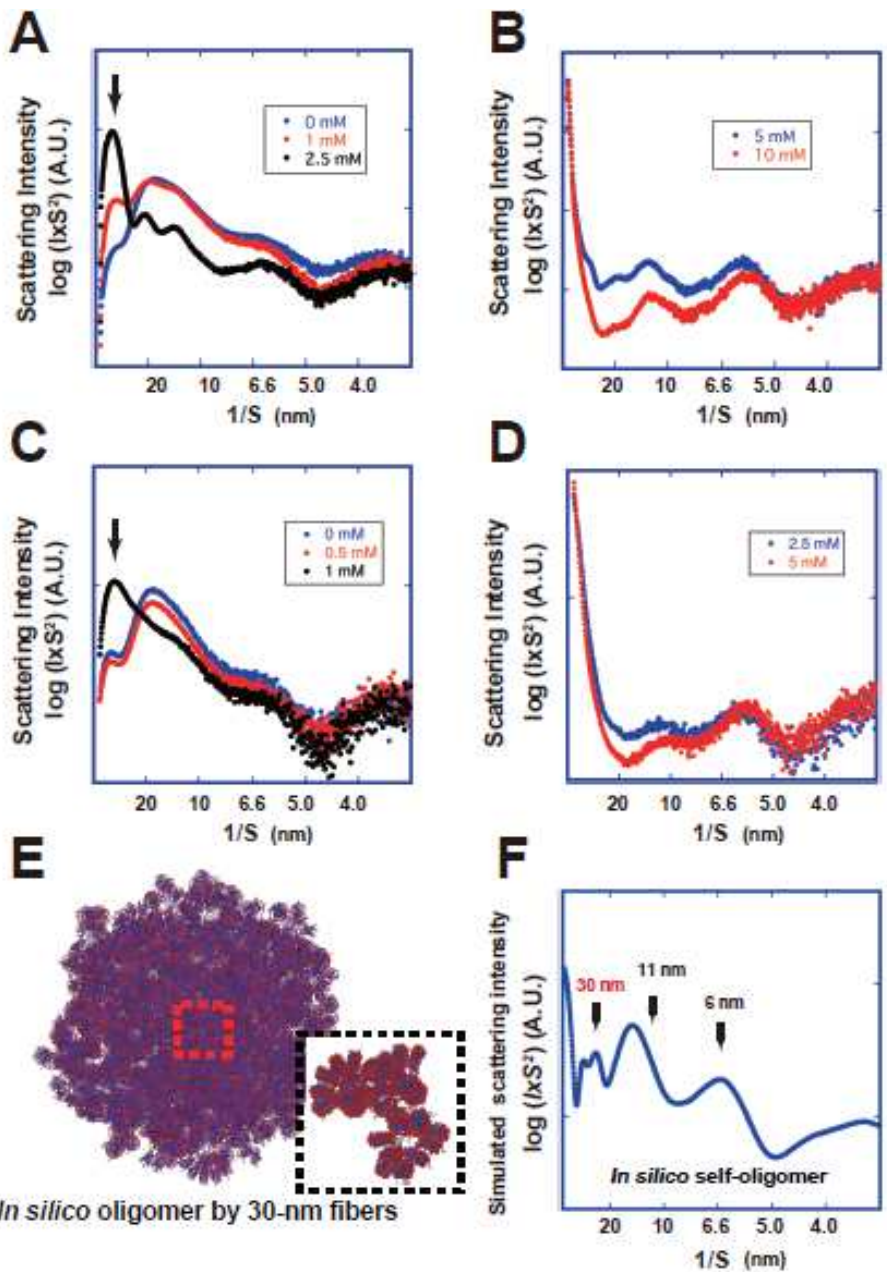


Figure 3.14) SAXS profiles of the H1-oligomers, native chicken chromatin and reconstructed *in silico* oligomer models. **A, B)** SAXS profiles of the H1-nucleosomal arrays in 0 (TE), 1, 2.5 mM MgCl₂ (**A**) and 5, 10 mM MgCl₂ (**B**) are shown as plots of log($I \times S^2$) vs. 1/S (I , intensity; S , scattering vector (1/nm)). **C, D)** SAXS profiles of the native chicken chromatin in 0 (TE), 0.5, 1 mM MgCl₂ (**C**) and 2.5, 5 mM MgCl₂ (**D**) are shown as plots of log($I \times S^2$) vs. 1/S (I , intensity; S , scattering vector (1/nm)). **E)** The "*in silico* oligomer" models were constructed in environments containing 100, 50, and 25 randomly and tightly packed 12-mer 30-nm fiber models (Fig. 3E). The nucleosome concentration was 0.5 mM. The 100-fiber model was drawn using MolScript (Kraulis, 1991). The broken-lined squares show magnified regions. **F)** The modeled scattering profiles, yielding average among-model values, have prominent peaks at ~30-40, 11, and 6 nm. This shows that the *in silico* oligomers retain characteristics of 30-nm fibers. Note that the modeled scattering profile is very distinct from the SAXS profiles in Figs. 3B, 7B and D, and also 8B (center and right).

3.2.4 Low salt disassembles higher order chromatin structures in nuclei *in situ*

Our *in vitro* studies suggest that the oligomers formed by nucleosomal arrays in the absence and presence of histone H1 are good *in vitro* models for interphase chromosome structure in nuclei. Given that the oligomers are stable in 5 mM MgCl₂ but not in <1 mM MgCl₂ (Fig. 3.1), we predicted that chromatin structure and organization *in situ* would appear normal in 5 mM MgCl₂ but would be disrupted by exposure to EDTA, which reduces the MgCl₂ concentration to essentially zero. To test our hypothesis the effects of MgCl₂ on the higher order chromatin structures present *in situ* in isolated HeLa nuclei were determined using FM and SAXS. To visualize nuclear structure, isolated nuclei were exposed to DAPI and analyzed by FM. In 1 mM and 5 mM MgCl₂, all of the nuclei examined showed both bright regions resulting from areas of intense DAPI staining (heterochromatin-rich) interspersed with dark regions that were less concentrated with DAPI (euchromatin) (Fig. 3.15A, center and right panels). The DAPI-intense regions were especially prominent near the nuclear periphery and around nucleoli. These images show that canonical interphase chromatin organization is retained in 1 mM and 5 mM MgCl₂. In distinct contrast, uniform DAPI staining was observed in nuclei exposed to EDTA (Fig. 3.15A, left panel), demonstrating that higher order chromatin organization *in situ* was disrupted in the absence of cations. Quantitation of the nuclear sizes indicated that the nuclei in EDTA on the average were twice as large as those in 1 mM and 5 mM MgCl₂ (Fig. 3.15A), indicative of extensive chromatin decondensation. Independently, SAXS analysis of HeLa nuclei was used to examine bulk interphase chromatin as a function of salt. The scattering profiles in 1 mM and 5 mM MgCl₂ (Fig. 3.15B, center and right panels) closely resembled those observed previously for intact nuclei (Joti *et al.*, 2012), and the H1-oligomers (Fig. 3.14B), with a prominent downturned slope in the range of $1/S > 15$ nm and peaks at 6 and 11 nm.

When the isolated HeLa nuclei were incubated in EDTA buffer, the scattering profile (Fig. 3.15B, left panel) changed to one that much more closely resembled those of the nucleosomal array and H1-nucleosomal array monomers (Figs. 3.8A, D and 3.14A). The FM and SAXS results together demonstrate that higher order chromatin structure in isolated nuclei *in situ* is disassembled in the absence of cations, conditions that also dissociate oligomeric nucleosomal arrays *in vitro*. These results also indicate that HeLa nuclear chromatin *in situ* is stabilized by lower MgCl₂ concentration (~1 mM) than the nucleosomal array oligomers and H1-oligomers, probably because the nuclear chromatin is at much higher concentration and complexed with more proteins than the model systems used in the *in vitro* experiments. The differential centrifugation assay of isolated HeLa chromatin is a good agreement with this finding, i.e., the Mg⁵⁰ for oligomerization of the HeLa chromatin is ~1 mM MgCl₂, compared to ~2.5 mM MgCl₂ for H1- nucleosomal arrays and ~4 mM MgCl₂ for nucleosomal arrays (Fig. 3.16 and Fig. 3.1).

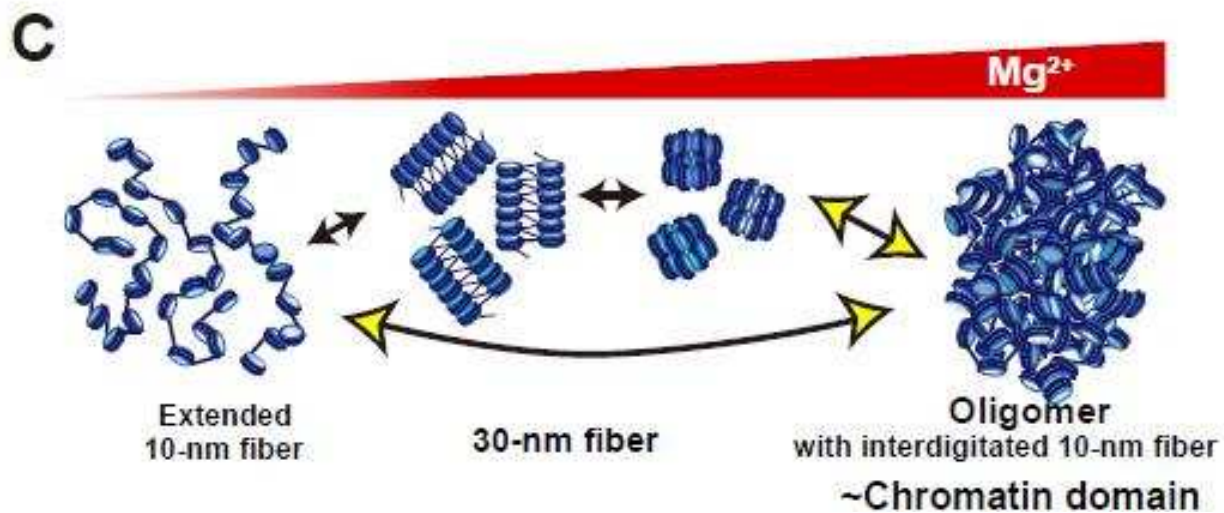
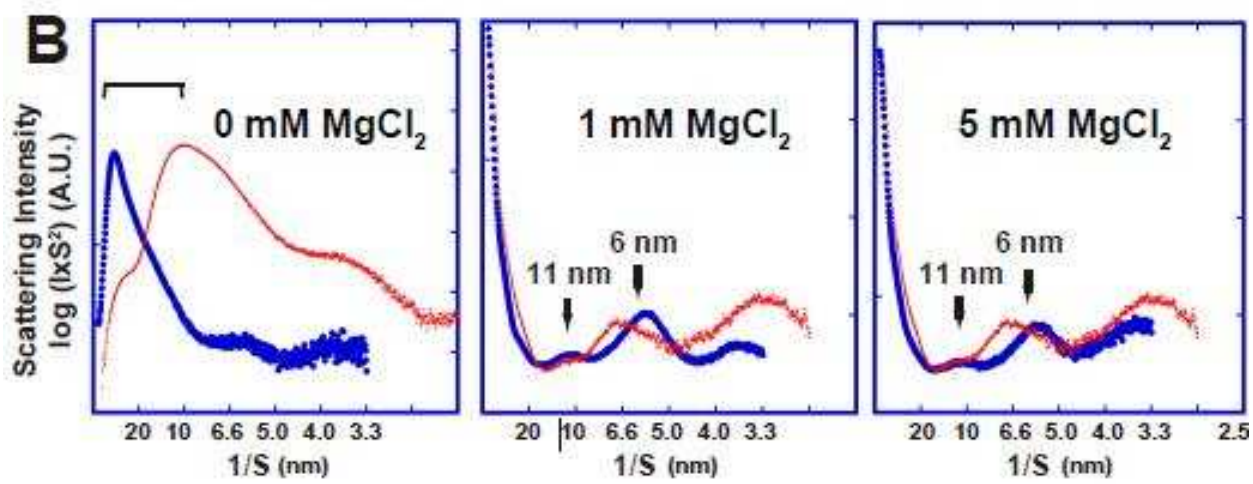
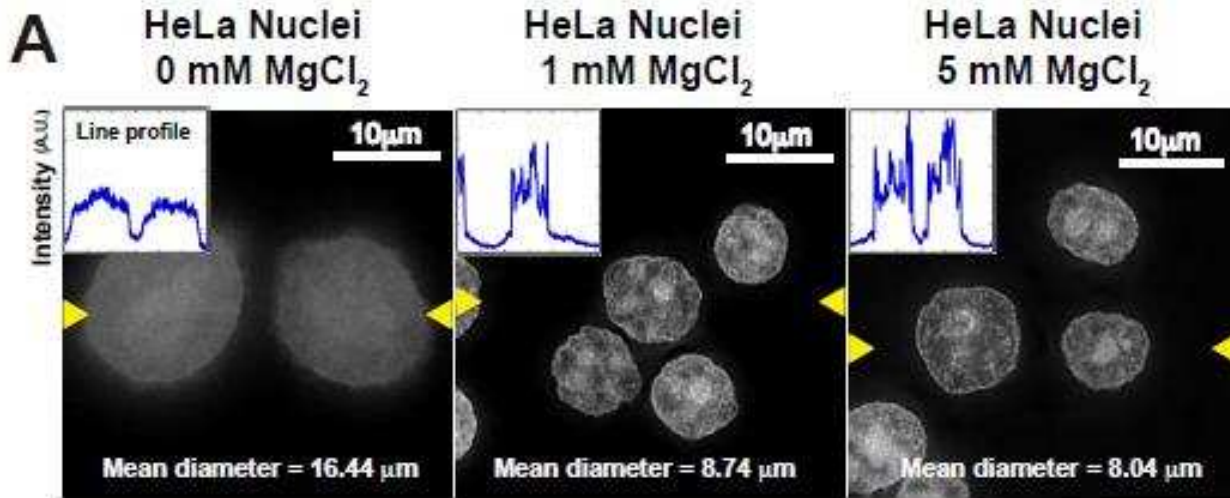


Figure 3.15) Effect of MgCl₂ concentration on the chromatin structure of isolated HeLa nuclei. **A)** FM images of chromatin structure in the nuclei with 0 mM (left), 1 mM (center) and 5 mM MgCl₂ (right). Insets show the intensity line profiles between the two marked arrow heads in the images. **B)** SAXS profiles of the isolated HeLa nuclei. SAXS profiles of the nuclei in 0 mM (left), 1 mM (center) and 5 mM MgCl₂ (right). Note that with 1 mM and 5 mM MgCl₂ the peaks at 6 and 11 nm are detectable, but no ~30-40 nm peak although these property almost disappeared. Although there is ~30-40 nm peak in 0 mM MgCl₂, the peak seems to derive from regular 30- 40-nm spatial distances between constrained nucleosomes in the nuclei, but not the 30-nm fibers. Differently from flexible nucleosomal arrays in solution, where they can freely move and stretch, the fibers in the nuclei are constrained in a space (e.g., Fig. 8A). This constraint can cause constant nucleosome distances of 30-40-nm in the nuclei (e.g. Fig 4 in (Eltsov et al., 2008).

C) Model scheme. The 12-mer nucleosomal array is a well-defined model chromatin system. In 1-2 mM Mg²⁺, the nucleosomal array folds into a folded 30-nm chromatin fiber structure. With further increases in Mg²⁺, the nucleosome arrays assemble into supramolecular oligomers. The large oligomers are not assemblies of the 30-nm chromatin fibers, but are proposed to be interdigitated and melted structures of 10-nm nucleosomal arrays.

HeLa Chromatin

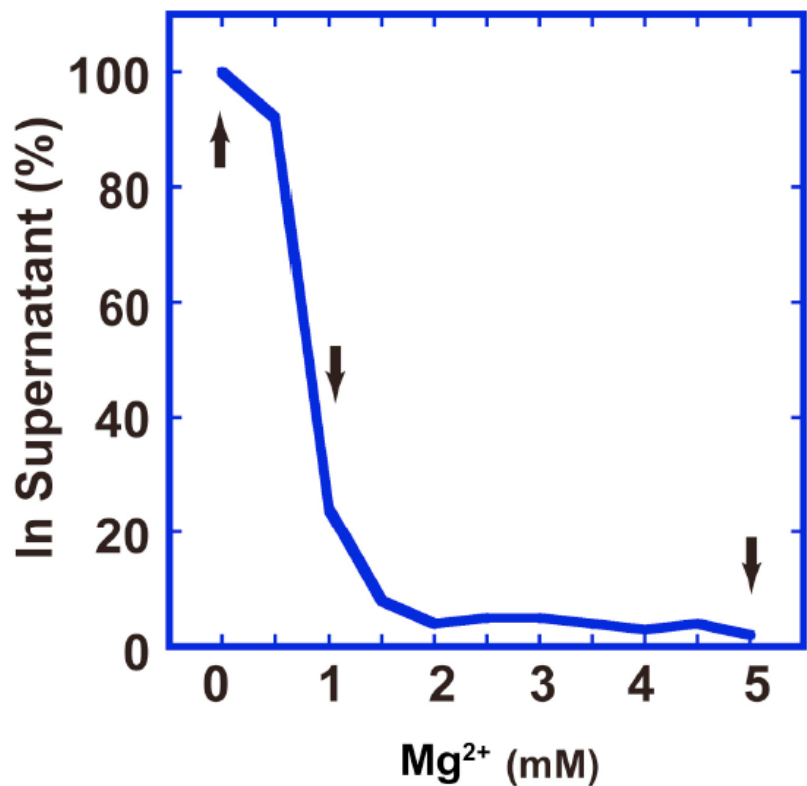


Figure 3.16) Differential centrifugation assay of isolated HeLa chromatin. Note that the HeLa chromatin was mostly pelleted in 1mM $MgCl_2$, indicating extensive oligomerization under these conditions.

3.3 Discussion

The oligomers characterized in our studies recapitulate key aspects of interphase chromosome structure and organization. Interphase chromosomes occupy discrete territories within the nucleus, and the territories appear globular when visualized by fluorescence *in situ* hybridization (Cremer & Cremer, 2010). Studies using chromosome conformation capture technology and its variants suggest that the long linear chromosomal chain of nucleosomes (Valouev *et al*, 2011) is assembled into arrays of higher order globular chromatin domains, often called topologically associating domains. Globular chromosomal domains also have been observed by fluorescence microscopy (Albiez *et al*, 2006). A typical chromatin domain contains ~0.1-10 Mb of DNA (Dekker *et al*, 2013; Eagen *et al*, 2015; Rao *et al*, 2014). In the case of *in vitro* oligomerization, the early stages of nucleosomal array self-association produce globular particles containing ~1-10 Mb DNA/oligomer (Fig. 3.4, Table 3.1). At their maximum, the globular oligomers are the size of chromosomes. When H1 is bound to nucleosomal arrays *in vitro*, the early stages of self-association produce globular oligomers consisting of ~0.5-1.0 Mb DNA/oligomer, quite similar to the average size observed for the chromatin domains in nuclei (Dekker *et al*, 2013; Eagen *et al*, 2015; Rao *et al*, 2014). These observations indicate that the globular oligomers characterized in our studies span the size range of the chromatin domains present in nuclei, and suggest that the oligomers are good *in vitro* model systems for studying interphase chromosome structure and organization.

The single nucleosome fiber that makes up an interphase chromosome behaves as a flexible random coil polymer chain e.g. (Barbieri *et al*, 2014). Thus, widely separated stretches of chromosomal nucleosomes will be able to interact over Mb distances, and the self-association of 12-mer nucleosomal arrays should be an *in vitro* reflection of the self-interactions of a condensed chromosomal fiber. The biological relevance of nucleosome

oligomerization was addressed experimentally by examining the effect of MgCl₂ concentration on the structure of isolated human nuclei. In our hypothesis the conditions that disassemble the oligomers *in vitro* should disrupt long-range chromosomal fiber interactions and perturb higher order chromatin structure in the nucleus. Our FM and SAXS analyses of isolated nuclei demonstrate that the heterochromatin and euchromatin compartments present in ~1 mM MgCl₂ *in situ* were abolished by exposure to EDTA, concomitant with extensive chromatin decondensation (Fig. 3.15). In recent related studies, chromatin condensation within permeabilized cell nuclei increased dramatically as the divalent cation and polyamine concentration were increased from 0 mM into the physiological range (Visvanathan et al., 2013), and hypotonic treatment (low salt) in living mammalian cells caused extensive chromatin decondensation (Albiez et al, 2006). Collectively, the *in situ* results indicate that very low salt concentrations that destabilize nucleosome oligomers *in vitro* also destabilize the chromatin domains and higher order chromatin structures in isolated nuclei. This in turn suggests that core and linker histone-mediated long-range nucleosome-nucleosome interactions contribute significantly to interphase chromosome structure and organization. Of note, histone-mediated long-range nucleosome-nucleosome interactions also appear to be applicable to mitotic chromosome structure. Isolated mitotic chromosomes behave like interphase chromatin in the presence and absence of salt. Without MgCl₂ the chromosomes are highly swollen and the chromosomal fibers are stretched into 10 nm-like fibers (Earnshaw & Laemmli, 1983; Eltsov et al, 2008; Takata et al, 2013), whereas in the presence of MgCl₂ the chromosomes are highly condensed (Earnshaw & Laemmli, 1983; Eltsov et al, 2008; Takata et al, 2013). Mg²⁺-dependent mitotic chromosome decondensation and condensation is highly reversible (Hudson et al, 2003).

The widely held paradigm for chromosomal DNA packaging *in vivo* maintains that helical 30-nm chromatin structures are requisite folding intermediates in the establishment of higher order chromosomal domains, i.e., the nucleosome chain must first fold into 30-nm fibers before assembling into successively more condensed chromatin structures (for reviews, e.g. (Grigoryev & Woodcock, 2012; Hansen, 2002; Robinson *et al*, 2006; Li & Zhu, 2015; Maeshima *et al*, 2014b). This view is based in large part on the fact that 10-nm fibers initially fold into 30-nm fibers when salt is titrated into solution *in vitro*. However, there is very little direct evidence for the existence of bulk 30-nm fibers in chromosomes. Although a ~30-40 nm peak was observed in SAXS studies of living cells, isolated nuclei and mitotic chromosomes (Joti *et al*, 2012; Langmore & Paulson, 1983; Nishino *et al*, 2012), if the nuclei and mitotic chromosomes were first stripped of contaminating ribosomes, the ~30-40 nm peak was absent (Joti *et al*, 2012; Nishino *et al*, 2012). Consistent with these results, cryo-EM studies of interphase chromatin and mitotic chromosome (Bouchet-Marquis *et al*, 2006; Eltsov *et al*, 2008; Gan *et al*, 2013) and electron spectroscopic imaging studies of mouse nuclei (Fussner *et al*, 2012) visualized packaged 10-nm fibers but no folded 30-nm fibers, even in the heterochromatin regions. Recent studies using super-resolution imaging also observed heterogeneous groups of nucleosomes (Ricci *et al*, 2015). Collectively, these studies argue for a new chromosome assembly paradigm that does not require folding into 30-nm fibers. Our SAXS analysis of the packaging of nucleosomal array oligomers provides biochemical evidence in support of an alternative model. In our control SAXS experiments, folding of monomeric arrays into 30- nm structures in 2.5 mM MgCl₂ was indicated by the appearance of a peak in the scattering profile at ~30-40 nm (Figs. 3.8A, 3.14A). However, this peak was noticeably absent in the SAXS profiles of both the H1-bound and H1-free oligomers, indicating that the subunit structure of the oligomers is not the 30-nm fiber. Instead, the lack of observed repetitive structures above 20 nm indicates that the subunits adopt extended 10-nm structures. We thus conclude that when studied *in vitro* nucleosomal

arrays and H1-chromatin only form 30-nm fibers under very specific ionic conditions. In addition, given that the peaks at 6 and 11 nm arise from face-to-face and edge-to-edge nucleosome-nucleosome interactions, respectively (Fig. 3.8C)(Langmore & Paulson, 1983), and the fact that linker DNA contributes to oligomer stability (Fig. 3.9), we propose that the individual 10-nm nucleosomal array subunits interdigitate to form a polymer-melt-like structure when packaged into the oligomers. Our studies ultimately provide a rigorous biochemical basis for how long-range chromatin condensation can occur without first forming 30-nm fibers.

Oligomerization absolutely requires the core histone tail domains of the nucleosome. Tailless nucleosomal arrays do not self-associate (Dorigo *et al*, 2003; Schwarz *et al*, 1996; Gordon *et al*, 2005), even in the presence of linker histones (Carruthers & Hansen, 2000). When the H2A, H2B, H3 and H4 tail domains are deleted individually, in each case the MgCl₂ concentration at which 50% of the sample pellets (Mg⁵⁰) is shifted toward higher MgCl₂ concentrations (Dorigo *et al*, 2003; Gordon *et al*, 2005). Removal of the H4 tail has the largest effect on the Mg⁵⁰ (Dorigo *et al*, 2003; Gordon *et al*, 2005), suggesting that it is a particularly important determinant. The need for more MgCl₂ when the tails are deleted implies that they function through an electrostatic-based mechanism. We speculate that the tails at least in part bind to linker DNA and screen negative charge, promoting interdigitated nucleosome-nucleosome interactions and oligomer assembly. In support of this hypothesis, the H4 and H3 tails can be cross-linked in trans to the DNA of other arrays within the packaged oligomers (Kan *et al*, 2009; Zheng *et al*, 2005). Moreover, linker DNA contributes significantly to oligomer stability (Fig. 3.9), as would be expected if it was the binding site for the tails. The H4 tail domain mediates 30-nm fiber folding by binding the acidic patch present on the surface of neighboring nucleosomes (Kalashnikova *et al*, 2013b). However, oligomerization and 30-nm folding are mediated by distinct molecular

mechanisms, and in particular oligomerization does not require H2A/H2B (Schwarz *et al*, 1996). The involvement of the H4 tail in both folding and oligomerization, acting though different mechanisms, provides a potential explanation for why the subunits of the oligomers adopt the 10-nm fiber structure. That is, under conditions where the H4 tails mediate oligomerization they cannot simultaneously interact with the acidic patch of neighboring nucleosomes to promote 30-nm folding. Certain tail post-translational modifications affect the Mg⁵⁰, including H4 acetylation (Shogren-Knaak *et al*, 2006a; Szerlong *et al*, 2010), H4 sumoylation (Dhall *et al*, 2014), and both H2A and H2B ubiquitination (Fierz *et al*, 2011a; Jason *et al*, 2001a). Nucleosome-depleted regions such as those found near promoters and enhancers, and the core histone variant H2A.Z (Fan *et al*, 2002a), move the Mg⁵⁰ toward higher MgCl₂ concentrations relative to nucleosomal arrays alone. The macroH2A variant (Muthurajan *et al*, 2011a), and chromatin architectural proteins such as MeCP2 (Nikitina *et al*, 2007), and Sir3p (McBryant *et al*, 2008), all lower the MgCl₂ concentration at which oligomerization occurs. The large number of physiologically relevant determinants of oligomerization suggests that the equilibrium between local and global nucleosome-nucleosome interactions in any given region of a chromosomal fiber is a tightly regulated point of regulatory control.

3.4 Materials and Methods

3.4.1 Reconstitutions.

Nucleosomal arrays were reconstituted from 12x207 bp 601 or 5S sequence DNA and purified chicken erythrocyte histone octamers using salt dialysis as described (Rogge *et al*, 2013b). The DNA concentration was 0.5 mg/mL and molar ratio of histone octamers to DNA repeats was 1.0-1.1. The extent of template saturation achieved after reconstitution was determined by sedimentation velocity in low salt (Hansen & Lohr, 1993b). The

nucleosomal arrays used in our studies sedimented between 26-29S in TE buffer (Figs. EV2 and 3.7), indicating that about half of the samples contained 11 nucleosomes per template and the other half contained 12 nucleosomes per template (Hansen & Lohr, 1993b). H1-nucleosomal arrays was assembled by mixing purified chicken H1.0 (Talbert *et al*, 2012) and reconstituted nucleosomal arrays at one H1 per DNA repeat in 50 mM NaCl, followed by dialysis against TE buffer overnight, and sedimentation velocity in low salt to determine the extent of H1 binding (Lu *et al*, 2009).

3.4.2 Fluorescence light microscopy of nucleosomal arrays and isolated nuclei.

Two µg of nucleosomal array and H1-nucleosomal array samples were incubated with the desired concentration of MgCl₂ for 15 min on ice and spun onto poly-L-lysine-coated coverslips by centrifugation at 2380 × g for 15 min. The arrays were gently fixed with 2% formaldehyde (Wako, Japan) in the same buffer. After DNA staining with 4',6-diamidino-2- phenylindole (DAPI), the coverslips were sealed with a nail polish. Optical sectioning images with 200 nm thickness were recorded with DeltaVision microscope (Applied Precision) and deconvolved to remove out of focus information. Projected images with 5 sections were shown.

For nuclei imaging, HeLa nuclei isolation was performed as described previously (Takata *et al*, 2013). Isolated nuclei were suspended in H10Mg5 buffer (10 mM HEPES-KOH [pH 7.4] and 5 mM MgCl₂) and attached to poly-L-lysine-coated coverslips by centrifugation at 2380 × g for 15 min. The nuclei on the coverslips were gently placed in the following three buffers: H10Mg5, H10Mg1 (10 mM HEPES-KOH [pH 7.4] and 1 mM MgCl₂), H10E (10 mM HEPES-KOH [pH 7.4] and 1 mM EDTA (pH 8.0)) buffers and then fixed with 2% formaldehyde in the same three buffer. After DNA staining with DAPI, the coverslips were sealed with a nail polish. Sectioning images were recorded and demonstrated as described above.

3.4.3 Transmission electron microscopy.

Nucleosomal array or H1-nucleosomal array samples were incubated with the desired concentration of 30X MgCl₂ for 30 min at room temperature and fixed with 0.1% gluteraldehyde overnight on ice. The DNA concentration was 0.215 mg/mL. Samples (10 µL drops) were deposited on freshly glow discharged formvar and carbon coated copper grids for 2 minutes, either with no dilution, or at 1:20 and 1:40 dilutions. Excess sample was removed from the grids by blotting. The grids were successively stained for 2 min with 2% uranyl acetate, sample buffer, and 1.5% phosphotungstic acid, with blotting in between each. Grids were then examined and photographed using either a JEOL JEM-2000 EX II transmission electron microscope operated at 100kV and captured on film, or a JEOL JEM-1400 transmission electron microscope equipped with an Orius model 832.J76VV0 (Gatan, Inc.) digital camera and operated at 100kV. Images were collected at microscope magnifications from 30,000 to 300,000. Negatives were scanned at 1200 dpi using an Epson Perfection V700 photo scanner and Adobe Photoshop. Images of the grids were processed using ImageJ for figures. Magnified images of the oligomer interiors were obtained by cropping and rescaling the initial images in order to make fine details more apparent.

3.4.4 Analytical ultracentrifugation.

Sedimentation velocity analyses were carried out in a Beckman XL-A or XL-I analytical ultracentrifuge. Experiments measuring the salt-dependent folding of nucleosomal arrays and H1-nucleosomal arrays were performed using the absorbance optical system as described (Lu *et al*, 2009). Absorbance sedimentation velocity data were analyzed by the method of Demeler and van Holde (Demeler & van Holde, 2004a) to yield the diffusion-corrected integral distribution of sedimentation coefficients. Experiments characterizing nucleosomal array and H1-nucleosomal array oligomers were performed using the

interference optical system as described (Rogge & Hansen, 2015). The laser delay and duration for a sharp fringe pattern were determined using a sapphire window cell containing only buffer. The counterbalance was then used for radial calibration of the detector. For each interference sedimentation velocity run, a single nucleosomal array and H1-arrays sample was prepared to a final concentration of 0.215 mg/mL DNA and the desired 30X MgCl₂ concentration, loaded into a cell assembled with sapphire windows, and placed in an An60-Ti rotor. The temperature of the run was 20 °C. The speed of the runs initially was 3000 rpm. After collection of 20-60 interference scans at this speed the oligomeric fraction of the sample had pelleted. The speed was then increased to 25,000 rpm to monitor sedimentation of the unassociated fraction of the sample. The interference sedimentation velocity data initially were analyzed using the second moment method to obtain the weight averaged sedimentation coefficient (*ssm*), The second moment analysis yields *ssm* for each scan, providing that the scan has a defined plateau and meniscus (Demeler, 2005). The *ssm* was plotted against the scan number and linear region of the plot extrapolated to the y-axis to obtain the *ssm* values reported in Figures 3 and 6. The scans also were analyzed by the time derivative method to obtain the sedimentation coefficient distribution, *g(s*)* (Stafford, 1992). All sedimentation coefficients are expressed in Svedberg units (S); one Svedberg is equal to 10⁻¹³ sec. All data editing and analyses were conducted using the UltraScanIII software (Demeler & Gorbet, 2016).

3.4.5 SAXS

SAXS experiments were performed at SPring-8 using the BL45XU beamline. Following the approach of Langmore and Paulson (Langmore & Paulson, 1983), The SAXS data in this paper are shown as plots of $\log(I \times S^2)$ vs. $1/S$, obtained after subtracting buffer scattering. Here, *I* and $1/S$ are the average intensity and inverse of the scattering vector,

respectively. $I \times S^2$ gives the true relative strength (power) of the structural periodicities in the samples (Langmore & Paulson, 1983). A peak in the X-ray scattering at a $1/S$ nm shows a periodicity of $1/S$ nm in the object. The data were averaged within concentric annuli of different radii about the experimental center to yield the average intensity I as a function of S .

BL45XU was set up for the SAXS experiment as follows (Fujisawa et al., 2000). The X-ray wavelength and sample-to-detector distances were 1.0 Å (13.8 keV) and 2.1 m. The sample cell is made of stainless steel with 3mm-thickness sealed by 0.02mm-thick synthetic quarts windows. The sample volume of it is 25µl. The nucleosome array solutions were exposed to the X-ray beam for about 60 sec. Scattering data for the chromosome samples and buffer were collected at room temperature using an imaging plate system (R-AXIS IV++; Rigaku). Native chicken chromatin (Figs. 7C and D) was purified described as (Ura & Kaneda, 2001) with minor modifications.

3.4.6 Micrococcal nuclease digestion

Four µg of 601-nucleosome arrays was incubated in H10Mg5+Ca buffer (10 mM HEPES-KOH [pH 7.4], 0.15 mM CaCl₂, 0.1 mM PMSF, and 5mM MgCl₂) to form the oligomers. For MNase digestion, the oligomers were digested for 5 minutes at 37°C using 1.6 U of MNase per µg of DNA. The reaction was stopped with 1 mM EGTA. The samples were subjected to fluorescence microscopy (FM) imaging or the differential centrifugation assay (10000 rpm for 5min). For FM imaging, the samples were spun onto BSA-coated coverslips and processed as described for the nuclei imaging. For verification of complete MNase digestion, DNA was purified, electrophoresed on 1.2 % agarose gel, and visualized by staining with ethidium bromide.

3.4.7 Computer modeling.

We constructed model structures for a dinucleosome (PDB code: 1kx5), one-start and two-start 30-nm chromatin fiber models with 12-mer nucleosomes, and simulated oligomers containing tightly packed 30-nm chromatin fiber models. The 12-mer nucleosome models for the one-start and the two-start helices were constructed based on the atomic coordinate models with 22-mer nucleosomes, which were kindly provided by Dr. D. Rhodes, LMB, UK (Robinson & Rhodes, 2006; Schalch *et al*, 2005a). The simulated oligomers were modeled as follows. (i) The position and orientation of the first 12-mer (one-start helix or two-start helix) were generated randomly within a sphere with the radius R (Appendix Table SI). (ii) The position and orientation of the second 12-mer were generated randomly within a sphere with the radius R (Appendix Table SI), so that the two 12-mers have a contact. Here two 12-mers are defined to have a contact if the distance between closest nucleosomes of the two 12-mers is less than 12 nm. Selection of the model (one-start or two-start) was done using the random number. (iii) The position and orientation of the third and later 12-mers were generated randomly within a sphere with the radius R (Appendix Table SI), so that the 12-mer has at least two contacts with the previous 12-mers.

In the computation of SAXS profiles for the simulated oligomers, we generated three kinds of simulated oligomers containing 13, 42, and 100 of the 12-mer. SAXS profiles of 10 structures of each simulated oligomer were calculated and their average was obtained. Appendix Table SI summarizes the parameters used in the modeling of the oligomeric structures.

SAXS profiles of the constructed model structures were calculated using the following equation:

$$I(S) = \sum_{i,j} f_i(S) f_j(S) \frac{\sin(2\pi S r_{ij})}{2\pi S r_{ij}}$$

where $f_i(S)$ and r_{ij} are the form factor of the i -th atom and the distance between i -th and j -th atoms, respectively. Here the summation is over non-hydrogen atoms in each model. Software of our own making, which is parallelized using a message passing interface (MPI) library, was adopted to compute SAXS profiles for a few tens of millions of atoms efficiently.

Chapter 4

Unpublished Experiments on Chromatin Oligomers and Future Directions

4.1 Introduction

While the previous chapter details a number of important features of self-associated chromatin oligomers, I have conducted further unpublished experiments that expand upon the published results. The first experiments repeated the results of our previous experiments using chicken erythrocyte histone octamers with core histone octamers constructed with recombinant histone proteins. Native chicken chromatin has long been a model for chromatin structure (Qian *et al*, 1997; Woodcock, 1994; Cui & Bustamante, 2000). The use of the chicken octamers, while very convenient, results in a model system that is not highly manipulatable, as we are limited to chromatin proteins that can be easily isolated from chicken erythrocytes. It would be ideal in the future to move into a model system that uses recombinant histone octamer. The use of recombinant octamers will allow us to interrogate how it is that individual components of chromatin, as well as chromatin architectural proteins, contribute to the structure of chromatin oligomers. As previously mentioned, the contribution of the tails and the effect of replacing the canonical histones with histone variants are attractive research areas (Gordon *et al*, 2005). The feasibility of these experiments is dependent on the chromatin self-association process being similar in these systems and not a unique phenomenon to the chicken histone proteins. We have preliminary results suggesting that the formation of large globular chromatin oligomers occurs with nucleosomal arrays reconstituted using recombinant *Xenopus laevis*.

We have also further investigated the digestion of the chromatin oligomers with micrococcal nuclease as an assay for the accessibility of the chromatin oligomers. The ability of nuclease to digest chromatin samples has frequently been used as an assay for the accessibility of DNA (Holmqvist *et al*, 2005). In addition to experiments which had completely

removed the linker DNA by nuclease digestion (Fig. 3.9), we have conducted experiments in which the linker DNA regions are only partially digested. The partial digest results in a laddering effect with bands of DNA for mononucleosomes, dinucleosomes, trinucleosomes, etc. all the way up to full length 12-mer DNA. Chromatin complexes with more accessible linker DNA are more prone to digestion down to the mononucleosome. We used these experiments to probe the accessibility of chromatin oligomers over a range of Mg²⁺ concentrations, and tested the effect of linker histone inclusion. These experiments suggest that all of DNA within the oligomers is accessible by enzymes and suggests interesting experiments such as *in vitro* transcription assays, which would allow us to investigate interesting biological activities of the self-associated chromatin.

The sedimentation velocity experiments on self-associated chromatin with linker histone yielded unmeasurable results in high magnesium conditions (Fig. 3.12A). The massive increase in size with increasing Mg²⁺ is strange behavior when compared to the plateau in size of the chromatin oligomers without linker histone (Fig 3.4A). Initial transmission electron microscopy experiments with the linker histone containing chromatin oligomers contained a strange branching internal structure. These experiments have not been replicated, but when examined along with the massive increase in sedimentation suggest a possible structural transition in the self-associated chromatin oligomers. While the branched structure may represent a structure which is irrelevant to *in vivo* chromosomes, the transition warrants further investigation. These results have a striking resemblance to chromatin as seen by AFM measurements on chromatin from ruptured chicken erythrocyte nuclei (Qian *et al*, 1997).

4.2 Results

4.2.1 Sedimentation velocity of chromatin oligomers made with recombinant *Xenopus laevis* chromatin oligomers.

We have preliminary data suggesting that the sedimentation of nucleosomal arrays assembled with recombinant *Xenopus* octamers can be measured using the interference optical system. Our control DCA assay demonstrates that these oligomers begin forming at a Mg²⁺ concentration of around 1.5 mM, have an Mg50 of approximately 1.8 mM Mg²⁺, and are entirely oligomeric at a concentration of 3 mM Mg²⁺ (Fig. 4.1A). These results are similar to those of published experiments which utilized *Xenopus laevis* recombinant histone octamers to examine the role of the histone N-terminal tails in chromatin self-association (Dorigo *et al*, 2003; Gordon *et al*, 2005). When we examine the second moment sedimentation coefficient averages these complexes first have an average of around 45,000 S in 1.75 mM Mg²⁺ and increase in size to just over 90,000 S under 4 mM Mg²⁺ conditions (Fig 4.1 B). These results are very similar to what we obtained for oligomers of chromatin made with chicken octamers. These are slightly smaller than the maximum noted with the chicken octamers, however we did not reach the plateau concentration of Mg²⁺ at which we no longer see an increase in sedimentation coefficient before running out of sample for these experiments. In all conditions the chromatin oligomers have a minimum size of 10,000 to 20,000 S with the averages and maximum oligomer size increasing with Mg²⁺ concentration, reaching a maximum size of approximately 350,000 S in 4 mM Mg²⁺ (Fig. 4.1C). Given their similar behavior and distribution of sedimentation coefficients, we believe that the *Xenopus* arrays are likely to reach a maximum size as the chicken chromatin oligomers in previous experiments (Fig. 3.4A). While this needs to be tested further, these results suggest that the recombinant octamers are a tractable system which can be used to test how specific chromatin components contribute to the structure of self-associated chromatin oligomers. Experiments in a recombinant system will allow us to test how

the components of the core histone octamers, histone variants, and additional chromatin architectural proteins affect chromatin oligomers.

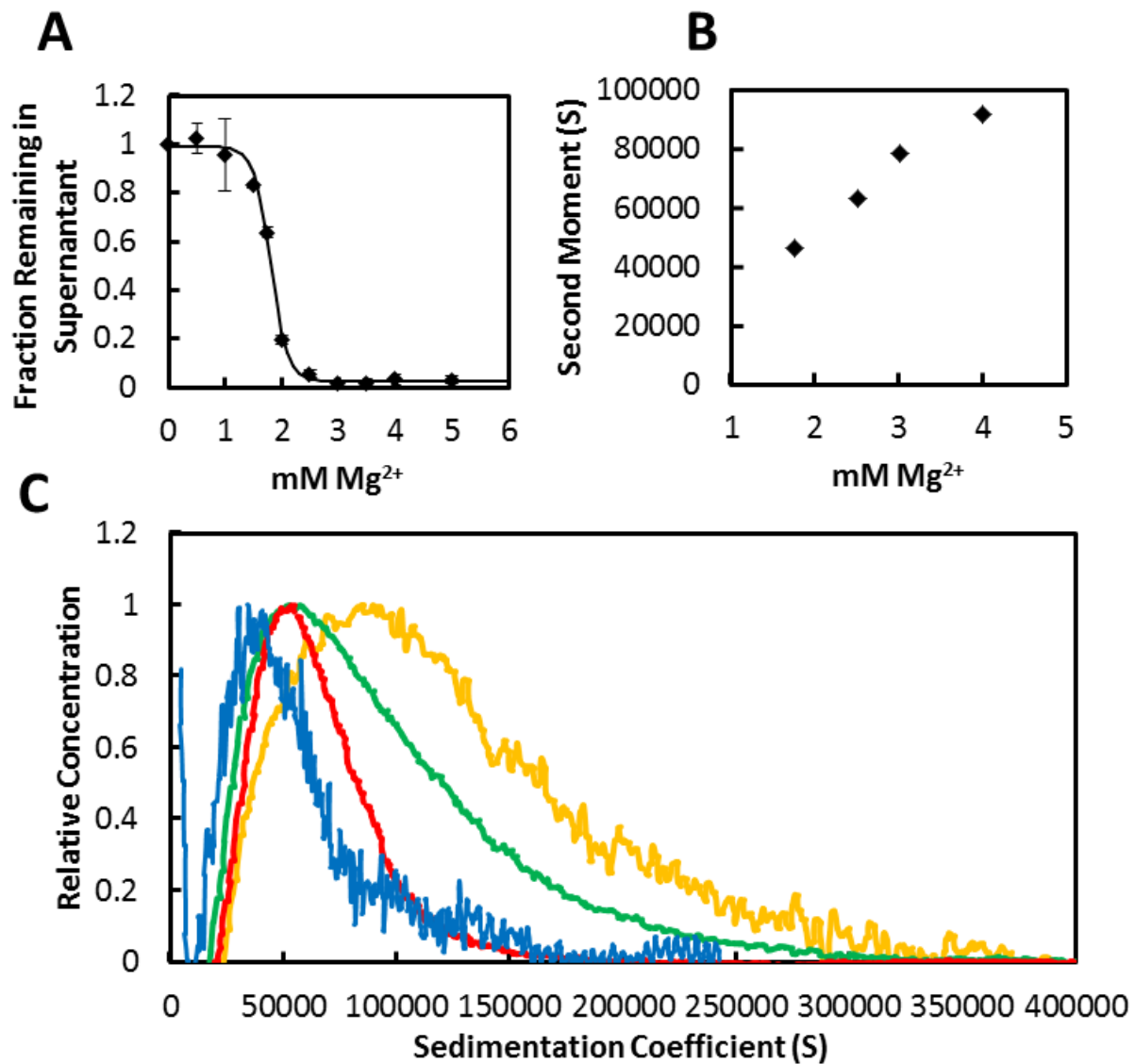


Figure 4.1) Sedimentation of chromatin oligomers constructed with recombinant *Xenopus laevis* octamers. **A.)** DCA assay of self-associated chromatin showing the Mg^{2+} range at which the chromatin forms oligomers. Error bars represent the standard deviation between triplicate results **B.)** Second moment analysis of sediment ion velocity experiments showing the mass average S under increasing Mg^{2+} concentrations. **C.)** Time derivative analysis of sedimentation velocity experiments showing the distribution of oligomer sedimentation coefficients in each condition. The distribution increase with increasing Mg^{2+} concentration with 1.75 mM (blue), 2.5 mM (red), 3 mM (green) and 4 mM

4.2.2 Accesibility of chromatin oligomers assayed using digestion by micrococcal nuclease.

Micrococcal nuclease assays have allowed us to investigate the accessibility of the chromatin oligomers to a small diffusing enzyme. Oligomeric chromatin digested with micrococcal nuclease has shown that increasing the Mg^{2+} concentration leads to a decrease in the ability of the nuclease to cleave the linker DNA (Fig. 4.2A). It is also clear that with increased digestion the chromatin oligomers can be reduced to mononucleosomes suggesting that nearly all linker DNA within the oligomers can be accessed by the enzyme (Fig. 4.2B). The chromatin oligomers containing linker histone are significantly more resistant to digestion by micrococcal nuclease at all Mg^{2+} concentrations tested (Fig. 4.2). The decrease in accessibility of the nuclease to the chromatin oligomers with increasing Mg^{2+} concentration is not apparent in the chromatin oligomers containing linker histone (Fig. 4.2A). These results would seem to indicate that the size of the oligomers is not the primary barrier to accessibility. The linker histone chromatin oligomers are significantly smaller (Fig 3.12A), and yet much less accessible to the micrococcal nuclease under all conditions tested. While these assays offer some insight into the chromatin oligomers, they also indicate that more biologically complex assays on the chromatin oligomers are possible. Experiments testing the ability of polymerase to transcribe DNA in the context of these oligomers are an attractive experiment. These experiments would provide significant support for the biological relevance of self-associated chromatin and provide an excellent model system for determining how structural components of chromatin affect transcription.

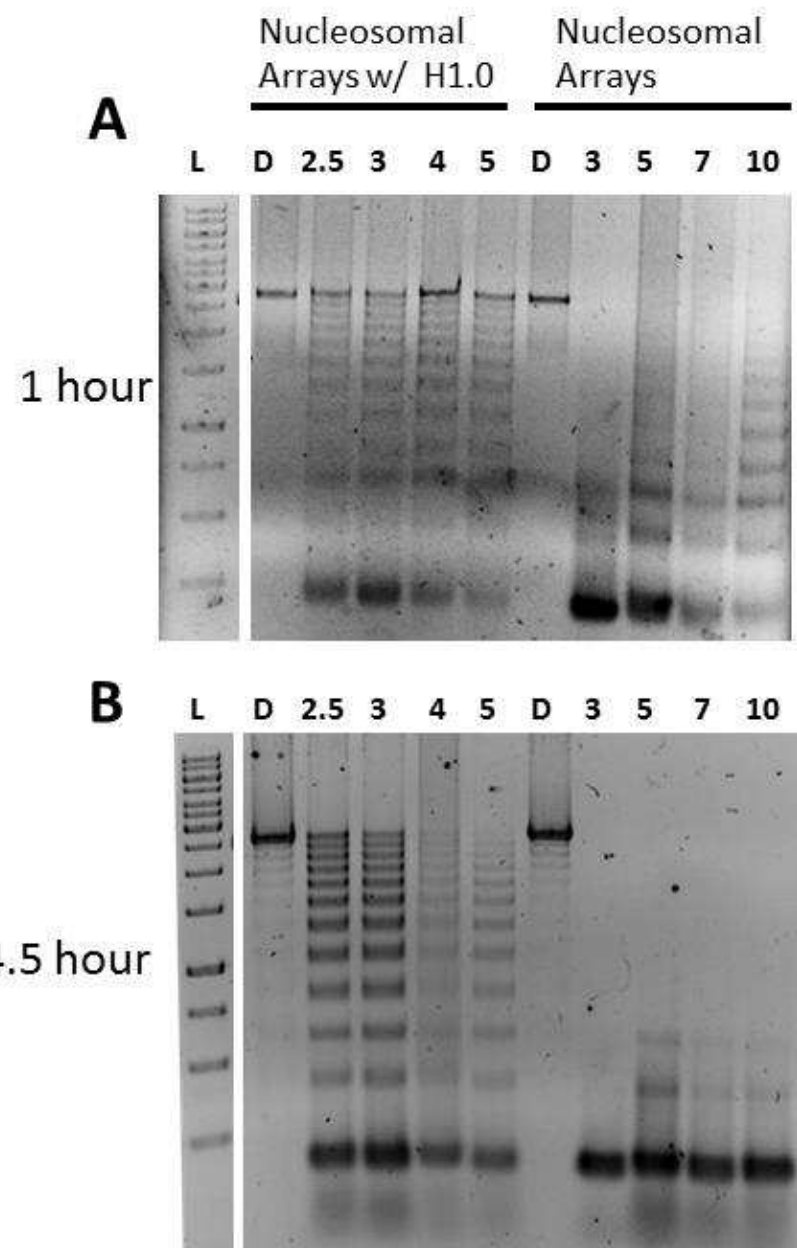


Figure 4.2) Accessibility of chromatin oligomers to digestion by micrococcal nuclease. **A.)** Digestion of chromatin oligomers both with and without chicken linker histone H1.0 for 1 hour. **B.)** Digestion of chromatin oligomers with and without linker histone for 4.5 hours.

4.2.3 Unique internal structure of linker histone chromatin in solution containing high concentrations of Mg²⁺ when examine by TEM.

When we performed sedimentation velocity experiments on chromatin oligomers containing linker histone we determined that the oligomers sedimented far too quickly for us to measure their rate accurately (Fig. 3.12A). Some of these chromatin oligomers also displayed a strange structure when examined by TEM (Fig. 4.3A). These conditions produced incredibly large highly branched structures under these conditions. The subunit structure within the branches appears to be on the order of 10nm which would indicate that these are composed of the self-associated nucleosome arrays (Fig. 4.3B). These samples also contained the more typical globular oligomers noted under all other conditions tested (Fig. 4.3C). These structures may be an artifact of the drying and negative staining which are necessary for the TEM visualizations. They are also highly suggestive of a fundamental change of state. It may be that these highly branched structures exist in solution. These highly connected large branched structures would explain the sedimentation velocity results. It is also possible that while this structure is unique to the staining process for TEM, that it results due to increased interaction between the chromatin complexes in solution. This would also help to explain the rapid sedimentation of the chromatin, attractive forces between the oligomeric complexes could result in an increase in the sedimentation rate.

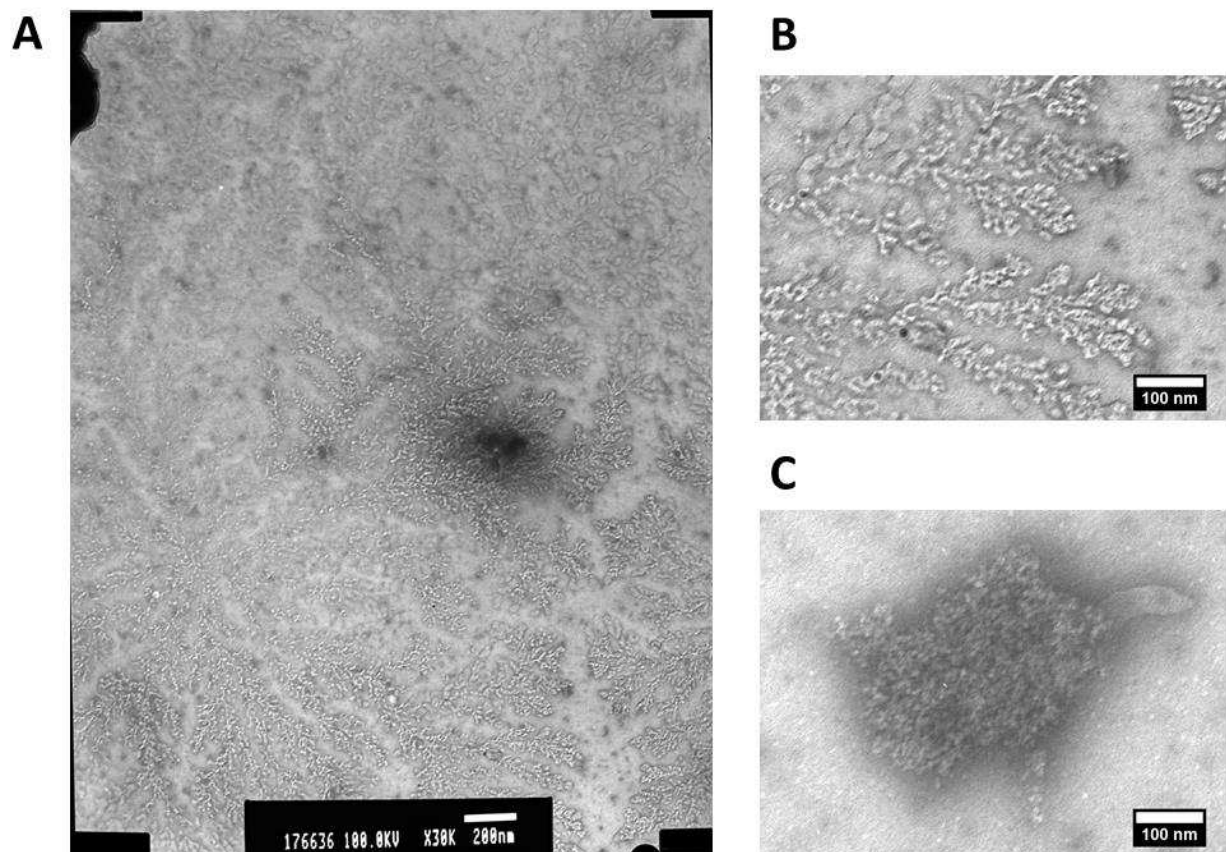


Figure 4.3) Negative stained TEM images of chromatin oligomers with linker histone in 5 mM Mg²⁺. **A.)** Expansive highly branched structures were prevalent on grids containing linker histone chromatin samples self-associated in 5 mM Mg²⁺. Shown is the entire film exposure at 30,000X magnification, the scale bar is 200 nm. **B.)** Enlarged and cropped images of branching subunit structure of these large complexes. **C.)** Globular self-associated chromatin complexes were found under the same conditions on the same EM grids.

4.3 Methods

4.3.1 Sedimentation velocity experiments on chromatin assembled with recombinant *Xenopus laevis* octamer.

Histone octamers were reconstituted with lyophilized proteins from the PEPF at Colorado State University. The histone octamers were assembled by combining equimolar amounts in a chaotropic unfolding buffer containing followed by dialysis into high NaCl Tris buffer. The core histone octamers were purified away from other histone complexes using size exclusion chromatography. The core histone octamer were used to form nucleosomal arrays on 601(207bp)-12mer DNA using step dialysis from high salt buffer to low salt. Assembled nucleosomal arrays were quality controlled for saturation using sedimentation velocity experiments (Hansen & Lohr, 1993b; Rogge *et al*, 2013a). Interference sedimentation velocity experiments were carried out as described in Chapter 2. Analysis of the data was done using UltrascanIII (Demeler, 2005).

4.3.2 Micrococcal nuclease digestion of chromatin oligomers.

Digestion of the chromatin oligomers was carried out by first self-associating the chromatin using the appropriate amount of Mg²⁺ and then separating the oligomeric and monomeric chromatin by centrifugation. Samples were spun for 10 min at 16,000 g. The supernatant was then removed and the oligomeric fraction resuspended in buffer containing the same amount of Mg²⁺ as the samples were self-associated in. Micrococcal nuclease was then added to a concentration of 0.4 U per µg of DNA, as well as CaCl₂ to a final concentration of .075 mM. Samples were then incubated at 37 °C for the desired amount of time. Reactions were stopped by the addition of 0.2 mM EGTA to chelate the Ca²⁺, which is a necessary cofactor for micrococcal nuclease function. Digests were carried out in bulk with 1ug samples pulled and stopped with EGTA and frozen for later analysis. Before agarose gel electrophoresis the samples of chromatin were then deproteinized by treatment with 6 µg of proteinase K and

and SDS at a final concentration of 1 %. These samples were then incubated at 55 °C for 1 hour. Samples were then run on 1.5% agarose gels and imaged using ethidium bromide.

4.3.3 Transmission electron microscopy.

The transmission electron microscopy experiments were performed as in Chapter 3, specific instructions can be found under section 3.4.3.

4.4 Discussion, Future Directions, Speculations

4.4.1 Discussion of unpublished experimental results

In vitro chromatin experiments have been valuable model systems for understanding how the molecular features of chromatin fibers affect the structure and function of chromosomes. The bulk of our experiments have been conducted with purified native chicken octamers, because they are a well characterized, abundant, and relatively easily purified from an industrial byproduct (Yager *et al*, 1989). While endogenous chicken octamers have been a very useful tool allowing for the assembly of large amounts of uniform chromatin, the use of recombinant proteins allows for a range of experiments in which we can dissect the contribution of specific portions of the histone proteins to chromatin self-association. Our preliminary results suggest that interference sedimentation velocity experiments will be a useful assay in studying more tractable chromatin systems. An attractive study is the contributions of the core histone tails to the self-associated structures. Many of the tools to accomplish this study are in place for the lab. The PEPF facility in particular has many of the histone mutants necessary to assemble core histone octamers with deleted tails.

Given that the interference sedimentation velocity experiments require large amounts of sample, the most interesting mutant to begin testing would be those lacking the H4 tails. Previous studies using the DCA technique to test nucleosomal array constructs which were assembled to test the deletion of each of the four histone tails, determined that the H4 tail had

the most significant effect on increasing the amount of Mg²⁺ necessary to induce self-association (Gordon *et al*, 2005). The H4 tails have been shown to be important for nucleosome-nucleosome interactions in a number of studies. The H4 tail interacts with a patch of basic residues on the core histone surface for the formation of folded “30-nm” fibers, but appears to primarily interact with nucleosomal array DNA during self-association (Pepenella *et al*, 2014; Kan *et al*, 2009). The presence of the H4 tail is necessary for intra-array folding, but is not necessary for inter-array interactions and self-association (Dorigo *et al*, 2003). *In vivo* the neutralization of the charges on the H4 tail through acetylation is associated with less compacted chromatin structures and increased transcription (Tse *et al*, 1998; Hebbes *et al*, 1988). One might speculate that the deletion of the H4 tails from the core histones, while shifting the Mg²⁺ necessary to induce self-association, would cause the chromatin oligomers to become smaller in size and more accessible to diffusing proteins. However, our linker histone MNase experiments suggest that the size of complexes is not a primary factor in their accessibility (Fig 4.2, Fig 3.12). In this case the size of the oligomeric complexes may be more closely related to the rate at which the complexes nucleate. A decreased affinity between the nucleosomal arrays might lead to slower rates of new oligomer nucleation, and thus fewer and ultimately larger chromatin oligomers.

A number of additional chromatin factors are known to affect the self-association of chromatin *in vitro*, as determined by the DCA assay. These factors, which were discussed previously, include post-translational modifications of the histone proteins, incorporation of histone variants, and the effects of additional chromatin architectural proteins. Factors known to affect the self-association of chromatin *in vitro* are shown in Table 4.1. These particular components of chromatin are attractive targets for analysis with our expanded set of assays for chromatin oligomer structure. While experiments examining the effect of chromatin composition

on chromatin oligomer structures are important, it would be interesting to develop assays of chromatin function to dissect structure-function relationships in chromatin fibers.

Component	DCA EC ⁵⁰ Shift	Reference	Type
Core Histone Tail Removal	Up	(Gordon <i>et al</i> , 2005)	Core Histone
H2A.Z	Up	(Fan <i>et al</i> , 2002)	Histone Variant
H4 Acetylation	Up	(Allahverdi <i>et al</i> , 2011)	Histone Post-Translational Modification
MacroH2A Linker Domain	Down	(Muthurajan <i>et al</i> , 2011)	Histone Variant
H2A L119 Ub	Down	(Jason <i>et al</i> , 2001)	Histone Post-Translational Modification
Linker Histone	Down	(Lu & Hansen, 2004)	Linker Histone
MeCP2	Down	(Nikitina <i>et al</i> , 2007)	Chromatin Architectural Protein
SIR3p	Down	(McBryant <i>et al</i> , 2008)	Chromatin Architectural Protein

Table 4.1) Chromatin components and their affect on conditions which self-associate nucleosomal arrays *in vitro*. EC⁵⁰ is the effective concentration of cation which induces the arrays to self-associate. For most experiments the cation used was Mg²⁺ and so the EC⁵⁰ is equivalent to the Mg⁵⁰. However, in Allahverdi *et al* multiple cations were tested and in the Fan *et al* self-association was determined under increasing amounts of Zn²⁺.

4.4.2 Future avenues of investigation.

In vitro chromatin transcription experiments are an excellent method for testing how specific chromatin factor might affect the expression of genes. These experiments have been performed relatively frequently, and in most circumstances under conditions which our experiments would indicate the chromatin is likely self-associated. Transcription assays on chromatin templates require Mg²⁺ for the function of RNA Pol II, and generally contain 5 to 10 mM MgCl₂ (Tse *et al*, 1998; Szerlong *et al*, 2010). While these buffers are fairly complex and contain nuclear extracts as another complicating factor, the study by Szerlong *et al* utilizes the results of experiments with significant fractions of self-associated as evidenced by the DCA assay. The samples under these conditions are still transcriptionally active, and in fact display increased transcription as compared to free DNA. These experiments support the idea that the chromatin oligomers are biologically relevant. We could expand upon them by utilizing the methods we have developed to add structural characterizations of the chromatin oligomers under the same buffer conditions necessary for transcription. Assays analyzing the transcription of chromatin oligomers *in vitro* would further illuminate structure-function relationships of self-associated chromatin.

While the sedimentation velocity experiments with the interference optics have been very insightful, they require large amounts of sample and saturated nucleosomal arrays are labor intensive projects. If one was interested in further studying chromatin oligomers it would be prudent to examine alternative methods for sizing the chromatin particles, both to limit the amount of sample used as well as confirm our previous results. Dynamic light scattering experiments might provide a valuable alternative assay for chromatin oligomers. These experiments measure the hydrodynamic properties of particles in solutions. The change in the particles light scattering patterns is directly related the particles Brownian motion, and the rate at which the particles diffuse due to the random motion is dependent on the how much solution the

particles displace (i.e. volume). By tracking the change in light The PMF at CSU has recently acquired a new dynamic light scattering instrument making accomplishing these experiments much easier. These experiments could augment the sedimentation velocity experiments and provide an alternative assay for sizing the chromatin particles.

Our experiments thus far assume that the interactions between separate arrays in solution are representative of long range interactions along a single chromosome. If these globular chromatin oligomers are representative of those along a single polymer, then a single chromatin fiber if long enough should contain a globular compacted state with only intra-array nucleosome-nucleosome interactions. This state should be detectable using modelling tools built into the UltrascanIII software for analyzing sedimentation velocity experiments (Demeler, 2005). The data from a sedimentation velocity experiment can be replicated using the Lamm equation. This requires defining two parameters for the species in solution the sedimentation coefficient (S) as well as the diffusion coefficient (D) which can be modelled using UltraScanIII (Brookes *et al*, 2010). If a reasonable estimate of the partial specific volume can be made, the inverse of the density of macromolecular complex, then shape information can be inferred from the data. This shape information allows for the calculation of a frictional ratio (f/f_0). Frictional ratios are a minimum of 1 for perfect spheres ($f=f_0$), and increase for shapes with higher surface to volume ratios. For extended arrays frictional ratios between 3 and 4 are typical. Ken Lyon, a rotation student in the lab was able to create a DNA template for nucleosome arrays containing 60 repeats of the 601 nucleosome positioning sequence. This long of an array would make a very long folded 30nm fiber with an axial ratio of approximately 20 (600 nm long by 30 nm wide). It should be possible to detect both folded “30 nm” and globular complexes which form only due to intra-array nucleosome interactions in this construct, and to differentiate this state from the extended and folded 30 nm fiber states. The extended nucleosome arrays in low salt should have a frictional ratio of around 4 in low salt conditions. When folded into “30 nm” fibers the

60mer arrays should have a frictional ratio of approximately 1.9. A reduction of frictional ratio past this point without any self-association would be indicative of a globular yet monomeric compacted chromatin fiber. This result could be confirmed using the TEM visualization experiments described previously. One of the primary difficulties in accomplishing these experiments would be ensuring that a majority of the 60mer arrays are saturated. The 12mer arrays have a large body of research, allowing for easy quality control of saturation using sedimentation velocity experiments (Hansen & Lohr, 1993; Jason *et al*, 2001; Garcia-Ramirez *et al*, 1992). The 60mer has not been as well characterized in the literature. Saturation could be controlled for using reconstitution methods which rely on the use of competitor DNA sequences, which have a lower affinity for nucleosome formation (Huynh *et al*, 2005). These competitor sequences are then typically removed using differences in Mg²⁺ self-association concentrations in order to selectively sediment the saturated complexes. It also may be possible to simply characterize the sedimentation coefficient of the large 60mer complexes in the presence of competitor DNA, followed by large scale reconstitutions to match the sedimentation coefficient values. These *in vitro* results would be a small step towards simulating the structural dynamics unique to the incredibly large chromosome polymers found *in vivo*.

4.4.3 Summary and conclusions.

Our experiments suggest a mechanism by which interphase chromosomes can self-organize both in to local domains as well as chromatin territories. The nucleosome alone is sufficient for recapitulating many of the features of chromosomes *in vivo*. While many traditional models of chromosome structure involve the folding of chromatin into a larger helical structure, many new experiments fail to find evidence of the “30nm” fiber as a global chromatin structure. For *in vitro* chromatin structure experiments to further illuminate chromosome structure, it was necessary to investigate chromatin structural dynamics other than the folding of nucleosomal arrays into 30 nm fibers. Our experiments suggest a possible mechanism by which

nucleosome-nucleosome interactions could lead to chromosome formation, and a new model system for understanding how chromatin components ultimately affect chromosomes. The effects of histone modifications, the incorporation of histone variants, and additional chromatin architectural proteins are likely to modulate local chromosome structures and function. Self-associated chromatin oligomers provide an attractive *in vitro* model system for studying these molecular mechanisms of chromatin structure and function.

Bibliography

- Ahmad K & Henikoff S (2002) The Histone Variant H3 . 3 Marks Active Chromatin by Replication-Independent Nucleosome Assembly. *9*: 1191–1200
- Alberts B, Johnson A, Lewis J, Raff M, Roberts K & Walter P (2007) No Title. *Mol. Biol. Cell, Fifth Ed.*
- Albiez H, Cremer M, Tiberi C, Vecchio L, Schermelleh L, Dittrich S, Kupper K, Joffe B, Thormeyer T, von Hase J, Yang S, Rohr K, Leonhardt H, Solovei I, Cremer C, Fakan S & Cremer T (2006) Chromatin domains and the interchromatin compartment form structurally defined and functionally interacting nuclear networks. *Chromosom. Res* **14**: 707–733
- Allahverdi A, Yang R, Korolev N, Fan Y, Davey C a, Liu C-F & Nordenskiöld L (2011) The effects of histone H4 tail acetylations on cation-induced chromatin folding and self-association. *Nucleic Acids Res.* **39**: 1680–91
- Allan J, Hartman P, Crane-Robinson C & Aviles F (1980) The structure of histone H1 and its location in chromatin. *Nature* **288**: 675–679 Available at: <http://www.nature.com/nature/journal/v288/n5792/abs/288675a0.html> [Accessed September 26, 2012]
- Ausio J (2000) Analytical Ultracentrifugation for the Analysis of Chromatin Structure. *Biophys. Chem.* **86**: 141–153
- Bannister AJ & Kouzarides T (2011) Regulation of chromatin by histone modifications. *Nat. Publ. Gr.* **21**: 381–395 Available at: <http://dx.doi.org/10.1038/cr.2011.22>
- Barbieri M, Chotalia M, Fraser J, Lavitas L-M, Dostie J, Pombo A & Nicodemi M (2012) Complexity of chromatin folding is captured by the strings and binders switch model. *Proc. Natl. Acad. Sci. U. S. A.* **109**: 16173–8 Available at: <http://www.ncbi.nlm.nih.gov/pubmed/22988072> [Accessed February 28, 2013]
- Barbieri M, Fraser J, Lavitas LM, Chotalia M, Dostie J, Pombo A & Nicodemi M (2014) A polymer model explains the complexity of large-scale chromatin folding. *Nucleus* **4**: 267–273
- Bazett-Jones DP, Li R, Fussner E, Nisman R & Dehghani H (2008) Elucidating chromatin and nuclear domain architecture with electron spectroscopic imaging. *Chromosome Res.* **16**: 397–412 Available at: <http://www.ncbi.nlm.nih.gov/pubmed/18461480> [Accessed October 9, 2012]
- Black JC, Rechem C Van & Whetstine JR (2012) Review Histone Lysine Methylation Dynamics : Establishment , Regulation , and Biological Impact. *Mol. Cell* **48**: 491–507 Available at: <http://dx.doi.org/10.1016/j.molcel.2012.11.006>
- Blacketer MJ, Feely SJ & Shogren-Knaak M a (2010) Nucleosome interactions and stability in an ordered nucleosome array model system. *J. Biol. Chem.* **285**: 34597–607 Available at: <http://www.ncbi.nlm.nih.gov/pmc/articles/PMC2966075/> [Accessed October 9, 2012]

ertype=abstract [Accessed January 23, 2014]

Bolzer A, Kreth G, Solovei I, Koehler D, Saracoglu K, Fauth C, Müller S, Eils R, Cremer C, Speicher MR & Cremer T (2005) Three-dimensional maps of all chromosomes in human male fibroblast nuclei and prometaphase rosettes. *PLoS Biol.* **3**: 0826–0842

Bouchet-Marquis C, Dubochet J & Fakan S (2006) Cryo-electron microscopy of vitrified sections: a new challenge for the analysis of functional nuclear architecture. *Histochem Cell Biol* **125**: 43–51

Brookes E, Cao W & Demeler B (2010) A two-dimensional spectrum analysis for sedimentation velocity experiments of mixtures with heterogeneity in molecular weight and shape. *Eur. Biophys. J.* **39**: 405–414

Brown PH & Schuck P (2006) Macromolecular size-and-shape distributions by sedimentation velocity analytical ultracentrifugation. *Biophys. J.* **90**: 4651–61 Available at: <http://www.ncbi.nlm.nih.gov/pmc/articles/PMC2267303/> [Accessed April 9, 2012]

Carruthers L, Marton L & Peterson C (2007a) Polyamine analogues: potent inducers of nucleosomal array oligomerization and inhibitors of yeast cell growth. *Biochem. J.* **62**: 453–468 Available at: <http://www.ncbi.nlm.nih.gov/pmc/articles/PMC2267303/> [Accessed August 21, 2012]

Carruthers LM, Bednar J, Woodcock CL & Hansen JC (1998) Linker histones stabilize the intrinsic salt-dependent folding of nucleosomal arrays: mechanistic ramifications for higher-order chromatin folding. *Biochemistry* **37**: 14776–87 Available at: <http://www.ncbi.nlm.nih.gov/pubmed/9778352>

Carruthers LM & Hansen JC (2000) The core histone N termini function independently of linker histones during chromatin condensation. *J Biol Chem* **275**: 37285–37290 Available at: http://www.ncbi.nlm.nih.gov/entrez/query.fcgi?cmd=Retrieve&db=PubMed&dopt=Citation&list_uids=10970897 [Accessed September 11, 2012]

Carruthers LM, Marton LJ & Peterson CL (2007b) Polyamine analogues : potent inducers of nucleosomal array oligomerization and inhibitors of yeast cell growth. *545*: 541–545

Chincholi B, Havlik A & Vold R (1974) Specific refractive index increments of polymer systems at four wavelengths. *J. Chem. Eng. Data* **19**: 4–8 Available at: <http://pubs.acs.org/doi/abs/10.1021/je60061a006>

Correll SJ, Schubert MH & Grigoryev S a (2012) Short nucleosome repeats impose rotational modulations on chromatin fibre folding. *EMBO J.* **31**: 2416–26 Available at: <http://www.ncbi.nlm.nih.gov/pubmed/22473209> [Accessed July 14, 2012]

Cremer T & Cremer M (2010) Chromosome territories. *Cold Spring Harb Perspect Biol* **2**: a003889 Available at: <http://www.ncbi.nlm.nih.gov/pubmed/24504674>

Cui Y & Bustamante C (2000) Pulling a single chromatin fiber reveals the forces that maintain its higher-order structure. *Proc. Nat. Acad. Sci. USA* **97**: 127–132

- Dekker J, Marti-Renom MA & Mirny LA (2013) Exploring the three-dimensional organization of genomes: interpreting chromatin interaction data. *Nat Rev Genet* **14**: 390–403
- Demeler B (2005) UltraScan: a comprehensive data analysis software package for analytical ultracentrifugation experiments. *Mod. Anal. ultracentrifugation Tech.* ...: 210–230
- Demeler B & Gorbet GE (2016) Analytical Ultracentrifugation Data Analysis with UltraScan-III . In *Analytical Ultracentrifugation: Instrumentation, Software, and Applications.* , Uchiyama S Stafford WF & Laue T (eds) Springer
- Demeler B & van Holde KE (2004a) Sedimentation velocity analysis of highly heterogeneous systems. *Anal Biochem* **335**: 279–288
- Demeler B & van Holde KE (2004b) Sedimentation velocity analysis of highly heterogeneous systems. *Anal. Biochem.* **335**: 279–88 Available at:
<http://www.ncbi.nlm.nih.gov/pubmed/15556567> [Accessed June 14, 2012]
- Dhall A, Wei S, Fierz B, Woodcock CL, Lee TH & Chatterjee C (2014) Sumoylated human histone H4 prevents chromatin compaction by inhibiting long-range internucleosomal interactions. *J Biol Chem* **289**: 33827–33837
- Dixon JR, Selvaraj S, Yue F, Kim A, Li Y, Shen Y, Hu M, Liu JS & Ren B (2012) Topological domains in mammalian genomes identified by analysis of chromatin interactions. *Nature* **485**: 376–380 Available at:
<http://www.ncbi.nlm.nih.gov/pmc/articles/PMC3356448/> [Accessed January 20, 2014]
- Dong F, Hansen JC & van Holde KE (1990) {DNA} and protein determinants of nucleosome positioning on sea urchin 5{S} r{RNA} gene sequences in vitro. *Proc Natl Acad Sci U S A* **87**: 5724–5728
- Doniach S (2001) Changes in Biomolecular Conformation Seen by Small Angle X-ray Scattering. *Chem. Rev.* **101**: 1763–1778
- Dorigo B, Schalch T, Bystricky K & Richmond TJ (2003) Chromatin fiber folding: requirement for the histone H4 N-terminal tail. *J. Mol. ...* **2836**: 85–96 Available at:
<http://www.ncbi.nlm.nih.gov/pmc/articles/PMC1283603000251/> [Accessed September 11, 2012]
- Dorigo B, Schalch T, Kulangara A, Duda S, Schroeder RR & Richmond TJ (2004) Nucleosome arrays reveal the two-start organization of the chromatin fiber. *Science* **306**: 1571–3 Available at: <http://www.ncbi.nlm.nih.gov/pmc/articles/PMC1556786/> [Accessed July 26, 2012]
- Dubin SB, Benedek GB, Bancroft FC & Freifelder D (1970) Molecular Weights of Coliphages and Coliphage DNA. *J. Mol. Biol.* **54**: 547–556
- Eagen KP, Hartl TA & Kornberg RD (2015) Stable Chromosome Condensation Revealed by Chromosome Conformation Capture. *Cell* **163**: 934–946 Available at: http://ac.els-cdn.com/S0092867415013409/1-s2.0-S0092867415013409-main.pdf?_tid=6c0bc948-c498-11e5-96a1-00000aacb361&acdnat=1453859643_9bf7b5f70190736bd473501aa399fa76

- Earnshaw WC & Laemmli UK (1983) Architecture of metaphase chromosomes and chromosome scaffolds. *J Cell Biol* **96**: 84–93
- Eberharter A & Becker PB (2002) Histone acetylation : a switch between repressive and permissive chromatin Second in review series on chromatin dynamics. *3*: 224–229
- Eltsov MM, Maclellan KM, Maeshima K, Frangakis AS & Dubochet J (2008) Analysis of cryo-electron microscopy images does not support the existence of 30-nm chromatin fibers in mitotic chromosomes in situ. *Proc. Natl. Acad. Sci. U. S. A.* **105**: 19732–7 Available at: <http://www.pubmedcentral.nih.gov/articlerender.fcgi?artid=2604964&tool=pmcentrez&rendertype=abstract>
- Fan JY, Gordon F, Luger K, Hansen JC & Tremethick DJ (2002a) The essential histone variant H2A.Z regulates the equilibrium between different chromatin conformational states. *Nat Struct Biol* **9**: 172–176
- Fan JY, Gordon F, Luger K, Hansen JC & Tremethick DJ (2002b) The essential histone variant H2A.Z regulates the equilibrium between different chromatin conformational states. *Nat. Struct. Biol.* **9**: 172–6 Available at: <http://www.ncbi.nlm.nih.gov/pubmed/11850638> [Accessed July 16, 2012]
- Fan Y, Nikitina T, Morin-Kensicki EM, Zhao J, Magnuson TR, Woodcock CL & Skoultchi AI (2003) H1 linker histones are essential for mouse development and affect nucleosome spacing in vivo. *Mol Cell Biol* **23**: 4559–4572
- Fan Y, Nikitina T, Zhao J, Fleury TJ, Bhattacharyya R, Bouhassira EE, Stein A, Woodcock CL & Skoultchi AI (2005) Histone H1 depletion in mammals alters global chromatin structure but causes specific changes in gene regulation. *Cell* **123**: 1199–1212
- Fierz B, Chatterjee C, McGinty K, Bar-dagan M & Muir W (2011a) Histone H2B ubiquitylation disrupts local and higher-order chromatin compaction. *Nat. Chem. Biol.* **7**: 1–7 Available at: <http://dx.doi.org/10.1038/nchembio.501>
- Fierz B, Chatterjee C, McGinty RK, Bar-Dagan M, Raleigh DP, Muir TW, McGinty K, Muir W, Bar-Dagan M & Muir W (2011b) Histone H2B ubiquitylation disrupts local and higher-order chromatin compaction. *Nat. Chem. ...* **7**: 113–119 Available at: <http://dx.doi.org/10.1038/nchembio.501> [Accessed September 26, 2012]
- Finch JT & Klug a (1976) Solenoidal model for superstructure in chromatin. *Proc Natl Acad Sci U S A* **73**: 1897–1901 Available at: <http://www.pubmedcentral.nih.gov/articlerender.fcgi?artid=430414&tool=pmcentrez&rendertype=abstract>
- Fletcher T, Serwer P & Hansen J (1994) Quantitative analysis of macromolecular conformational changes using agarose gel electrophoresis: application to chromatin folding. *Biochemistry* **33**: 10859–10863 Available at: <http://pubs.acs.org/doi/abs/10.1021/bi00202a002> [Accessed September 11, 2012]
- Fussner E, Strauss M, Djuric U, Li R, Ahmed K, Hart M, Ellis J & Bazett-Jones DP (2012) Open and closed domains in the mouse genome are configured as 10-nm chromatin fibres. *EMBO Rep.* **13**: 1–5 Available at: <http://www.ncbi.nlm.nih.gov/pubmed/22986547>

[Accessed October 4, 2012]

Gajiwala KS & Burley SK (2000) Winged helix proteins. *Curr. Opin. Struct. Biol.* **10**: 110–6
Available at: <http://www.ncbi.nlm.nih.gov/pubmed/10679470>

Gan L, Ladinsky MS & Jensen GJ (2013) Chromatin in a marine picoeukaryote is a disordered assemblage of nucleosomes. *Chromosoma* **122**: 377–386

Garcia-Ramirez M, Dong F & Ausio J (1992) Role of the histone ‘tails’ in the folding of oligonucleosomes depleted of histone H1. *J. Biol. Chem.* **267**: 19587–95 Available at: <http://www.ncbi.nlm.nih.gov/pubmed/1527076>

Gilbert N, Boyle S, Fiegler H, Woodfine K, Carter NP & Bickmore WA (2004) Chromatin architecture of the human genome: gene-rich domains are enriched in open chromatin fibers. *Cell* **118**: 555–566

Gordon F, Luger K & Hansen JC (2005) The Core Histone N-terminal Tail Domains Function Independently and Additively during Salt-dependent Oligomerization of Nucleosomal Arrays *. *J. Biol. Chem.* **280**: 33701–33706 Available at: <http://www.ncbi.nlm.nih.gov/pubmed/16033758> [Accessed March 17, 2012]

Grigoryev SA, Arya G, Correll S, Woodcock CL & Schlick T (2009) Evidence for heteromorphic chromatin fibers from analysis of nucleosome interactions. *Proc Natl Acad Sci U S A* **106**: 13317–13322

Grigoryev SA & Woodcock CL (2012) Chromatin organization — The 30 nm fiber. *Exp. Cell Res.* : 8–15 Available at: <http://dx.doi.org/10.1016/j.yexcr.2012.02.014>

Hansen JC (2002) Conformational dynamics of the chromatin fiber in solution: determinants, mechanisms, and functions. *Annu. Rev. Biophys. Biomol. Struct.* **31**: 361–92 Available at: <http://www.ncbi.nlm.nih.gov/pubmed/11988475> [Accessed June 23, 2011]

Hansen JC, Ausio J, Stanik VH & van Holde KE (1989) Homogeneous reconstituted oligonucleosomes, evidence for salt-dependent folding in the absence of histone H1. *Biochemistry* **28**: 9129–36 Available at: <http://www.ncbi.nlm.nih.gov/pubmed/2605246> [Accessed January 23, 2014]

Hansen JC & Lohr D (1993a) Assembly and structural properties of subsaturated chromatin arrays. *J. Biol. Chem.* **268**: 5840–8 Available at: <http://www.ncbi.nlm.nih.gov/pubmed/8449950> [Accessed June 14, 2012]

Hansen JC & Lohr D (1993b) Assembly and structural properties of subsaturated chromatin arrays. *J. Biol. Chem.* **268**: 5840–8 Available at: <http://www.ncbi.nlm.nih.gov/pubmed/8449950> [Accessed June 14, 2012]

Happel N & Doenecke D (2009) Histone H1 and its isoforms: contribution to chromatin structure and function. *Gene* **431**: 1–12 Available at: <http://www.ncbi.nlm.nih.gov/pubmed/19059319> [Accessed March 19, 2012]

Hashimoto H, Takami Y, Sonoda E, Iwasaki T, Iwano H, Tachibana M, Takeda S, Nakayama T, Kimura H & Shinkai Y (2010) Histone H1 null vertebrate cells exhibit altered nucleosome

architecture. *Nucleic Acids Res.* **38**: 3533–3545

Hayes JJ & Wolffe A P (1993) Preferential and asymmetric interaction of linker histones with 5S DNA in the nucleosome. *Proc. Natl. Acad. Sci. U. S. A.* **90**: 6415–9 Available at: <http://www.ncbi.nlm.nih.gov/pmc/articles/PMC46942/> [Accessed August 13, 2012]

Hebbes TR, Thorne AW & Crane-Robinson C (1988) A direct link between core histone acetylation and transcriptionally active chromatin. *EMBO J.* **7**: 1395–1402 Available at: <http://www.ncbi.nlm.nih.gov/pmc/articles/3409869/> [Accessed August 13, 2012]

Hihara S, Pack C-GG, Kaizu K, Tani T, Hanafusa T, Nozaki T, Takemoto S, Yoshimi T, Yokota H, Imamoto N, Sako Y, Kinjo M, Takahashi K, Nagai T & Maeshima K (2012) Local nucleosome dynamics facilitate chromatin accessibility in living mammalian cells. *Cell Rep* **2**: 1645–1656 Available at: <http://www.ncbi.nlm.nih.gov/pmc/articles/2324600/> [Accessed August 2, 2014]

Hirano T (2015) Chromosome Dynamics during Mitosis. *Cold Spring Harb Perspect Biol* **7**:

Holde K Van & Weischet W (1978) Boundary analysis of sedimentation velocity experiments with monodisperse and paucidisperse solutes. *Biopolymers* **17**: 1387–1403 Available at: <http://onlinelibrary.wiley.com/doi/10.1002/bip.1978.360170602/abstract> [Accessed August 21, 2012]

Holmqvist P-H, Belikov S, Zaret KS & Wrangé O (2005) FoxA1 binding to the MMTV LTR modulates chromatin structure and transcription. *Exp. Cell Res.* **304**: 593–603 Available at: <http://www.ncbi.nlm.nih.gov/pmc/articles/1574890/> [Accessed November 7, 2011]

Hudson DF, Vagnarelli P, Gassmann R & Earnshaw WC (2003) Condensin is required for nonhistone protein assembly and structural integrity of vertebrate mitotic chromosomes. *Dev Cell* **5**: 323–336

Hussain S, Goutte-gattat D, Becker N, Meyer S, Shubhdarshan Shukla M, Hayes JJ, Everaers R, Angelov D, Bednar J & Dimitrov S (2010) Single-base resolution mapping of H1-nucleosome interaction and 3D organization of the nucleosome. *Proc. Natl. Acad. Sci.* **107**: 1–6

Huynh VAT, Robinson PJJPJJ & Rhodes D (2005) A Method for the In Vitro Reconstitution of a Defined ‘30nm’ Chromatin Fibre Containing Stoichiometric Amounts of the Linker Histone. *J. Mol. Biol.* **345**: 957–968 Available at: <http://www.sciencedirect.com/science/article/pii/S0022283604013968> [Accessed August 13, 2012]

Igarashi K & Kashiwagi K (2000) Polyamines : Mysterious Modulators of Cellular Functions. *564*: 559–564

Jason L, Moore S, Ausió J & Lindsey G (2001a) Magnesium-dependent association and folding of oligonucleosomes reconstituted with ubiquitinated H2A. *J. Biol. Chem.* **276**: 14597–14601 Available at: <http://www.jbc.org/cgi/doi/10.1074/jbc.M011153200> [Accessed August 21, 2012]

Jason LJ, Moore SC, Ausió J, Lindsey G, Ausio J & Lindsey G (2001b) Magnesium-dependent association and folding of oligonucleosomes reconstituted with ubiquitinated H2A. *J. Biol. Chem.* **276**: 14597–601 Available at: <http://www.ncbi.nlm.nih.gov/pubmed/11278847> [Accessed August 21, 2012]

Jason LJMLJ, Moore SCSC, Ausio J, Lindsey G, Ausió J, Lindsey G, Ausio J & Lindsey G (2001c) Magnesium-dependent association and folding of oligonucleosomes reconstituted with ubiquitinated H2A. *J. Biol. Chem.* **276**: 14597–14601 Available at: <http://www.jbc.org/cgi/doi/10.1074/jbc.M011153200> [Accessed August 21, 2012]

Joti Y, Hikima T, Nishino Y, Kamada F, Hihara S, Takata H, Ishikawa T & Maeshima K (2012) Chromosomes without a 30-nm chromatin fiber. *Nucleus* **3**: 404–10 Available at: <http://www.pubmedcentral.nih.gov/articlerender.fcgi?artid=3474659&tool=pmcentrez&rendertype=abstract>

Kalashnikova AA, Porter-Goff ME, Muthurajan UM, Luger K & Hansen JC (2013a) The role of the nucleosome acidic patch in modulating higher order chromatin structure. *J. R. Soc. Interface* **10**: 20121022 Available at: <http://www.pubmedcentral.nih.gov/articlerender.fcgi?artid=3627075&tool=pmcentrez&rendertype=abstract>

Kalashnikova AA, Porter-Goff ME, Muthurajan UM, Luger K & Hansen JC (2013b) The role of the nucleosome acidic patch in modulating higher order chromatin structure. *J R Soc Interface* **10**: 20121022

Kalashnikova AA, Winkler DD, Mcbryant SJ, Henderson RK, Herman JA, Deluca JG, Luger K, Prenni JE & Hansen JC (2013c) Linker histone H1 . 0 interacts with an extensive network of proteins found in the nucleolus. *41*: 4026–4035

Kamakaka RT & Biggins S (2005) Histone variants : deviants ? : 295–310

Kan PY, Caterino TL & Hayes JJ (2009) The H4 tail domain participates in intra- and internucleosome interactions with protein and DNA during folding and oligomerization of nucleosome arrays. *Mol Cell Biol* **29**: 538–546

Korolev N, Allahverdi A, Yang Y, Fan Y, Lyubartsev AP & Nordenskiöld L (2010) Electrostatic origin of salt-induced nucleosome array compaction. *Biophys. J.* **99**: 1896–905 Available at: <http://www.pubmedcentral.nih.gov/articlerender.fcgi?artid=2941033&tool=pmcentrez&rendertype=abstract> [Accessed September 26, 2012]

Langmore JP & Paulson JR (1983) Low angle x-ray diffraction studies of chromatin structure in vivo and in isolated nuclei and metaphase chromosomes. *J. Cell Biol.* **96**: 1120–31 Available at: <http://www.pubmedcentral.nih.gov/articlerender.fcgi?artid=2112310&tool=pmcentrez&rendertype=abstract>

Langmore JP & Schutt C (1980) The higher order structure of chicken erythrocyte chromosomes in vivo. *Nature* **288**: 620–622

Li G & Zhu P (2015) Structure and organization of chromatin fiber in the nucleus. *FEBS Lett*

Lieberman-Aiden E, van Berkum NL, Williams L, Imakaev M, Ragoczy T, Telling A, Amit I, Lajoie BR, Sabo PJ, Dorschner MO, Sandstrom R, Bernstein B, Bender MA, Groudine M, Gyorke A, Stamatoyannopoulos J, Mirny L a, Lander ES & Dekker J (2009) Comprehensive mapping of long-range interactions reveals folding principles of the human genome. *Science* **326**: 289–93 Available at: <http://www.pubmedcentral.nih.gov/articlerender.fcgi?artid=2858594&tool=pmcentrez&rendertype=abstract> [Accessed July 13, 2012]

Liu Y, Lu C, Yang Y, Fan Y, Yang R, Liu C-FF, Korolev N, Nordenskiold L, Nordenskiöld L & Nordenskiold L (2011) Influence of histone tails and H4 tail acetylations on nucleosome-nucleosome interactions. *J. Mol. Biol.* **414**: 749–64 Available at: <http://www.ncbi.nlm.nih.gov/pubmed/22051513> [Accessed July 19, 2012]

Lowary PT & Widom J (1998) New DNA sequence rules for high affinity binding to histone octamer and sequence-directed nucleosome positioning. *J Mol Biol* **276**: 19–42 Available at: <http://www.sciencedirect.com/science/article/pii/S0022283697914947>

Lu X, Hamkalo B, Parseghian MH & Hansen JC (2009) Chromatin condensing functions of the linker histone C-terminal domain are mediated by specific amino acid composition and intrinsic protein disorder. *Biochemistry* **48**: 164–72 Available at: <http://www.pubmedcentral.nih.gov/articlerender.fcgi?artid=2644900&tool=pmcentrez&rendertype=abstract>

Lu X & Hansen JC (2004) Identification of specific functional subdomains within the linker histone H10 C-terminal domain. *J. Biol. Chem.* **279**: 8701–7 Available at: <http://www.ncbi.nlm.nih.gov/pubmed/14668337> [Accessed March 8, 2012]

Lu X, Klonoski JM, Resch MG & Hansen JC (2006) In vitro chromatin self-association and its relevance to genome architecture. *Biochem. cell ...* **84**: 411–417 Available at: <http://www.ingentaconnect.com/content/nrc/bcb/2006/00000084/00000004/art00003> [Accessed August 21, 2012]

Lu X & Simon M (2008) The effect of H3K79 dimethylation and H4K20 trimethylation on nucleosome and chromatin structure. *Nat. Struct. ...* **15**: 1122–1124 Available at: <http://www.nature.com/nsmb/journal/vaop/ncurrent/full/nsmb.1489.html> [Accessed August 21, 2012]

Luger K, Mader AW, Richmond RK, Sargent DF & Richmond TJ (1997) Crystal structure of the nucleosome core particle at 2.8 Å resolution. *Nature* **7**: 251–260 Available at: <http://128.122.244.100/research/sb/PSB/PSB08/Week2/Luger.pdf> [Accessed June 13, 2012]

MacRaild CA, Hatters DM, Lawrence LJ & Howlett GJ (2003) Sedimentation velocity analysis of flexible macromolecules: self-association and tangling of amyloid fibrils. *Biophys J* **84**: 2562–2569 Available at: <http://www.pubmedcentral.nih.gov/articlerender.fcgi?artid=1302822&tool=pmcentrez&rendertype=abstract>

Maeshima K, Hihara S & Eltsov M (2010) Chromatin structure: does the 30-nm fibre exist in vivo? *Curr Opin Cell Biol* **22**: 291–297 Available at: <http://www.ncbi.nlm.nih.gov/pubmed/20346642> [Accessed March 1, 2012]

Maeshima K, Imai R, Hikima T & Joti Y (2014a) Chromatin structure revealed by X-ray scattering analysis and computational modeling. *Methods* **70**: 154–161 Available at: <http://www.ncbi.nlm.nih.gov/pubmed/25168089> [Accessed September 17, 2014]

Maeshima K, Imai R, Tamura S & Nozaki T (2014b) Chromatin as dynamic 10-nm fibers. *Chromosoma*

Maeshima K, Rogge R, Joti Y, Hikima T, Tamura S, Szerlong H, Krause C, Herman J, Ishikawa T, DeLuca J & Hansen JC (2015) Nucleosomal arrays self-assemble into hierarchical globular structures lacking 30nm fibers. *Manuscr. Prep.*

Maze I, Noh K, Soshnev AA & Allis CD (2014) Every amino acid matters : essential contributions of histone variants to mammalian development and disease. *Nat. Publ. Gr.* **15**: 259–271 Available at: <http://dx.doi.org/10.1038/nrg3673>

McBryant SJ, Krause C, Woodcock CL & Hansen JC (2008) The silent information regulator 3 protein, SIR3p, binds to chromatin fibers and assembles a hypercondensed chromatin architecture in the presence of salt. *Mol Cell Biol* **28**: 3563–3572

McBryant SSJSSJ, Adams VHV & Hansen JJC (2006) Chromatin architectural proteins. *Chromosome Res.* **14**: 39–51 Available at: <http://www.springerlink.com/index/T212N7327721P7T6.pdf> [Accessed June 13, 2012]

Misteli T, Gunjan A, Hock R, Bustin M & Brown DT (2000) Dynamic binding of histone H1 to chromatin in living cells. *Nature* **408**: 877–881

Muthurajan UM, McBryant SJ, Lu X, Hansen JC & Luger K (2011a) The linker region of macroH2A promotes self-association of nucleosomal arrays. *J Biol Chem* **286**: 23852–23864

Muthurajan UM, McBryant SJ, Lu X, Hansen JC & Luger K (2011b) The linker region of macroH2A promotes self-association of nucleosomal arrays. *J. Biol. Chem.* **286**: 23852–64 Available at: <http://www.pubmedcentral.nih.gov/articlerender.fcgi?artid=3129167&tool=pmcentrez&rendertype=abstract> [Accessed August 20, 2012]

Nagano T, Lubling Y, Stevens TJ, Schoenfelder S, Yaffe E, Dean W, Laue ED, Tanay A & Fraser P (2013) variability in chromosome structure. Available at: <http://dx.doi.org/10.1038/nature12593>

Nikitina T, Shi X, Ghosh RP, Horowitz-Scherer RA, Hansen JC & Woodcock CL (2007) Multiple modes of interaction between the methylated DNA binding protein MeCP2 and chromatin. *Mol Cell Biol* **27**: 864–877

Nishino Y, Eltsov M, Joti Y, Ito K, Takata H, Takahashi Y, Hihara S, Frangakis AS, Imamoto N, Ishikawa T & Maeshima K (2012) Human mitotic chromosomes consist predominantly of irregularly folded nucleosome fibres without a 30-nm chromatin structure. *EMBO J.* **31**: 1644–1653 Available at: <http://www.ncbi.nlm.nih.gov/pubmed/22343941> [Accessed March 12, 2012]

Nora EP, Lajoie BR, Schulz EG, Giorgetti L, Okamoto I, Servant N, Piolot T, van Berlum NL,

- Meisig J, Sedat JW, Gribnau J, Barillot E, BLüthgen N, Dekker J & Heard E (2012) Spatial partitioning of the regulatory landscape of the X-inactivation centre. . *Nat.* **485**: 381–5.
- Ohta S, Wood L, Bukowski-Wills JC, Rappaport J & Earnshaw WC (2010) Building mitotic chromosomes. *Curr Opin Cell Biol* **23**: 114–121
- Ong C & Corces VG (2014) CTCF : an architectural protein bridging genome topology and function. *Nat. Publ. Gr.* **15**: 234–246 Available at: <http://dx.doi.org/10.1038/nrg3663>
- Pepegnella S, Murphy KJ & Hayes JJ (2014) Intra- and inter-nucleosome interactions of the core histone tail domains in higher-order chromatin structure. *Chromosoma* **123**: 3–13
- Qian RL, Liu ZX, Zhou MY, Xie HY, Jiang C, Yan ZJ, Li MQ, Zhang Y & Hu J (1997) Visualization of chromatin folding patterns in chicken erythrocytes by atomic force microscopy (AFM). *Cell Res.* **7**: 143–50 Available at: <http://www.ncbi.nlm.nih.gov/pubmed/9444393>
- Rao SS, Huntley MH, Durand NC, Stamenova EK, Bochkov ID, Robinson JT, Sanborn AL, Machol I, Omer AD, Lander ES & Aiden EL (2014) A 3D map of the human genome at kilobase resolution reveals principles of chromatin looping. *Cell* **159**: 1665–1680
- Ricci MAA, Manzo C, García-Parajo MF, Lakadamyali M, Cosma MPP, Garcia-Parajo MF, Lakadamyali M & Cosma MPP (2015) Chromatin fibers are formed by heterogeneous groups of nucleosomes in vivo. *Cell* **160**: 1145–1158 Available at: <http://linkinghub.elsevier.com/retrieve/pii/S0092867415001324>
- Robinson PJ & Rhodes D (2006) Structure of the ‘30 nm’ chromatin fibre: a key role for the linker histone. *Curr Opin Struct Biol* **16**: 336–343
- Robinson PPJJ, Fairall L, Huynh VAT & Rhodes D (2006) EM measurements define the dimensions of the ‘30-nm’ chromatin fiber: evidence for a compact, interdigitated structure. *Proc. ...* **103**: 6506–6511 Available at: <http://www.pnas.org/content/103/17/6506.short> [Accessed November 27, 2012]
- Roe R-J (2000) Methods of X-Ray and Neutron Scattering in Polymer Science.
- Rogge R a, Kalashnikova A a, Muthurajan UM, Porter-Goff ME, Luger K & Hansen JC (2013a) Assembly of nucleosomal arrays from recombinant core histones and nucleosome positioning DNA. *J. Vis. Exp.*: 1–10 Available at: <http://www.ncbi.nlm.nih.gov/pubmed/24056546> [Accessed December 4, 2013]
- Rogge RA & Hansen JC (2015) Sedimentation Velocity Analysis of Large Oligomeric Chromatin Complexes Using Interference Detection. *Methods Enzymol. Anal. Ultracentrifugation* : 1–14 Available at: <http://linkinghub.elsevier.com/retrieve/pii/S0076687915003055>
- Rogge RA, Kalashnikova AA, Muthurajan UM, Porter-Goff ME, Luger K & Hansen JC (2013b) Assembly of nucleosomal arrays from recombinant core histones and nucleosome positioning DNA. *J Vis Exp*
- Rossetto D, Avvakumov N & Côté J (2012) A chromatin modification involved in diverse nuclear events Histone phosphorylation. *7*: 1098–1108

Sanborn AL, Rao SSP, Huang S-C, Durand NC, Huntley MH, Jewett AI, Bochkov ID, Chinnappan D, Cutkosky A, Li J, Geeting KP, Gnrke A, Melnikov A, McKenna D, Stamenova EK, Lander ES & Aiden EL (2015) Chromatin extrusion explains key features of loop and domain formation in wild-type and engineered genomes. *Proc. Natl. Acad. Sci.* **112**: 201518552 Available at:
<http://www.ncbi.nlm.nih.gov/pmc/articles/PMC4664323/> [Accessed July 14, 2012]

Schalch T, Duda S, Sargent DF & Richmond TJ (2005a) X-ray structure of a tetranucleosome and its implications for the chromatin fibre. *Nature* **436**: 138–141

Schalch T, Duda S, Sargent DF & Richmond TJ (2005b) X-ray structure of a tetranucleosome and its implications for the chromatin fibre. *Nature* **436**: 138–41 Available at:
<http://www.ncbi.nlm.nih.gov/pubmed/16001076> [Accessed July 14, 2012]

Schuck P (2013) Analytical Ultracentrifugation as a Tool for Studying Protein Interactions. *Biophys Rev* **5**: 159–171

Schuck P & Demeler B (1999) Direct sedimentation analysis of interference optical data in analytical ultracentrifugation. *Biophys. J.* **76**: 2288–96 Available at:
<http://www.ncbi.nlm.nih.gov/pmc/articles/PMC1300201/> [Accessed July 14, 2012]

Schwarz PM, Felthauser A, Fletcher TM & Hansen JC (1996) Reversible oligonucleosome self-association: dependence on divalent cations and core histone tail domains. *Biochemistry* **35**: 4009–15 Available at: <http://www.ncbi.nlm.nih.gov/pubmed/8672434>

Schwarz PM & Hansen JC (1994) Formation and stability of higher order chromatin structures. Contributions of the histone octamer. *J Biol Chem* **269**: 16284–16289

Sexton T, Yaffe E, Kenigsberg E, Bantignies F, Leblanc B, Hoichman M, Parrinello H, Tanay A & Cavalli G (2012) Three-Dimensional Folding and Functional Organization Principles of the Drosophila Genome. *Cell* **148**: 458–472

Shaw BR, Herman TM, Kovacic RT, Beaudreau GS & Holde KEVAN (1976) Analysis of subunit organization in chicken erythrocyte chromatin. *Proc. Natl. Acad. Sci. United States Am.* **73**: 505–509

Shogren-Knaak M, Ishii H, Sun JM, Pazin MJ, Davie JR & Peterson CL (2006a) Histone H4-K16 acetylation controls chromatin structure and protein interactions. *Science (80-.).* **311**: 844–847 Available at: <http://classic.sciencemag.org/content/311/5762/844.full.pdf>

Shogren-Knaak M, Ishii H, Sun J-MM, Pazin MJ, Davie JR & Peterson CL (2006b) Histone H4-K16 acetylation controls chromatin structure and protein interactions. *Science* **311**: 844–7 Available at: <http://classic.sciencemag.org/content/311/5762/844.full.pdf> [Accessed July 20, 2012]

Simpson RT, Thoma F & Brubaker JM (1985) Chromatin reconstituted from tandemly repeated cloned DNA fragments and core\ histones: a model system for study of higher order structure. *Cell* **42**: 799–808

- Sirotkin AM, Edelmann W, Cheng G, Klein-szantot A, Kucherlapati R & Skoultchi AI (1995) Mice develop normally without the H10 linker histone. *92*: 6434–6438
- Smallwood A & Ren B (2013) Genome organization and long-range regulation of gene expression by enhancers. *Curr Opin Cell Biol* **25**: 387–394
- Song F, Chen P, Sun D, Wang M, Dong L, Liang D, Xu RM, Zhu P & Li G (2014) Cryo-EM study of the chromatin fiber reveals a double helix twisted by tetranucleosomal units. *Science* (80-.). **344**: 376–380 Available at: <http://www.ncbi.nlm.nih.gov/pubmed/24763583>
- Stafford WF (1992) Boundary analysis in sedimentation transport experiments: A procedure for obtaining sedimentation coefficient distributions using the time derivative of the concentration profile. *Anal. Biochem.* **203**: 295–301
- Strick R, Strissel PL, Gavrilov K & Levi-Setti R (2001) Cation-chromatin binding as shown by ion microscopy is essential for the structural integrity of chromosomes. *J. Cell Biol.* **155**: 899–910 Available at: <http://www.ncbi.nlm.nih.gov/article/2150894> [tool=pmcentrez&rendertype=abstract] [Accessed December 30, 2014]
- Szerlong HJ, Herman JA, Krause CM, Deluca JG, Skoultchi A, Winger QA, Prenni JE & Hansen JC (2015) Proteomic Characterization of the Nucleolar Linker Histone H1 Interaction Network. *J. Mol. Biol.* **427**: 2056–2071 Available at: <http://dx.doi.org/10.1016/j.jmb.2015.01.001>
- Szerlong HJ, Prenni JE, Nyborg JK & Hansen JC (2010) Activator-dependent p300 acetylation of chromatin in vitro: enhancement of transcription by disruption of repressive nucleosome-nucleosome interactions. *J. Biol. Chem.* **285**: 31954–64 Available at: <http://www.ncbi.nlm.nih.gov/article/2952196> [tool=pmcentrez&rendertype=abstract] [Accessed June 13, 2012]
- Takata H, Hanafusa T, Mori T, Shimura M, Iida Y, Ishikawa K, Yoshikawa K, Yoshikawa Y & Maeshima K (2013) Chromatin compaction protects genomic DNA from radiation damage. *PLoS One* **8**: e75622
- Talbert PB, Ahmad K, Almouzni G, Ausio J, Berger F, Bhalla PL, Bonner WM, Cande WZ, Chadwick BP, Chan SW, Cross GA, Cui L, Dimitrov SI, Doenecke D, Eirin-Lopez JM, Gorovsky MA, Hake SB, Hamkalo BA, Holec S, Jacobsen SE, et al (2012) A unified phylogeny-based nomenclature for histone variants. *Epigenetics Chromatin* **5**: 7
- Tse C & Hansen JC (1997a) Hybrid trypsinized nucleosomal arrays: identification of multiple functional roles of the H2A/H2B and H3/H4 N-termini in chromatin fiber compaction. *Biochemistry* **36**: 11381–8 Available at: <http://www.ncbi.nlm.nih.gov/pubmed/9298957>
- Tse C & Hansen JC (1997b) Hybrid trypsinized nucleosomal arrays: identification of multiple functional roles of the H2A/H2B and H3/H4 N-termini in chromatin fiber compaction. *Biochemistry* **36**: 11381–8 Available at: <http://www.ncbi.nlm.nih.gov/pubmed/9298957>
- Tse C, Sera T, Wolffe AP & Hansen JC (1998) Disruption of Higher-Order Folding by Core Histone Acetylation Dramatically Enhances Transcription of Nucleosomal Arrays by RNA Polymerase III Disruption of Higher-Order Folding by Core Histone Acetylation Dramatically

Enhances Transcription of Nucleosoma. *Mol. Cell. Biol.* **18**: 4629–4638

Tumolo T, Angnes L & Baptista MS (2004) Determination of the refractive index increment ($\Delta n/dc$) of molecule and macromolecule solutions by surface plasmon resonance. *Anal. Biochem.* **333**: 273–279

Ugarte F, Sousae R, Cinquin B, Martin EW, Krietsch J, Sanchez G, Inman M, Tsang H, Warr M, Passegu?? E, Larabell CA & Forsberg EC (2015) Progressive chromatin condensation and H3K9 methylation regulate the differentiation of embryonic and hematopoietic stem cells. *Stem Cell Reports* **5**: 728–740

Ura K & Kaneda Y (2001) Reconstitution of chromatin in vitro. *Methods Mol Biol* **181**: 309–325

Valouev A, Johnson SM, Boyd SD, Smith CL, Fire AZ & Sidow A (2011) Determinants of nucleosome organization in primary human cells. *Nature* **474**: 516–520

Widom J & Klug A (1985) Structure of the 3008 Chromatin Filament : X-Ray Diffraction from Oriented Samples. *Cell* **43**: 207–213

Woodcock CL (1994) Chromatin fibers observed in situ in frozen hydrated sections. Native fiber diameter is not correlated with nucleosome repeat length. *J. Cell Biol.* **125**: 11–9 Available at:

Woodcock CL & Horowitz RA (1991) Ultrastructure of chromatin. *J. Cell Sci.* **99**: 99–106

Woodcock CL, Skoultschi AI & Fan Y (2006) Role of linker histone in chromatin structure and function: H1 stoichiometry and nucleosome repeat length. *Chromosom. Res* **14**: 17–25

Woodcock CLF, Frado LY & Rattner JB (1984) The Higher-order Structure of Chromatin : Evidence for a Helical Ribbon Arrangement Fibers from Interphase Nuclei and Chromosome. *99*:

Yager TD, McMurray CT & van Holde KE (1989) Salt-induced release of DNA from nucleosome core particles. *Biochemistry* **28**: 2271–81 Available at:
<http://www.ncbi.nlm.nih.gov/pubmed/2719953>

Zhao H, Brown PH & Schuck P (2011) On the distribution of protein refractive index increments. *Biophys. J.* **100**: 2309–2317 Available at: <http://dx.doi.org/10.1016/j.bpj.2011.03.004>

Zheng C, Lu X, Hansen JC & Hayes JJ (2005) Salt-dependent intra- and internucleosomal interactions of the H3 tail domain in a model oligonucleosomal array. *J Biol Chem* **280**: 33552–33557

Ziv Y, Bielopolski D, Galanty Y, Lukas C, Taya Y, Schultz DC, Lukas J, Bekker-Jensen S, Bartek J & Shiloh Y (2006) Chromatin relaxation in response to DNA double-strand breaks is modulated by a novel ATM- and KAP-1 dependent pathway. *Nat. Cell Biol.* **8**: 870–876 Available at:
<http://www.nature.com/doifinder/10.1038/ncb1446npapers3://publication/doi/10.1038/ncb1446>